

MIXING AND DISPERSION OF VISCOUS LIQUIDS AND POWDERED SOLIDS*

J. M. Ottino, P. DeRoussel, S. Hansen, and D. V. Khakhar

Department of Chemical Engineering Northwestern University Evanston, IL 60208

I. Preliminaries	105
II. Mixing and Dispersion of Immiscible Fluids	124
A. Breakup	130
B. Coalescence	151
C. Breakup and Coalescence in Complex Flows	155
III. Fragmentation and Aggregation of Solids	159
A. Fragmentation	163
B. Aggregation	180
IV. Concluding Remarks	194
References	198

I. Preliminaries

Mixing and dispersion of viscous fluids—blending in the polymer processing literature—is the result of complex interaction between flow and events occurring at drop length-scales: breakup, coalescence, and hydrodynamic interactions. Similarly, mixing and dispersion of powdered solids in viscous liquids is the result of complex interaction between flow and

* Note on notation: Relations from breakup, coalescence, fragmentation, and aggregation are based on either actual experiments or numerical simulations, the latter commonly referred to as “computer experiments.” Computer experiments are often based on crude simplifying assumptions and actual experiments are always subject to errors; the strict use of the equality sign in many of the final results may therefore be misleading. In order to accurately represent the uncertainty associated with the results, the following notation is adopted:

\approx	Used in relations when the error is generally less than 25%
\sim	Used to denote proportionality and order of magnitude
\approx, \approx	Used in conditional statements when the limiting value given is correct within a factor of 2
$=, >, <$	Used in expressions related to modeling and standard mathematical manipulations

events—erosion, fragmentation and aggregation—occurring at agglomerate length scales. Important applications of these processes include the compounding of molten polymers and the dispersion of fine particles in polymer melts. Reynolds numbers in both cases are small, even more so given the small length scales that dominate the processes.

There are similarities and, undoubtedly, substantial differences between these two processes. The following analogies are apparent (Fig. 1):

Breakup \leftrightarrow Fragmentation

Coalescence \leftrightarrow Aggregation

The ratio of deforming viscous forces to resisting interfacial tension forces in the case of droplets is the *capillary number*, Ca . Similarly, the ratio of viscous to cohesive forces in agglomerates is the *fragmentation number*, Fa .

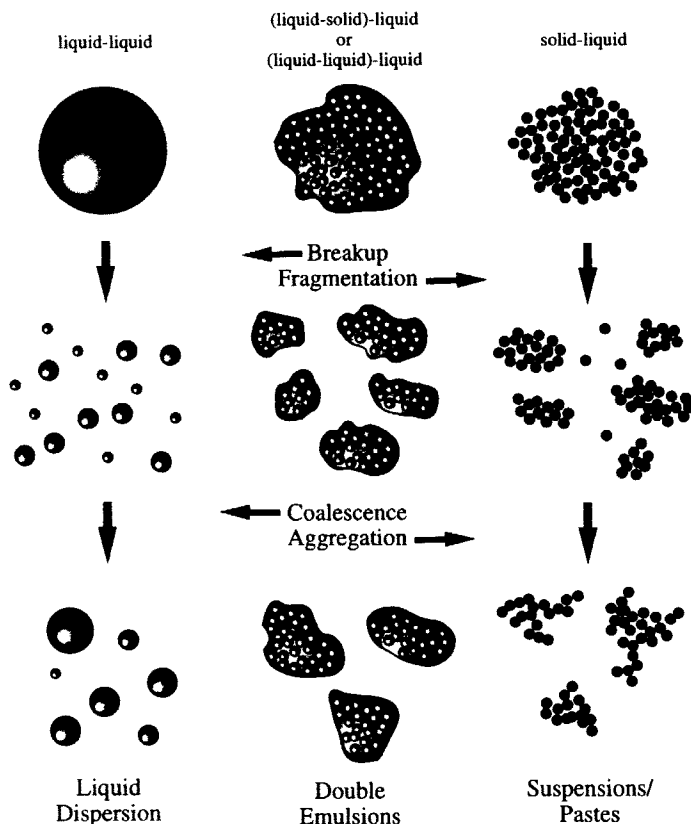


FIG. 1. Schematic diagram illustrating the analogies between dispersion of immiscible liquids and dispersed solids.

Thus, $Ca < O(1)$ and $Fa < O(1)$ determine conditions where no breakup or fragmentation is possible. Both processes, breakup and coalescence for drops, and fragmentation and aggregation for solids, lead to time-varying distributions of drops and cluster sizes that become time-invariant when scaled in suitable ways. There are also parallels between aggregation and fragmentation that underscore mathematical similarity: Both *Smoluchowski's equation* and the *fragmentation equation* are amenable to scaling solutions.

These similarities notwithstanding, it may be argued that it is differences that have hindered understanding. This state of affairs has not been helped by proliferation of terminology: alloying, compounding, and blending all appear in the polymer processing literature; fragmentation and rupture in the solids dispersion literature; breakup, rupture, and burst in the fluid mechanics literature. Both agglomerates and flocs refer to particle clusters. Undoubtedly, droplets are easier to deal with than agglomerates whose structure is complex and can only be known in a statistical sense. Thus, breakup and coalescence, being placed squarely in the realm of classical fluid mechanics, are on more sure footing than fragmentation and aggregation, which demand knowledge of physical chemistry and colloid science, and have been studied to a lesser extent.

Realistic mixing problems are inherently difficult owing to the complexity of the *flow* fields, to the fact that the *fluids* themselves are rheologically complex, and to the coupling of length scales. For this very reason, mixing problems have been attacked traditionally on a case-by-case basis. Modeling becomes intractable if one wants to incorporate all details at once. Nevertheless it appears important to focus on common features and to take a broad view.

Two reviews, published in the same book, may be considered to be the launching basis for the material presented here: Meijer and Janssen (1994) and Manas-Zloczower (1994). In both reviews the fundamentals of the processes are considered at a small length scale (drops, agglomerates), focusing on the effects of flow. Meijer and Janssen (1994) review fundamental studies of droplet breakup and coalescence in the context of the analysis of polymer blending. Manas-Zloczower (1994), on the other hand, focuses on dispersion of fine particles in polymers. The primary objective of the present work is to present both topics in a unified format together with the basics of particle aggregation. The unified presentation serves to highlight the analogies between the processes and consequently to increase understanding. A related goal is to introduce potentially useful recent advances in fundamentals that have not yet been applied to the analysis of practical processing and structuring problems (Villadsen, 1997).

There have been substantial advances in the understanding of *viscous*

mixing of single fluids. This has been driven primarily by theoretical developments based on chaos theory and increased computational resources, as well as by advances in fluid mechanics and a host of new experimental results. Such an understanding forms a fabric for the evolution of breakup, coalescence, fragmentation, and aggregation. These processes can in fact be viewed as a population of “microstructures” whose behavior is driven by a chaotic flow; microstructures break, diffuse, and aggregate, causing the population to evolve in space and time. *Self-similarity* is common to all these problems; examples arise in the context of the distribution of stretchings within chaotic flows, in the asymptotic evolution of fragmentation processes, and in the equilibrium distribution of drop sizes generated upon mixing of immiscible fluids.

It may be useful at this juncture to draw the distinction between *theory* and *computations* (or numerical experiments), as the material presented here is somewhat tilted toward theory. Computations are not theory, but theory often requires computations. To the extent that it is not possible to put all elements of a problem into a complete picture, assumptions are necessary—often entailing mechanistic views of the behavior of the system. Nontrivial assumptions leading to nontrivial consequences lead to significant theories. Assuming that a flow field can be imagined as an assembly of weak regions (where stretching of passive elements is linear) and strong regions (where stretching of passive elements is exponential) could form the basis of a theory; real flows are manifestly more complex, but this is clearly a useful approximation. In fact, G. I. Taylor’s (1932) pioneering work in drop dynamics can be traced back to this crucial element. A binary breakup assumption, on the other hand, may not form as strong a basis, especially if more precise knowledge can be incorporated with little or no difficulty into the picture: Drops and fluid filaments break, often producing, in single events, a distribution of sizes. Thus, a “theory” based on binary breakup could be revisited and may be successfully augmented. Similar comments apply to fragmentation of agglomerates.

This paper is divided into two main, interconnected parts—breakup and coalescence of immiscible fluids, and aggregation and fragmentation of solids in viscous liquids—preceded by a brief introduction to mixing, this being focused primarily on stretching and self-similarity.

The treatment of mixing of immiscible fluids starts with a description of breakup and coalescence in homogeneous flows. Classical concepts are briefly reviewed and special attention is given to recent advances—satellite formation and self-similarity. A general model, capable of handling breakup and coalescence while taking into account stretching distributions and satellite formation, is described.

The treatment of aggregation and fragmentation processes parallels that

of breakup and coalescence. Classical concepts are briefly reviewed; special attention is given to fragmentation theory as well as to flow-driven processes in nonhomogeneous (chaotic) flows. The Péclet number in all instances is taken to be much greater than unity, so that diffusion effects are unimportant. In many examples, hydrodynamic interactions between clusters are neglected to highlight the effects of advection on the evolution of the cluster size distribution and the formation of fractal structures.

The paper is structured to be read at three levels. The main thread of the text is a review of fundamentals and previous studies. *Illustrations* focusing on specific systems or more detailed elaboration of concepts are interspersed in the text. Many of these include new results; they form a second level that can be read as independent subunits. Finally, the conclusions of each section, especially those with significance for practical applications, are summarized as heuristics.

1. Stretching and Chaotic Mixing

Fluid advection—be it regular or chaotic—forms a template for the evolution of breakup, coalescence, fragmentation, and aggregation processes. Let $\mathbf{v}(\mathbf{x}, t)$ represent the Eulerian velocity field (typically we assume that $\nabla \cdot \mathbf{v} = 0$). The solution of

$$\left(\frac{d\mathbf{x}}{dt}\right)_{\mathbf{x}} = \mathbf{v}(\mathbf{x}, t), \quad (1)$$

with \mathbf{X} representing the initial coordinates of material particles located at \mathbf{x} at time t , gives the motion

$$\mathbf{x} = \Phi_t(\mathbf{X}) \text{ with } \mathbf{X} = \Phi_{t=0}(\mathbf{X}), \quad (2)$$

i.e., the particle \mathbf{X} is mapped to the position \mathbf{x} after a time t . This is formally the solution to the so-called *advection* problem (Aref, 1984). The foundations of this area are now on sure footing and reviews are presented in Ottino (1989, 1990). The quantity of interest is stretching of fluid elements.

The stretches of a material filament $d\mathbf{x}$, λ , and material surface element $d\mathbf{a}$, η , are defined as

$$\lambda \equiv \lim_{|d\mathbf{X}| \rightarrow 0} \frac{|d\mathbf{x}|}{|d\mathbf{X}|}, \quad \eta \equiv \lim_{|d\mathbf{A}| \rightarrow 0} \frac{|d\mathbf{a}|}{|d\mathbf{A}|}, \quad (3)$$

where $d\mathbf{X}$ and $d\mathbf{A}$ represent the initial conditions of $d\mathbf{x}$ and $d\mathbf{a}$, respectively. The fundamental equations for the rate of stretch are

$$\frac{d(\ln \lambda)}{dt} = \mathbf{D} : \mathbf{mm}, \quad \frac{d(\ln \eta)}{dt} = \nabla \cdot \mathbf{v} - \mathbf{D} : \mathbf{nn}, \quad (4)$$

where $\mathbf{D} \equiv [\nabla \mathbf{v} + (\nabla \mathbf{v})^T]/2$ is the stretching tensor, and \mathbf{m} and \mathbf{n} are the instantaneous orientations ($\mathbf{m} = d\mathbf{x}/|d\mathbf{x}|$, $\mathbf{n} = d\mathbf{a}/|d\mathbf{a}|$). The Lagrangian histories $d(\ln \lambda)/dt = \alpha_\lambda(\mathbf{X}, \mathbf{M}, t)$ and $d(\ln \eta)/dt = \alpha_\eta(\mathbf{X}, \mathbf{N}, t)$ are called *stretching functions*. Flows can be compared in terms of their stretching efficiencies. The stretching efficiency $e_\lambda = e_\lambda(\mathbf{X}, \mathbf{M}, t)$ of the material element $d\mathbf{X}$ and the stretching efficiency $e_\eta = e_\eta(\mathbf{X}, \mathbf{N}, t)$ of the area element $d\mathbf{A}$ are defined as

$$e_\lambda \equiv \frac{1}{(\mathbf{D} : \mathbf{D})^{1/2}} \frac{d(\ln \lambda)}{dt} < 1, \quad e_\eta \equiv \frac{1}{(\mathbf{D} : \mathbf{D})^{1/2}} \frac{d(\ln \eta)}{dt} < 1. \quad (5)$$

If $\nabla \cdot \mathbf{v} = 0$, $e_i \leq (1/2)^{1/2}$ in two-dimensional (2D) flows and $(2/3)^{1/2}$ in three-dimensional (3D) flows, where $i = \lambda, \eta$. The efficiency can be thought of as the specific rate of stretching of material elements normalized by a factor proportional to the square root of the energy dissipated locally.

The key to effective mixing lies in producing stretching and folding, an operation that is referred to in the mathematics literature as a *horseshoe map*. Horseshoe maps, in turn, imply chaos. The 2D case is the simplest. The equations of motion for a two-dimensional area preserving flow can be written as

$$v_x = \frac{dx}{dt} = \frac{\partial \psi}{\partial y}, \quad v_y = \frac{dy}{dt} = -\frac{\partial \psi}{\partial x}, \quad (6)$$

where ψ is the stream function. If the velocity field is steady (i.e., ψ is independent of time), then it is integrable and the system cannot be chaotic. The mixing is thus poor: Stretching for long times is linear, the stretching function decays as $1/t$, and the efficiency decays to zero. On the other hand, if the velocity field, or equivalently ψ , is time-periodic, there is a good chance that the system will be chaotic (Aref, 1984). It is relatively straightforward to produce flow fields that can generate chaos. A necessary condition for chaos is the “crossing” of streamlines: Two successive streamline portraits, say at t and $(t + \Delta T)$ for time periodic flows or at z and $(z + \Delta z)$ for spatially periodic flows, when superimposed, should show intersecting streamlines. In 2D systems this can be achieved by time modulation of the flow field, for example by motions of boundaries or time periodic changes in geometry. Figures 2 and 3 show typical examples of mixing in such flows: the vortex mixing flow (VMF) and the cavity flow, respectively. The vortex mixing flow is generated by alternately rotating one of the cylinders for a fixed period of time; the cavity flow is generated by alternately moving the upper and lower walls of the cavity for a fixed time period. It is clear from the geometry of the systems that both achieve the required “crossing” of streamlines by the time modulation.

Numerous experimental studies have revealed the degree of order and

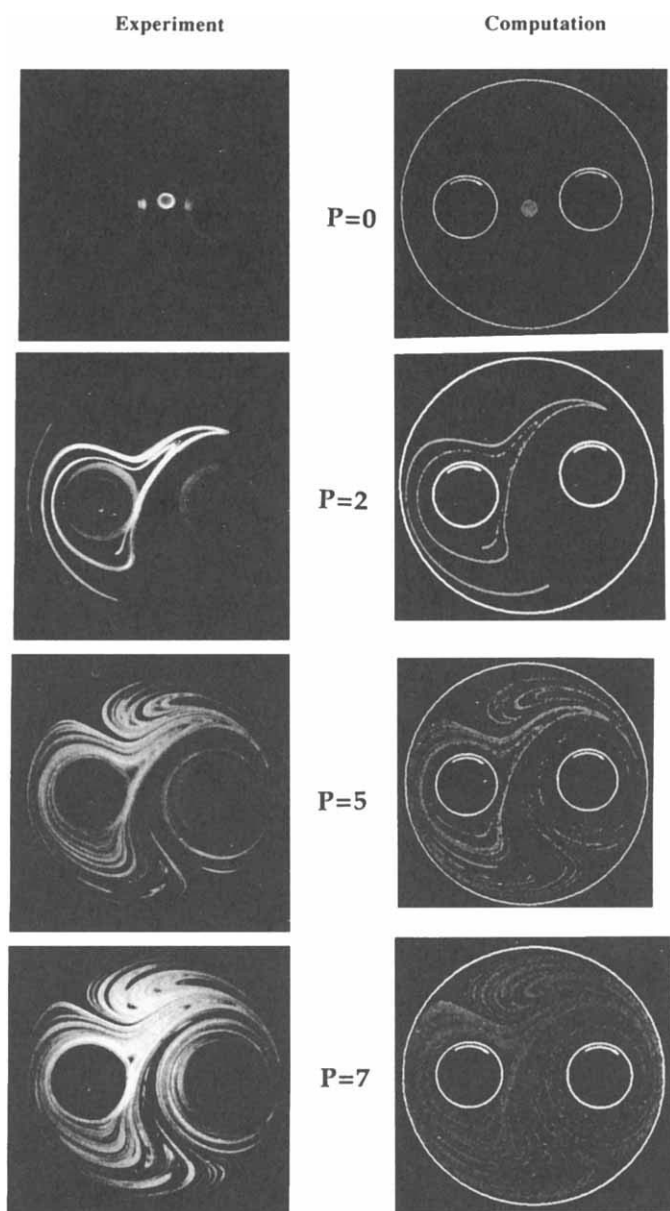


FIG. 2. Mixing in the vortex mixing flow with increasing periods of flow (P). The flow is time periodic with each cylinder rotating alternately for a fixed time period (Jana, Metcalfe and Ottino, 1994).

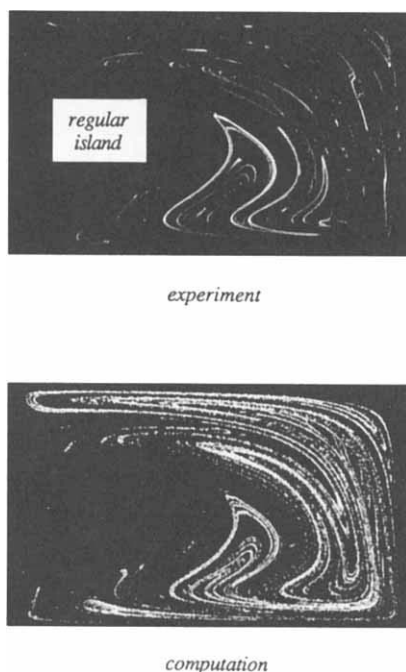


FIG. 3. Mixing in the cavity flow. The flow is time periodic with the upper and lower walls moving alternately for a fixed time period (Leong and Ottino, 1989).

disorder compatible with chaos in fluid flows. Experiments conducted in carefully controlled two-dimensional, time-periodic flows and spatially periodic flows reveal the complexity associated with chaotic motions. The most studied flows are the flow between two rotating eccentric cylinders, several classes of corotating and counterrotating cavity flows, and spatially periodic flows. Even within this theme, many variations are possible. For example, Leong (1990) considered the effect of cylindrical obstructions placed in a cavity flow; Schepens (1996) took this a step further and carried out computations and experiments for the case when the pin itself is allowed to rotate. The 2D time-periodic case is especially illustrative.

Dye structures of passive tracers placed in time-periodic chaotic flows evolve in an iterative fashion; an entire structure is mapped into a new structure with persistent large-scale features, but finer and finer scale features are revealed at each period of the flow. After a few periods, strategically placed blobs of passive tracer reveal patterns that serve as templates for subsequent stretching and folding. Repeated action by the flow generates a lamellar structure consisting of stretched and folded striations, with thicknesses $s(t)$, characterized by a probability density function, $f(s, t)$, whose

mean, on the average, decreases with time [$f(s,t)ds$ is the number of striations with striation thicknesses between s and $s + ds$]. The striated pattern quickly develops into a time-evolving complex morphology of poorly mixed regions of fluid (islands) and of well-mixed or chaotic regions (see Fig. 3). Computations capture the evolution of the structure reasonably well for short mixing times (Figs. 2 and 3) and are useful for analysis. Islands translate, stretch, and contract periodically and undergo a net rotation, preserving their identity returning to their original locations after multiples of the period of the flow, symmetry being a common feature of many flows (see Fig. 4). Stretch in islands, on the average, grows linearly and much slower than in chaotic regions, in which the stretch increases exponentially with time. Moreover, since islands do not exchange matter with the rest of the fluid they represent an obstacle to efficient mixing. An important parameter of the flow is the sense of rotation in the alternate periods—corotation tends to produce more uniform mixing.

Duct flows, like steady two-dimensional flows, are poor mixers. This class of flows is defined by the velocity field

$$v_x = \frac{\partial \psi}{\partial y}, \quad v_y = -\frac{\partial \psi}{\partial x}, \quad v_z = f(x, y), \quad (7)$$

which is composed of a two-dimensional cross-sectional flow augmented by a unidirectional axial flow; fluid is mixed in the cross-section while it is

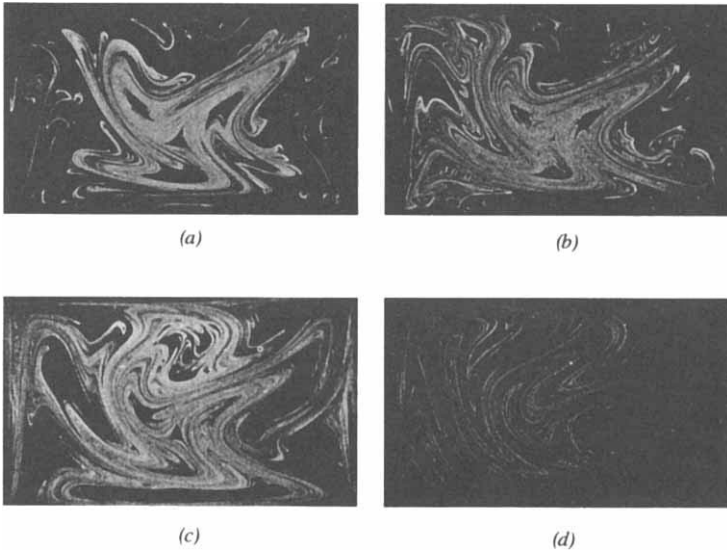


FIG. 4. Mixing in the time periodic cavity flow at increasing values of the time period. The mixed state is shown at long mixing times (Leong and Ottino, 1989).

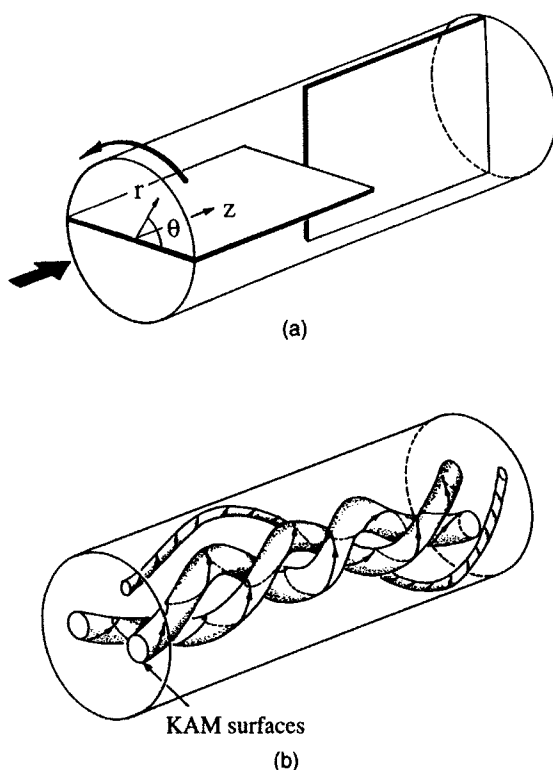
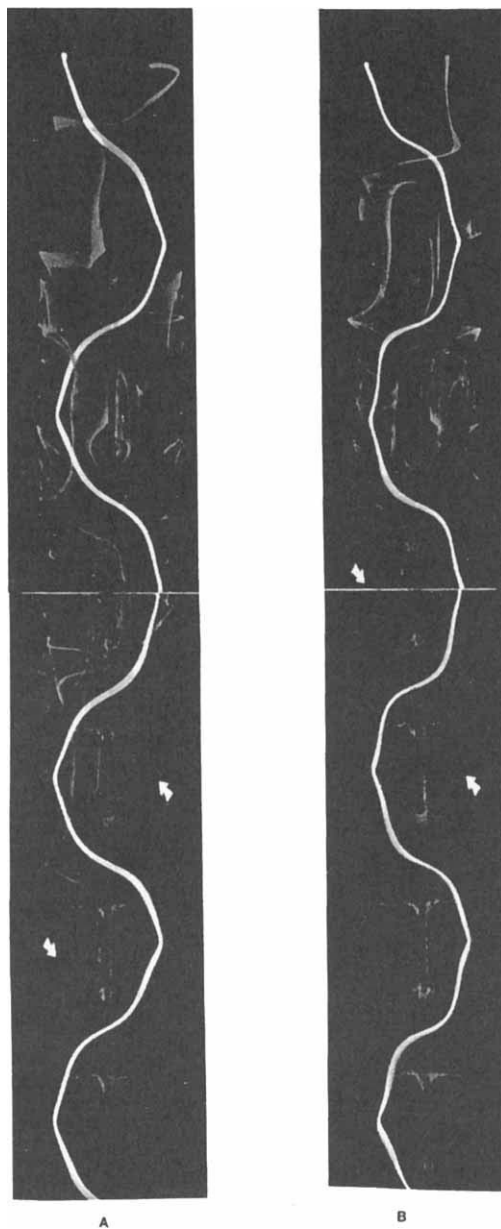


FIG. 5. Mixing in the partitioned pipe mixer. (a) Schematic view of the mixer geometry; one element of the mixer is shown, and the mixer comprises several such elements joined together. (b) KAM surfaces in flow bounding regions of regular flow. (c) A and B show examples of experimentally obtained streaklines: undeformed streaklines pass through KAM tubes, whereas streaklines in the chaotic region are well mixed. The white arrows indicate the location of a companion streak-tube. (Khakhar, Franjione, and Ottino, 1987; Kusch and Ottino, 1992).

simultaneously transported down the duct axis. In a duct flow, the cross-sectional and axial flows are independent of both time and distance along the duct axis, and material lines stretch linearly in time. A single screw extruder, for example, belongs to this class.

Duct flows can be converted into efficient mixing flows (i.e., flows with an exponential stretch of material lines with time) by time- modulation or by spatial changes along the duct axis. One example of the spatially periodic class is the partitioned-pipe mixer (PPM). This flow consists of a pipe partitioned with a sequence of orthogonally placed rectangular plates (Fig. 5a). The cross-sectional motion is induced through rotation of the pipe with respect to the assembly of plates, whereas the axial flow is caused by



(c)

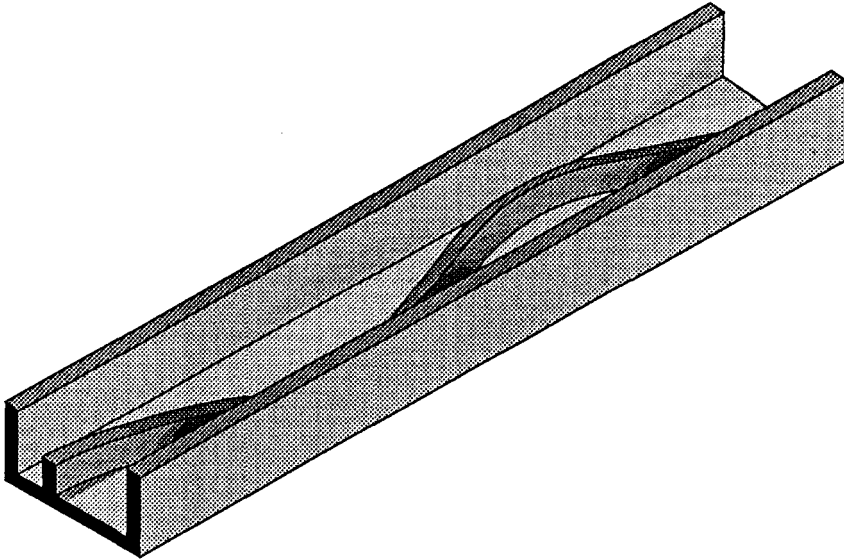
FIG. 5 (continued)

a pressure gradient; the behavior of the system is characterized by the ratio of cross-sectional twist to axial stretching, β (Khakhar, Franjione, and Ottino, 1987; Kusch and Ottino, 1992). The flow is regular for no cross-sectional twist ($\beta = 0$) and becomes chaotic with increasing values of β . The KAM (Kolmogorov–Arnold–Moser) surfaces (tubes) bound regions of regular flow and correspond to the islands in 2D systems (Fig. 5b). Experiments reveal the intermingled regular and chaotic regions: A streak-line starting in a KAM tube passes through the mixer with little deformation, whereas streaklines in the chaotic regions are mixed well (Fig. 5c a,b).

Illustration: Improved mixing in single screw extruders. The concept of improved mixing by reorienting the flow is often used in various types of single screw extruders. The extruder is divided into a small number of zones with a mixing section between each zone. Each mixing section consists of pins or blades that protrude into the flow and cause random reorientations of fluid elements in the flow; a random reorientation is better than no reorientation at all. The mixing efficiency climbs and mixing is dramatically improved. Such an approach was investigated by Chella and Ottino (1985).

Mixing in such systems can also be significantly improved by means of time-dependent changes in geometry. This idea can be readily implemented in the context of duct flows by adding a secondary baffle. Such a concept has obvious applications in polymer processing; for example, single screw extruders can be imagined as a channel with a moving lid (not shown) as in Fig. 6a. A two-dimensional analog of the extruder channel with a baffle is a cavity flow with steady motion of the top wall and periodic motion of the lower wall with a rectangular block (Fig. 6b). The mixing in this case is greatly improved as compared to a steady cavity flow. Similar designs have been arrived at empirically in engineering practice.

Illustration: Mixing of viscoelastic fluids. Driving a system faster, for example by moving boundaries at a higher speed under a *fixed* protocol, does not imply better mixing: Islands survive and do not go away. Yet another instance where faster action may actually lead to *worse* mixing is provided by the case of viscoelastic fluids. Niederkorn and Ottino (1993) studied, experimentally and computationally, the mixing of Boger fluids—viscoelastic fluids with a constant shear viscosity. The system considered was the flow between two eccentric cylinders, in which the inner and outer cylinders are rotated alternately. The flow is referred to as the “journal bearing flow” and is a classical system in chaotic mixing studies. In the limit of slow flow, a Boger fluid behaves as Newtonian; faster flows lead to viscoelastic effects quantified in terms of Weissenberg number (We), the ratio of the relaxation time of the fluid to a time scale of the flow, e.g., the inverse of the shear rate. Spectacular effects occur at moderate We



(a)

FIG. 6. (a) Schematic view of an extruder channel with an undulating baffle. (b) B, C, D: Steady flow streamlines with and without baffles for initial condition A. E, F: Mixing in a cavity flow with an oscillating baffle. The upper plate moves with a steady velocity while the lower plate with the baffle undergoes linear oscillatory motion (Jana, Tjahjadi, and Ottino, 1994).

(Nieder Korn and Ottino, 1993); Fig. 7 shows the contrast between the Newtonian ($We \approx 0$) and the non-Newtonian case ($We \approx 0.06$). In general, it appears that viscoelastic fluids mix more slowly than the corresponding Newtonian fluid; in most instances also, in the long time limit, the region occupied by regular islands is larger for the viscoelastic case, i.e., the mixing is poorer. This, however, is not always the case, and there are experimentally documented instances where the long-time degree of mixing in the viscoelastic case is better than in the Newtonian case. Shear thinning effects, on the other hand, appear to be milder than viscoelastic effects and relatively high degrees of shear thinning are required to produce substantial effects (Nieder Korn and Ottino, 1994).

Kumar and Homsey (1996) carried out a theoretical analysis of slightly viscoelastic flow and mixing in the journal bearing system described earlier. The effect of elasticity on the flow is to shift the stagnation streamline, which affects the size of the mixed region (Kaper and Wiggins, 1993). Depending on the mixing protocol, Kumar and Homsey (1996) found that the size of unmixed islands may increase or decrease with elasticity as in the experiments of Nieder Korn and Ottino (1994). Many other comparisons

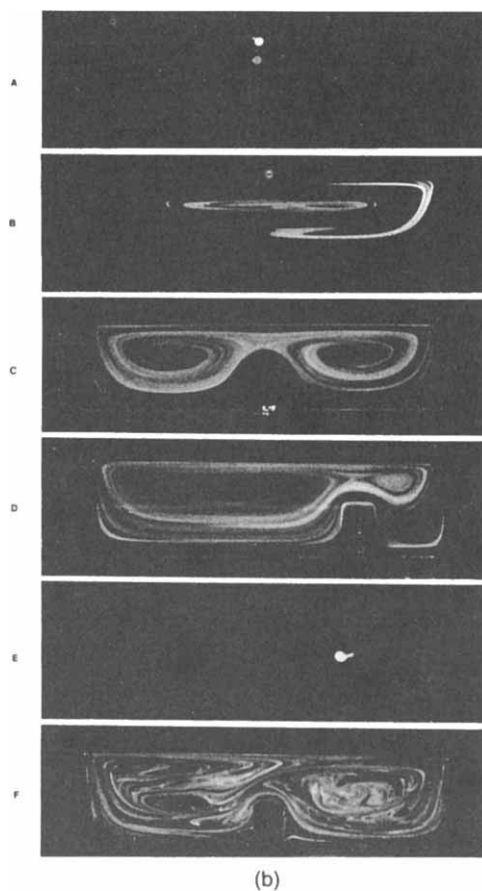


FIG. 6 (continued)

between chaotic advection of Newtonian and viscoelastic fluids are possible. For example, the critical modulation frequency of the inner cylinder at which the largest island disappears is lower for the viscoelastic fluid. Conclusions, however, are specific and dependent on mixing protocols, and little can be said in general about the effects of viscoelasticity. More work should be carried out in this area.

2. Stretching Distributions

Filaments in chaotic flows experience complex time-varying stretching histories. Computational studies indicate that within chaotic regions, the distribution of stretches, λ , becomes self-similar, achieving a scaling limit.

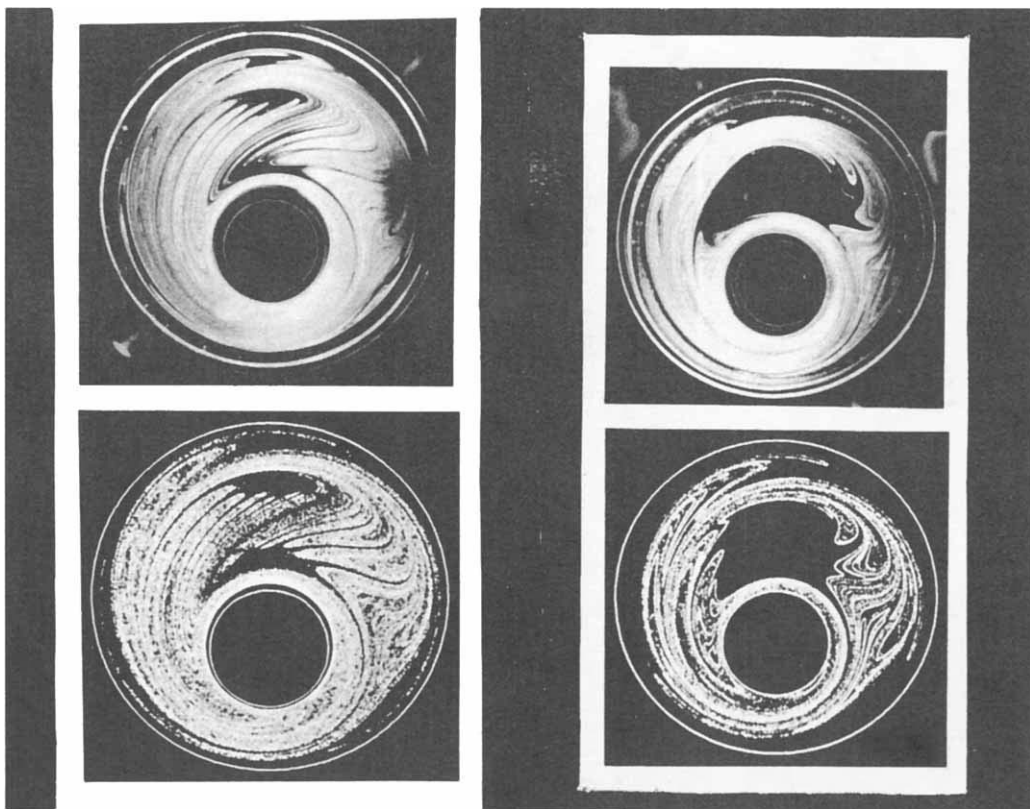


FIG. 7. Experiments and computations on the advection of a dye blob in an eccentric cylinder apparatus (from Niederkorn and Ottino, 1993). *Left:* Top, experiment using Newtonian fluid; bottom, numerical simulation of same situation. *Right:* Top, identical experiment as in upper left, but using viscoelastic fluid ($We \approx 0.06$); bottom, numerical simulation at $We = 0.04$.

The distribution of stretches can be quantified in terms of the probability density function $F_n(\lambda) \equiv dN(\lambda)/d\lambda$, where $dN(\lambda)$ is the number of points that have values of stretching between λ and $(\lambda+d\lambda)$ at the end of period n . Another possibility is to focus on the distribution of $\log \lambda$. In this case we define the measure $H_n(\log \lambda) \equiv dN(\log \lambda)/d(\log \lambda)$.

Muzzio, Swanson, and Ottino (1991a) demonstrated that the distribution of stretching values in a globally chaotic flow approaches a log-normal distribution at large n : A log-log graph of the computed distribution approaches a parabolic shape (Fig. 8a) as required for a log-normal distribution. Furthermore, as n increases, an increasing portion of the curves in the figure (Fig. 8b) overlap when the distribution is rescaled as

$$\mathcal{H}(z) = [\log \lambda]^2 \frac{H_n(\log \lambda)}{m_{\log \lambda}(n)}, \quad (8)$$

where $m_{\log \lambda}(n) = \sum \log \lambda H_n(\log \lambda)$ is the first moment of $H_n(\log \lambda)$ and $z = \log \lambda / \log \Lambda_g$, with $\log \Lambda_g = [\sum \log \lambda H_n(\log \lambda)] / [\sum H_n(\log \lambda)]$, and the sums are over a large number of fluid elements in the flow. The rescaled distribution is thus independent of the number of periods of the flow (n) at large n , and the distributions $H_n(\log \lambda)$ are said to be self-similar.

The explanation for the approach to a log-normal distribution is as follows. Consider, for simplicity, flows as those considered by Muzzio, Swanson, and Ottino (1991a): two-dimensional time periodic flows. Let $\lambda_{n,k}$ denote the length stretch experienced by a fluid element between periods n and k . The total stretching after m periods of the flow, $\lambda_{0,m}$, can be written as the product of the stretchings from each individual period:

$$\lambda_{0,m} = \lambda_{0,1} \lambda_{1,2} \lambda_{2,3} \dots \lambda_{m-1,m}. \quad (9)$$

The amount of stretching between successive periods (i.e., $\lambda_{1,2}$ and $\lambda_{2,3}$) is strongly correlated; however, the correlation in stretching between nonconsecutive periods (e.g., $\lambda_{0,1}$ and $\lambda_{4,5}$) grows weaker as the separation between periods increases as a result of chaos (the presence of islands in the flow complicates the picture, but these issues are not considered here). Thus, $\lambda_{0,m}$ is essentially the product of random numbers, which when rewritten as

$$\log \lambda_{0,m} = \log \lambda_{0,1} + \log \lambda_{1,2} + \log \lambda_{2,3} + \dots + \log \lambda_{m-1,m} \quad (10)$$

gives a sum of random numbers. According to the central limit theorem, any collection of sums of random numbers will converge to a Gaussian. So, when all material elements are considered, the distribution of $\lambda_{0,m}$ should be log-normal (Fig. 8a). This conjecture has been verified by numerous computations (Muzzio *et al.*, 1991a).

Illustration: Optimum strain per period in shear flows with periodic reorientation. Many practical mixing flows (e.g., single screw extruder with mixing

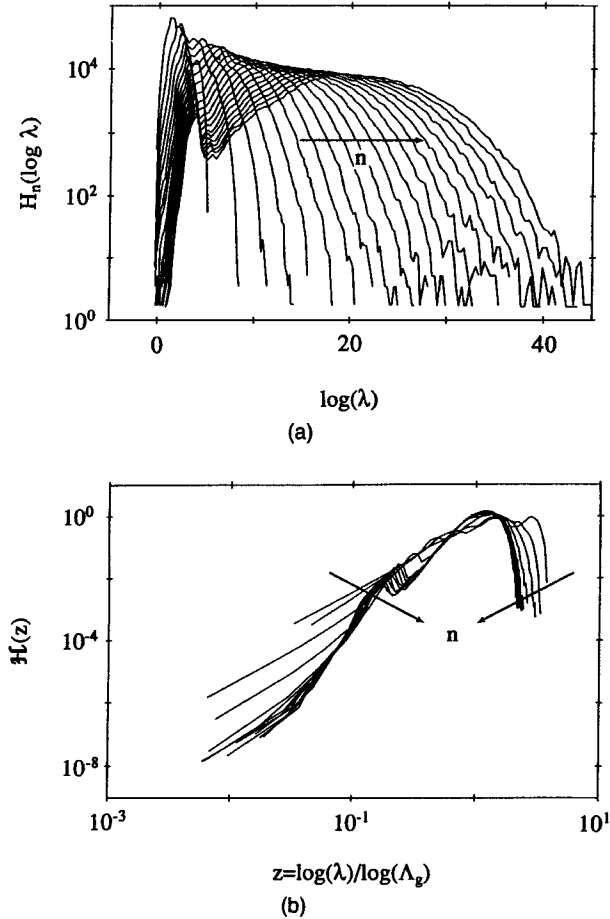


FIG. 8. (a) Distribution of length stretches ($\log \lambda$) for increasing periods of flow (n) in a journal bearing flow. The distribution approaches a log-normal form (parabolic shape) at large n . (b) Rescaled distribution of length stretches. Data in (a) collapse to a single curve, implying self-similarity (Muzzio *et al.*, 1991a).

zones), as well as the chaotic cavity flows discussed earlier, are composed of a sequence of shear flows with periodic random reorientation of material elements relative to the flow streamlines. In all cases, the effect of the reorientation is an exponential stretching of material elements. The interval between two successive reorientations is an important parameter of such systems, and the following argument demonstrates that an optimum interval must exist at which the total length stretch is maximum for a fixed time of mixing: In the limit of very small periods, material elements are stretched and compressed at random, and hence the average length stretch is small;

in the limit of very large time periods, the flow approaches a steady shear flow and again the length stretch is small. Khakhar and Ottino (1986a) showed a maximum in the average stretching efficiency when the strain per period was between 4 and 5 for a simple shear flow and a vortical flow with random periodic reorientation (Fig. 9). Since the average efficiency is simply the length stretch per period normalized by $(\mathbf{D}:\mathbf{D})^{1/2}$, which is proportional to the square root of the viscous dissipation, the optimum corresponds to the maximum stretching for a fixed energy input. Similar results are obtained when there is a distribution of shear rates.

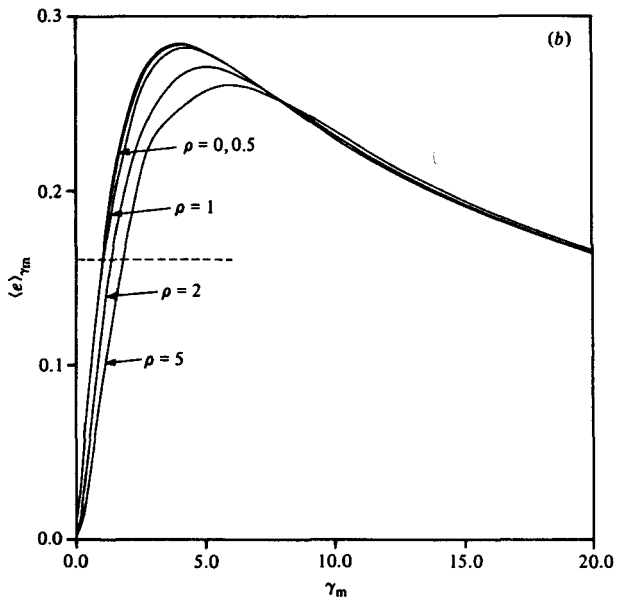
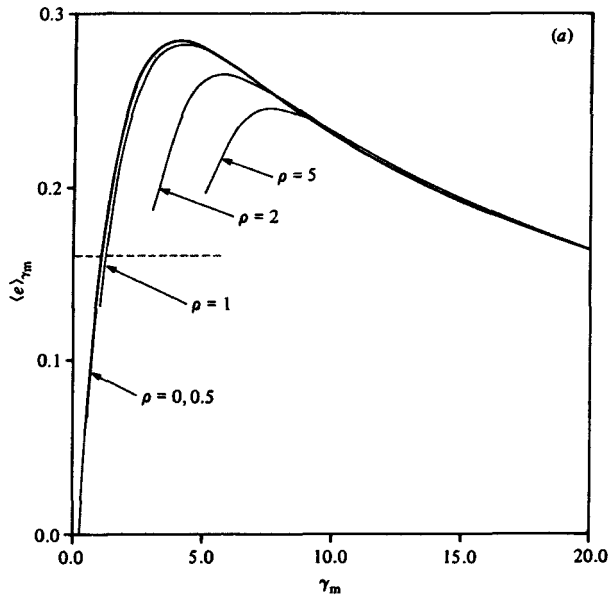
Numerical analysis provides an important tool for quantitative estimates of stretching in practical mixers. The flow in most such mixers is three-dimensional and time dependent, and numerical analysis is required to obtain the velocity field; stretching is then obtained computationally from this. Avalosse and Crochet (1997a,b) obtained the velocity field for a rotating cam mixer (a 2D time periodic flow) and a Kenics static mixer (a spatially periodic duct flow) using the finite element method (Avalosse, 1993). The 2D mixer comprises two triangular cams rotating in a cavity and is similar in design to the Banbury mixer (see Fig. 34). The Kenics static mixer comprises a pipe with inserts—helically twisted tape sections joined at right angles to each other—and the mixing action is similar to the partitioned pipe mixer. In both cases, an exponential increase in length of material line is obtained. As may be expected based on studies using idealized systems (Khakhar *et al.*, 1986) corotating cams are found to give much better mixing than counterrotating cams in the 2D mixer. Good agreement is obtained between the computed mixing patterns and experimental results for both flows. More recently, Hobbs and Muzzio (1997) carried out an analysis of the Kenics static mixer and showed that the stretching distributions produced are self-similar.

HEURISTICS

- 2D time periodic flows and spatially periodic duct flows can produce chaos. A necessary condition for chaos is crossing of streamlines.

FIG. 9. Average efficiency of stretching of material elements (ϵ_s) in a simple shear flow with random reorientation after an average length stretch γ_m . ρ gives the width of the distribution of length stretch about the mean value (γ_m). Results for a random distribution (top) and a normal distribution (bottom) of length stretch are shown. The maximum in the efficiency corresponds to the maximum length stretch for a fixed amount of energy dissipated and occurs at an average stretch of about 5 per period (Khakhar and Ottino, 1986a).

Importance of reorientation



- In general, time periodic (or spatially periodic) flows generate islands (or tubes). Stretching in islands and tubes is linear. Stretching in chaotic regions is exponential.
 - Stretchings of the order of 10^4 can be obtained in about six cycles (or reorientations). A stretch of about 4–5 per cycle seems to be optimal.
 - Corotational flows distribute material better than counterrotational flows.
 - Viscoelasticity (We as low as 0.06) results in substantially different patterns of mixing—larger islands and slower rates of mixing may result.
 - Shear thinning typically has little effect on mixing.
-

II. Mixing and Dispersion of Immiscible Fluids

1. Physical Picture

The importance of viscous mixing can be justified on purely business grounds. Consider the case of polymers. The world production (by volume) of plastics has surpassed that of metals, and new polymers with extraordinary properties are constantly being produced in laboratories around the world. Less than 2% of all new polymers, however, ever find a route to commercial application. There are two reasons for this low figure. The first is the inherent high cost of producing new materials. The second is that often new properties can be obtained by compounding, blending and alloying (all synonyms for mixing) existing polymers together with additives, to produce “tailored” materials with the desired properties. Mixing provides the best route to commercial competitiveness while optimizing properties-to-price ratio. Similar arguments can be made in the consumer products industry, where imparting the “right structure” is crucial to the value of the product (Villadsen, 1997).

Quenched, possibly metastable structures are ultimately responsible for the properties observed, so the key linkage is between *mixing* and *morphology*. Thus, for example, the properties of a polymer blend—e.g., permeability, mechanical properties—are a strong function of the mixing achieved, and this in turn depends strongly on the equipment used. Thin, ribbon-like anisotropic structures are produced in single screw extruders; fine drop dispersions in static mixers and twin screw extruders. Knowledge about the mixing process can be used to produce targeted properties (see, for example, Liu and Zumbrunnen, 1997).

Experiments reveal mechanisms at work. Figure 10 shows a 45/55 blend

of PS and HDPE; the processing temperature is such that the viscosities are nearly matched. Long ribbons of PS in the process of breakup by capillary instabilities, as well as coalesced regions, are apparent in this figure (Meijer *et al.*, 1988). In simple shear flow, the phenomena are somewhat different and pellets may be stretched into sheets that break by the formation and growth of holes (Sundaraj, Dori, and Macosko, 1995).

It may appear surprising that large length reductions—initial pellet sizes being on the order of a few millimeters, final drop scales on the order of microns—can be achieved in short residence times and relatively low shear rates. For example, in a typical extruder there are high-shear zones in which residence times (t_{res}) are short ($\dot{\gamma} \sim 100 \text{ s}^{-1}$, $t_{\text{res}} \sim 0.1 \text{ s}$), and low-shear zones with longer residence times ($\dot{\gamma} \sim 3 \text{ s}^{-1}$, $t_{\text{res}} \sim 10 \text{ s}$), with material elements visiting each zone several times (Janssen and Meijer, 1995). This leads to a strain of about 10 in high shear zones and 30 in low shear zones, which is considerably less than the length stretches shown in Fig. 10. The key to efficient mixing of immiscible liquids, as in the case of single fluids, lies in reorientations; six reorientations, with a stretch per reorientation of about 5, generate a stretch of 1.5×10^4 .

A precondition for stretching of initially spherical drops is that hydrodynamic stresses acting on the drop be large enough to overcome surface tension that tends to return the drop to a spherical shape; stretched drops eventually break by surface-tension-driven instabilities. Complex flow in mixers results also in collisions between dispersed phase drops and, eventually, coalescence if the film between the colliding drops breaks. The dynamic balance between breakup and coalescence, both driven by the flow, determines the distribution of drop sizes and morphology in the blend. Fundamental studies of single-drop breakup and coalescence of pairs of drops, mainly for Newtonian fluids, provide a basis for the analysis of the physical processes. The non-Newtonian rheology of blends and the effects of high loading of the dispersed phase (e.g., increase in effective viscosity and phase inversion) complicate the analysis, and much remains to be done at a basic level in this regard. Also, little will be said here about the mid-column in Fig. 1. The reader interested in this topic will find leads in the papers by Kao and Mason (1975) for cohesionless aggregates, and Ulbrecht *et al.* (1982), Stroeve and Varanasi (1984), Srinivasan and Stroeve (1986), and Varanasi *et al.* (1994) for the case of double emulsions.

2. Mixing: From Large to Small Scales

Mixing involves a reduction of length scales. Let us now consider a typical mixing process as it progresses from large to small scales, as illustrated in

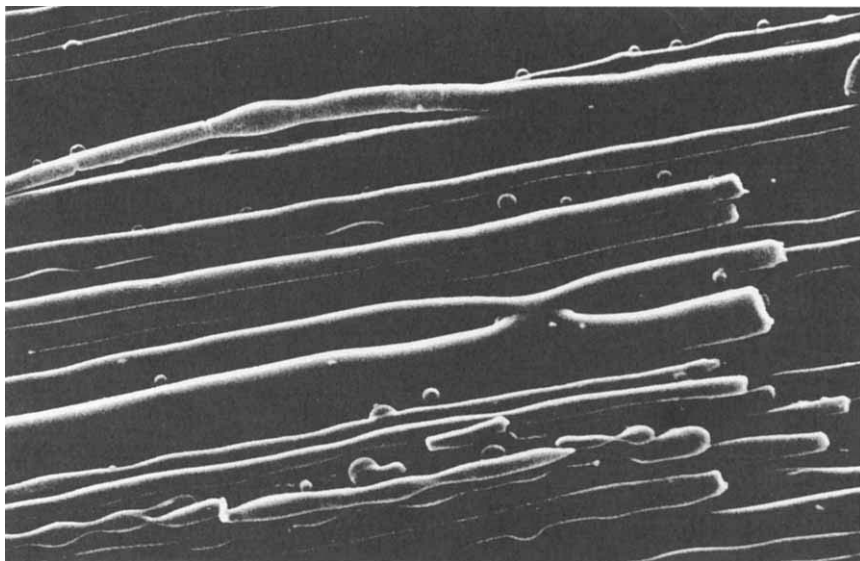


FIG. 10. Scanning electron micrograph of a fracture surface parallel to the direction of extrusion of an extrudate of a 45:55 PS-HDPE blend with a viscosity ratio $p \approx 1$. Fibrous PS is shown at different stages of breakup; the diameter of the largest fiber is about $1 \mu\text{m}$ (Meijer *et al.*, 1988).

Fig. 11. The initial condition corresponds to a large blob of the dispersed phase (d), suspended in the continuous phase (c). At the beginning of the mixing process, the capillary number, which is the ratio of the viscous forces to the interfacial forces, is large and interfacial tension is unimportant. A description of mixing essentially amounts to a description of the evolution of the interface between the two large masses of fluid: an initially designated material region of fluid (Fig. 11, top) stretches and folds throughout space. An exact description of mixing is thus given by the location of the interfaces as a function of space and time. This level of description is, however, rare because the velocity fields usually found in mixing processes are complex, and the deformation of the blobs is related in a complicated way to the velocity field. Moreover, relatively simple velocity fields can produce exponential area growth due to stretching and folding, and numerical tracking becomes impossible. Realistic problems can take years of computer time with megaflop machines (Franjione and Ottino, 1987).

The problem of following the interface for Newtonian fluids can be described by the Stokes equations,

$$\mu_i \nabla^2 \mathbf{v}_i = \nabla P_i, \quad \nabla \cdot \mathbf{v}_i = 0 \quad (i = c, d), \quad (11)$$

where c denotes the continuous phase and d denotes the dispersed phase. The boundary conditions at the interface come from a jump in the normal

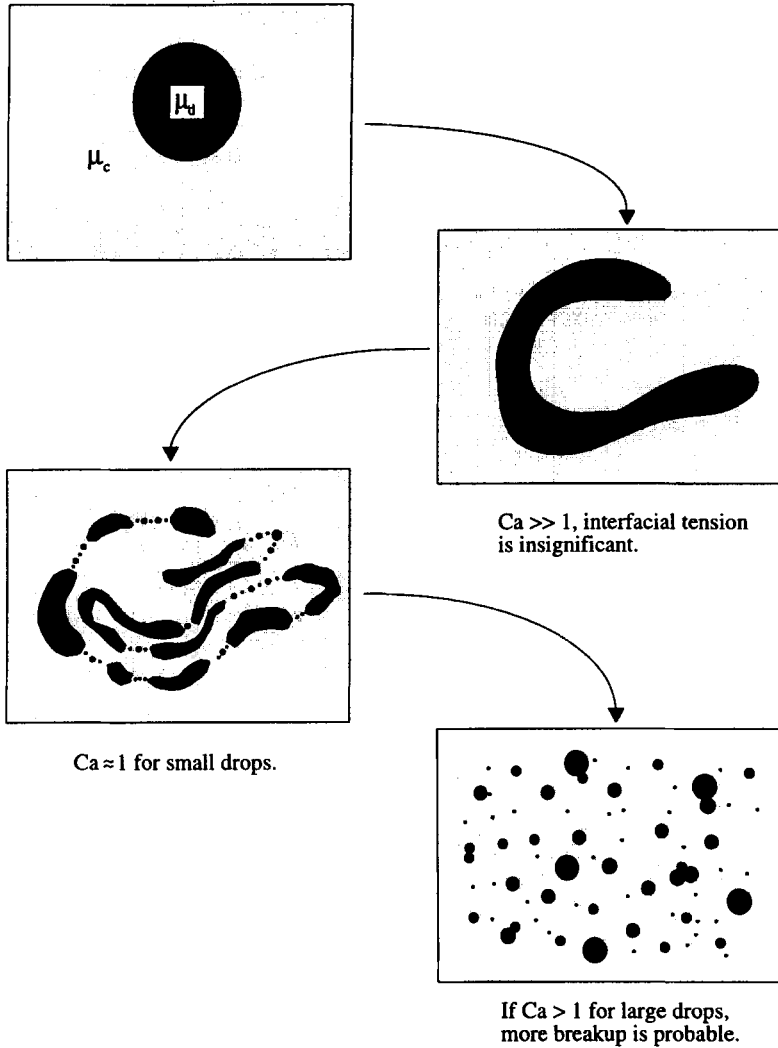


FIG. 11. Schematic view of the stages in the mixing of two immiscible viscous liquids. The large drop of the dispersed phase is stretched out and folded by the flow and breaks up into smaller droplets. Smaller drops may collide and coalesce to form larger drops.

stress due to the interfacial tension, σ , between the two fluids and the kinematic condition

$$\mathbf{n} \cdot (\mathbf{T}_c - \mathbf{T}_d) = \sigma \mathbf{n}(\nabla_s \cdot \mathbf{n}) \quad \text{for } \mathbf{x} = \mathbf{x}_s \quad (12)$$

$$\frac{d\mathbf{x}}{dt} = (\mathbf{v}_i \cdot \mathbf{n})\mathbf{n} \quad (i = c, d) \quad \text{for } \mathbf{x} = \mathbf{x}_s. \quad (13)$$

In addition, the velocity field is continuous across the interface

$$\mathbf{v}_c = \mathbf{v}_d, \quad (14)$$

and boundary conditions at the system boundaries and the initial condition must be specified. Points in both the dispersed and continuous phases are denoted by the position vector \mathbf{x} and points at the interface are given by \mathbf{x}_s . The stress tensors \mathbf{T}_c and \mathbf{T}_d are given by $\mathbf{T}_i = -P_i\mathbf{I} + 2\mu_i\mathbf{D}_i$, where $\mathbf{D}_i = [\nabla\mathbf{v}_i + (\nabla\mathbf{v}_i)^T]/2$. The mean curvature of the interface is given by $\nabla_s \cdot \mathbf{n}$, where the local normal \mathbf{n} is directed from the dispersed phase to the continuous phase and ∇_s denotes the surface gradient.

If the length scales associated with changes in velocity are normalized by ∇_v (characteristic length scale for Stokes flow), length scales associated with changes in curvature are normalized by δ_s (typical striation thickness) and velocities normalized by V (a characteristic velocity), then the normal stress condition becomes,

$$\mathbf{n} \cdot (\mathbf{T}'_c - p\mathbf{T}'_d) = \frac{1}{Ca} \mathbf{n}(\nabla'_s \cdot \mathbf{n}), \quad (15)$$

where p is the viscosity ratio, μ_d/μ_c , primed quantities denote dimensionless variables, and $Ca = \mu_c V \delta_s / (\delta_v \sigma)$ may be interpreted as the ratio of viscous forces, $\mu_c V / \delta_v$ (V/δ_v is the characteristic shear rate), to capillary forces, σ/δ_s . This ratio is the so-called *capillary number*. During the initial stages of mixing Ca is relatively large because of large striation thicknesses, δ_s , although interfacial tension effects may be noticeable in regions of high curvature, such as folds. However, as the mixing process proceeds, δ_s is reduced and interfacial tension starts to play a larger role. The coupling between the flow field and interfacial tension occurs at length scales of order $\sigma/\dot{\gamma}\mu$, where $\dot{\gamma} = V/\delta_v$ is a characteristic shear rate [i.e., $Ca = O(1)$].

Illustration: Initial stages of mixing. Bigg and Middleman (1974) and Chakravarthy and Ottino (1996) approached the problem depicted in Fig. 12 by solving the governing equations (11)–(14) using a modified finite difference technique. Using this method the evolution of the interface can be followed and the length stretch of the interface and striation thicknesses can be obtained. However, this technique eventually breaks down as the interface becomes highly convoluted. Numerical difficulties quickly arise because of the large number of points that must be used to follow the interface. Alternative methods for the numerical simulation of the early stages of mixing are presented by Chella and Viñals (1996) and Zumbrunnen *et al.* (e.g., Zhang and Zumbrunnen, 1996a,b) based on the spatial evolution of an *order parameter* (which is related to the mass fraction of the phases) due to convection and diffusion, together with fluid flow. The

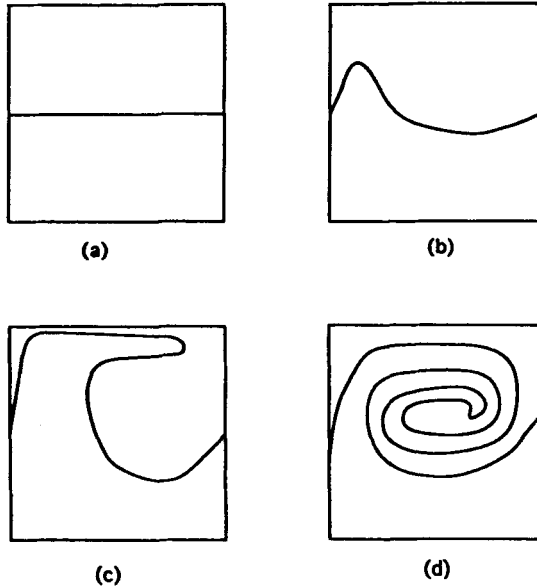


FIG. 12. Deformation of the interface between two immiscible viscous liquids in a steady cavity flow with increasing time of flow. The viscosity ratio is $p = 0.8$, and the upper fluid is of lower viscosity (Chakravarthy and Ottino, 1996).

interface between the phases is diffuse and is determined by the gradient of the order parameter. Interfacial tension forces are calculated from the order parameter field and are included in the fluid flow equations.

Illustration: Typical mixing in polymer processing. In order to illustrate the changing scales in mixing, consider a typical example in polymer processing where viscosities are on the order of $100 \text{ Pa} \cdot \text{s}$ and interfacial tension 0.005 N/m . Consider a typical screw with a diameter of 64 mm and a channel that can be approximated by the barrel wall moving over a cavity with dimensions 3 mm by 30 mm . If the screw rotates at 60 rpm , the relative speed of the upper wall to the screw is 0.2 m/s . A characteristic length scale for changes in velocity is around 3 mm and a typical initial value for δ_s is 1 mm . Using these typical values gives an initial capillary number of $Ca \sim 1300$, which clearly demonstrates that interfacial tension is unimportant in the initial stages of mixing. Interfacial tension stress does not become significant, $Ca = O(1)$, until the striation thickness is reduced to about 10^{-5} m ($10 \mu\text{m}$).

Illustration: Role of dispersed phases on flow structure. Dispersed fluid phases that have properties different from those of the continuous phase can disrupt the structure of chaotic and regular regions obtained for single

phase mixing. Zhang and Zumbrunnen (1996a) studied the patterns of mixing of a tracer in a time periodic cavity flow with and without a dispersed phase blob. The capillary number for the flow with the blob is small enough so that the blob does not deform significantly in the flow. The presence of the blob disturbs the flow in a random fashion when it is placed in the chaotic region, and thus eliminates islands by breaking KAM surfaces. From a macroscopic viewpoint, dispersed phases improve mixing. Put in another way, once some breakup has been achieved, further mixing becomes more efficient.

A. Breakup

1. Small Scales

As the mixing proceeds, the capillary number decreases. At $Ca = O(1)$, interfacial tension stresses become of the same order of magnitude as viscous stresses, and the extended thread breaks into many smaller drops. Large drops, corresponding to $Ca > 1$, may stretch and break again, while smaller drops begin to collide with each other and coalesce into larger drops, which may in turn break again.

To a first approximation, the velocity field with respect to a frame fixed on the drop's center of mass, denoted \mathbf{X} , and far away from it, denoted by the superscript ∞ , can be approximated by

$$\mathbf{v}^\infty = \mathbf{x} \cdot \mathbf{L} + \text{higher order terms}, \quad (16)$$

where $\mathbf{L} = \mathbf{L}(\mathbf{X}, t) = (\mathbf{D} + \Omega)$ is a function of the fluid mechanical path of the drop, and \mathbf{D} and Ω are defined as $\mathbf{D} \equiv [\nabla \mathbf{v}^\infty + (\nabla \mathbf{v}^\infty)^T]/2$, and $\Omega \equiv [\nabla \mathbf{v}^\infty - (\nabla \mathbf{v}^\infty)^T]/2$, respectively. The central point is to investigate the role of \mathbf{L} in the stretching and breakup of the drop.

As before, the problem is governed by the creeping flow equations and boundary conditions given earlier [Eqs. (11)–(14)]. The far field boundary condition in this case is

$$\mathbf{v} \rightarrow \mathbf{v}^\infty = \mathbf{x} \cdot \mathbf{L} \quad \text{as} \quad |\mathbf{x}| \rightarrow \infty. \quad (17)$$

The tensor \mathbf{L} defines the character of the flow. The capillary number for the drop deformation and breakup problem is

$$Ca = \frac{\mu_c \dot{\gamma} R}{\sigma}, \quad (18)$$

where R is the radius of the initially spherical drop, and $\dot{\gamma} = \sqrt{2\mathbf{D}:\mathbf{D}}$ is the shear rate.

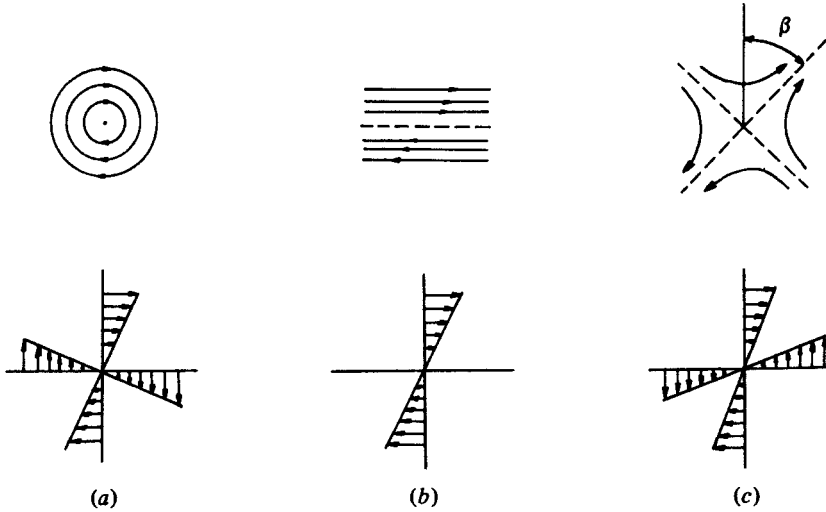


FIG. 13. Streamlines and velocity profiles for two-dimensional linear flows with varying vorticity. (a) $K = -1$: pure rotation, (b) $K = 0$: simple shear flow, (c) $K = 1$: hyperbolic extensional flow.

Illustration: Common flow types. Experimental studies of drop breakup have been mainly confined to linear, planar flows. All linear flows in 2D are encapsulated by the general velocity field equations

$$v_x = Gy, \quad v_y = KGx, \quad (19)$$

where K determines the vorticity of the flow and G is a measure of the shear rate. Planar extensional flow corresponds to $K = 1$ (zero vorticity) and simple shear flow corresponds to $K = 0$. Streamlines for the flows with different values of K are shown in Fig. 13. Uniaxial extensional flow is another common flow type encountered, and is defined by

$$v_z = \dot{\epsilon}z, \quad v_x = -\frac{1}{2}\dot{\epsilon}x, \quad v_y = -\frac{1}{2}\dot{\epsilon}y. \quad (20)$$

For comparison of the different flows, it is necessary to define a consistent shear rate for all the flows. A natural choice is

$$\dot{\gamma} = \sqrt{2\mathbf{D}:\mathbf{D}}. \quad (21)$$

This definition gives $\dot{\gamma} = G$ when applied to a simple shear flow (i.e., $K = 0$).

Flows may be classified as strong or weak (Giesekus, 1962; Tanner, 1976) based on their ability to stretch material elements after long times of stretching, and this characteristic can be inferred from the velocity field.

Flows that produce an exponential increase in length with time are referred to as strong flows, and this behavior results if the symmetric part of the velocity gradient tensor (\mathbf{D}) has at least one positive eigenvalue. For example, 2D flows with $K > 0$ and uniaxial extensional flow are strong flows; simple shear flow ($K = 0$) and all 2D flows with $K < 0$ are weak flows.

2. Critical Capillary Number

The degree of deformation and whether or not a drop breaks is completely determined by Ca , p , the flow type, and the initial drop shape and orientation. If Ca is less than a critical value, Ca_{crit} , the initially spherical drop is deformed into a stable ellipsoid. If Ca is greater than Ca_{crit} , a stable drop shape does not exist, so the drop will be continually stretched until it breaks. For linear, steady flows, the critical capillary number, Ca_{crit} , is a function of the flow type and p . Figure 14 shows the dependence of Ca_{crit} on p for flows between elongational flow and simple shear flow. Bentley and Leal (1986) have shown that for flows with vorticity between simple shear flow and planar elongational flow, Ca_{crit} lies between the two curves in Fig. 14. The important points to be noted from Fig. 14 are these:

- For $p > 4$, stretching of a drop into a thread is impossible for shear flow.
- It is easiest to stretch drops when $p \approx 1$.
- Elongational flow is more effective than simple shear flow for a given viscosity ratio.

It is also important to note Ca_{crit} says nothing about the drop sizes produced upon breakup: The value of Ca_{crit} only gives the *maximum* drop size that can survive in a given flow in the absence of coalescence. This result may appear to suggest that the most effective dispersion—leading to the finest drop sizes—occurs when viscosities are nearly matched. As we shall see later on, this perception turns out to be incorrect. Nevertheless, an understanding of Fig. 14 constitutes the minimum level of knowledge needed to rationalize dispersion processes in complex flows.

3. Affine Deformation

For $Ca > Ca_{crit}$ a drop continually stretches until it breaks. If $Ca > \kappa Ca_{crit}$, where κ is about 2 for simple shear flow and 5 for elongational flow (Janssen, 1993), the drop undergoes *affine deformation*, i.e., the drop acts as a material element, and it is stretched into an extended cylindrical thread with length L and radius R according to

$$(\text{Simple shear flow}) \quad \frac{L}{R_0} \sim \dot{\gamma} t, \quad \frac{R}{R_0} \sim (\dot{\gamma} t)^{-1/2} \quad (22)$$

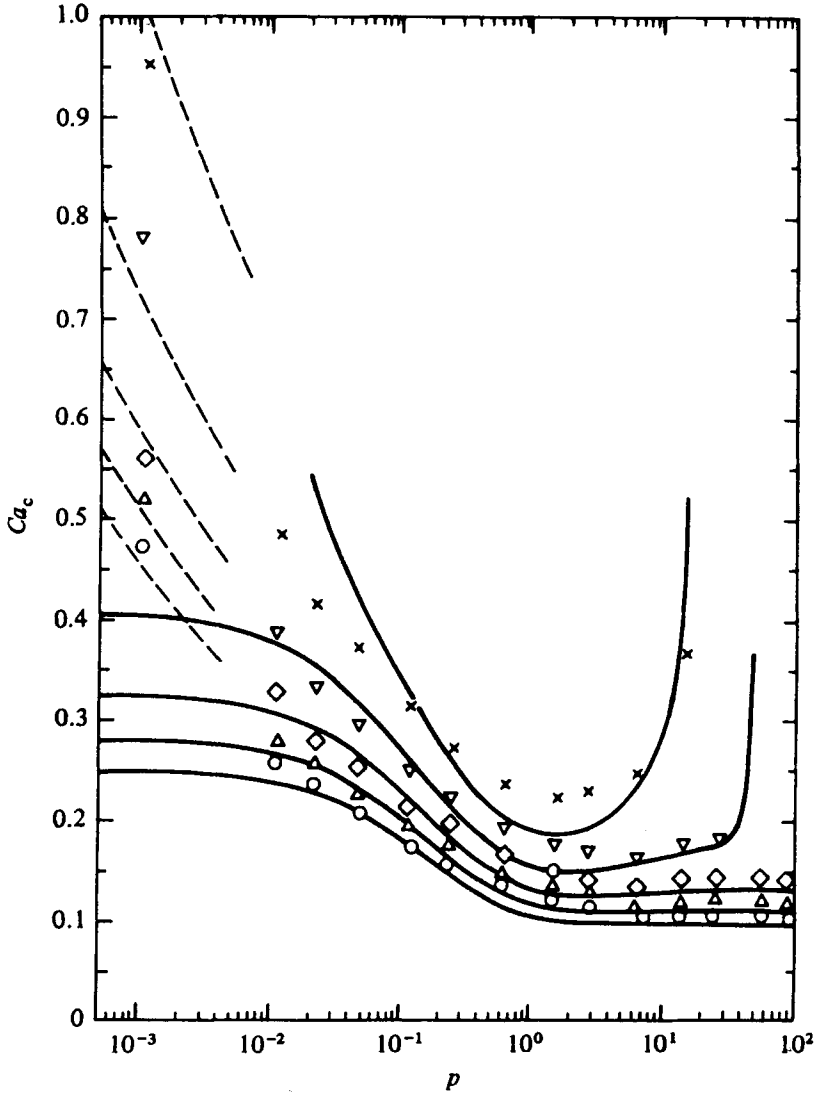


FIG. 14. Critical capillary number (Ca_{crit}) as a function of the viscosity ratio (p) for two-dimensional linear flows with varying vorticity (Bentley and Leal, 1986).

$$(\text{Extensional flow}) \quad \frac{L}{R_0} \sim \exp(\dot{\gamma}t), \quad \frac{R}{R_0} \sim \exp(-\dot{\gamma}t/2). \quad (23)$$

These expressions approach an exact equality as $\dot{\gamma}t$ becomes large. Figure 15 illustrates the point at which a highly stretched drop can be treated as

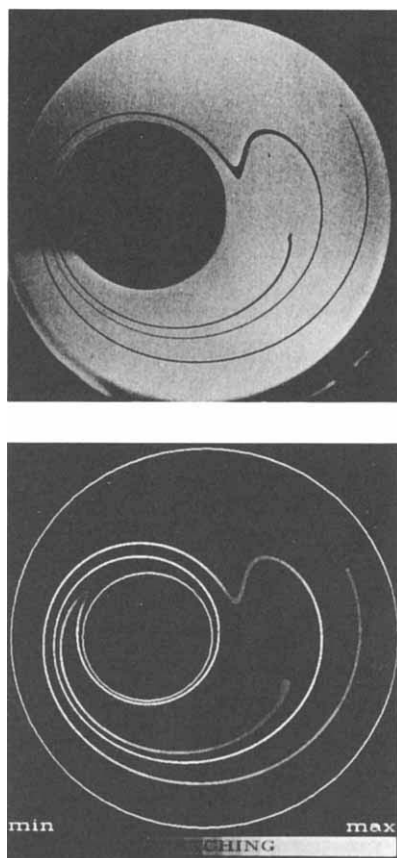


FIG. 15. Affine stretching of a filament in the journal bearing flow. Experiments (top) agree well with computations (bottom) carried out assuming that the filament deforms as the suspending fluid (*i.e.*, affine deformation) (Tjahjadi and Ottino, 1991).

a material element (*i.e.*, it deforms affinely). This figure shows computations and experiments done by Tjahjadi and Ottino (1991) where a drop of fluid is dispersed in a second fluid in the journal bearing flow (Swanson and Ottino 1990, Chaiken et al. 1986). In the computations, the drop was treated as a material element, and as can be seen, the agreement between the computations and experiments is quite good. A necessary condition for stretching is that Ca must surpass Ca_{crit} as illustrated in Fig. 16: One drop does not reach the critical Ca and remains underformed; the other breaks into thousands of drops.

Illustration: Importance of reorientations. The stretching rate of long filaments in shear flow can be improved from being linear to exponential

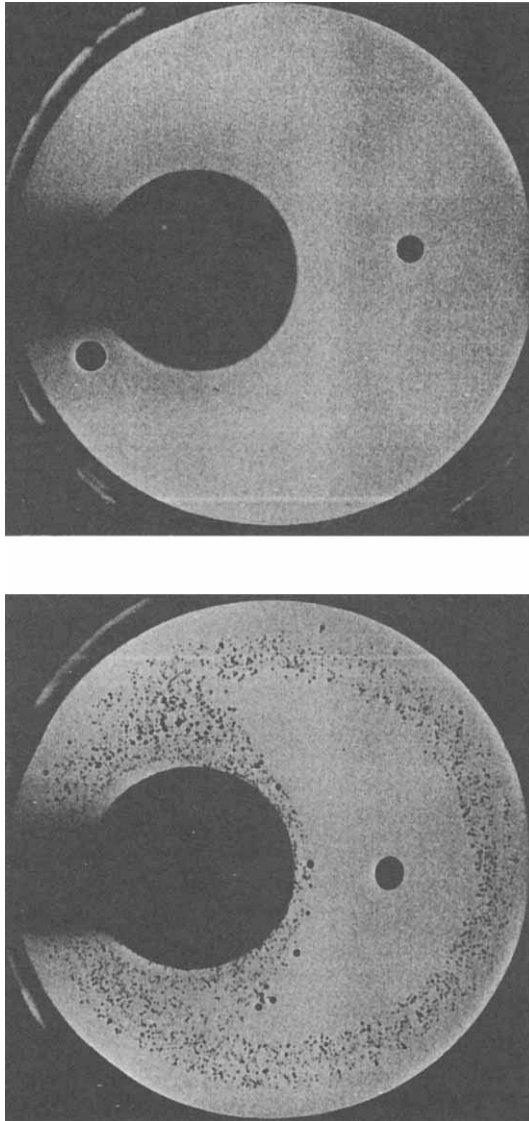


FIG. 16. Drop breakup in the journal bearing flow. The drop initially in the chaotic region of the flow deforms into a thin filament that breaks to produce a fine dispersion of droplets. The drop initially in the regular region of the flow (island) remains undeformed (Tjahjadi and Ottino, 1991).

by incorporating periodic reorientations in the flow, as seen earlier for material lines. The basic idea is instead of using one long shear flow to divide the flow into shorter sections with reorientations between each section. When this is done the amount of stretching is given by (Erwin, 1978)

$$\frac{L}{R_0} \sim \left(\frac{\gamma_{\text{tot}}}{n+1} \right)^{(n+1)}, \quad \frac{R}{R_0} \sim \left(\frac{\gamma_{\text{tot}}}{n+1} \right)^{-(n+1)/2}, \quad (24)$$

where γ_{tot} is the *total* shear in the mixer. The improvement with reorientations is illustrated in Fig. 17, where R_0/R is plotted vs time for the cases

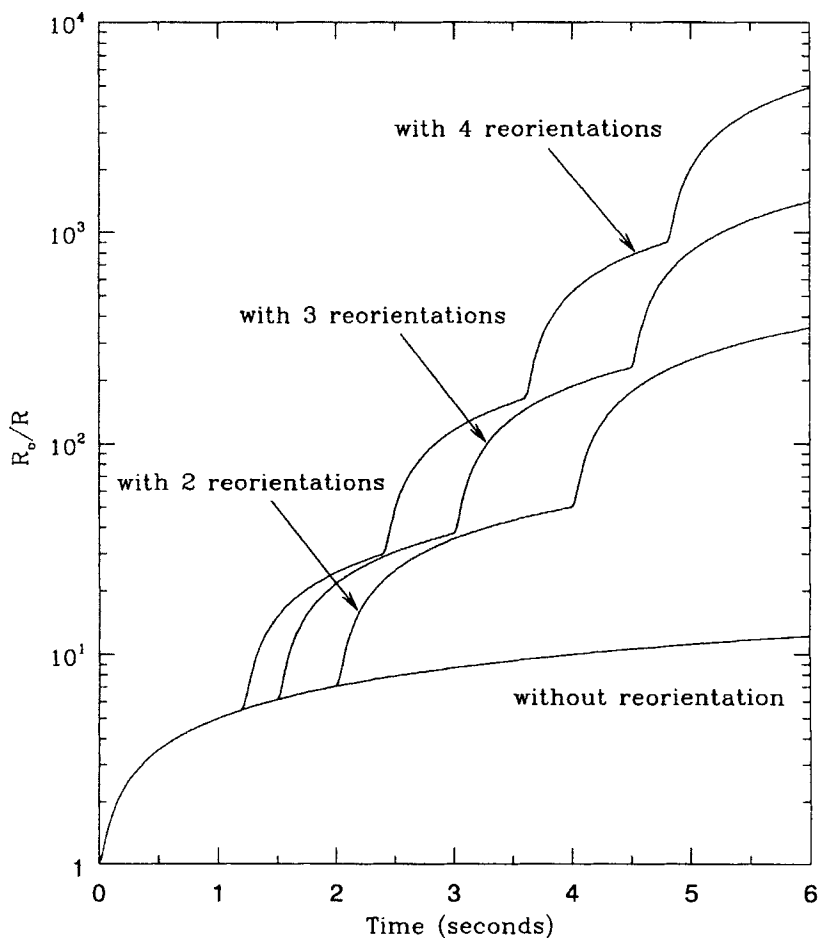


FIG. 17. Stretching of a filament in a simple shear flow with random reorientation at different time intervals. The length stretch is shown vs time for $\dot{\gamma} = 50 \text{ s}^{-1}$.

of 0, 2, 3, and 4 reorientations. After a total shear of 300 ($\dot{\gamma} = 50 \text{ s}^{-1}$ for 6 s), the length scale is reduced from 10^{-3} m to $6 \times 10^{-5} \text{ m}$. If a reorientation is added after every 2 s, the length scale is reduced from 10^{-3} to 10^{-6} m (a typical length scale reduction in polymer processing). To get this same reduction without reorientation would take approximately 5.5 h. Four or five reorientations are typically enough.

Although the preceding equations illustrate clearly the role of reorientation in stretching, it should be noted that the equations are valid only when the strain per period is large ($\gamma_{\text{tot}}/(n+1) > 1$). The length of the filament after n reorientations is in fact given by

$$\frac{L}{R_0} = \prod_{i=1}^{n+1} \left\{ \left(\cos \theta_i + \frac{\gamma_{\text{tot}}}{n+1} \right)^2 + \sin^2 \theta_i \right\}^{1/2}, \quad (25)$$

where θ_i is the angle between the filament and the streamlines at the start of the i th period (Khakhar and Ottino, 1986a). For large $\gamma_{\text{tot}}/(n+1)$ Eq. (25) reduces to Eq. (24). However, when this condition is not satisfied, actual strains may be less than or greater than unity depending on the orientation of the material element (θ_i). Consequently, Eq. (24) would not give an accurate estimate of the optimum number of reorientations when the length stretch is maximum.

Illustration: Stretching of low-viscosity-ratio elongated drops. For the case $p \ll 1$ and $\text{Ca}/\text{Ca}_{\text{crit}} = O(1)$, the dynamics of a nearly axisymmetric drop with pointed ends, characterized by an orientation \mathbf{m} ($|\mathbf{m}| = 1$) and a length $L(t)$, is given by (Khakhar and Ottino, 1986b,c)

$$\frac{1}{L} \frac{dL}{dt} = \mathbf{D} : \mathbf{m}\mathbf{m} - \left(\frac{\sigma}{2(5)^{1/2} \mu_c R} \right) \left(\frac{(L(t)/R)^{1/2}}{1 + 0.8p(L(t)/R)^3} \right) \quad (26a)$$

$$\frac{d\mathbf{m}}{dt} = (G\mathbf{D} + \Omega)^T \cdot \mathbf{m} - (G\mathbf{D} : \mathbf{m}\mathbf{m})\mathbf{m}, \quad (26b)$$

where $G(t) = (1 + 12.5R^3/L(t)^3)/(1 - 2.5R^3/L(t)^3)$. The underlined term in the first equation acts as a resistance to the deformation [contrast Eq. (26a) with Eq. (4) for stretching of a material element]. A very long drop, $[L(t)/a] \rightarrow \infty$, $G \rightarrow 1$, rotates and stretches as a passive element since the resistance to stretching becomes negligible. Note also that since $G > 1$ the droplet "feels" a flow that is slightly more extensional than the actual flow. The preceding equation is a special case of the linear vector model (Olbricht *et al.*, 1982), which describes the dynamics of deformation of an arbitrary microstructure that is specified by its length and orientation. We shall show later in this paper that the fragmentation and separation of agglomerates is also described by an equation very similar to the preceding equation.

In the context of the preceding model, a drop is said to break when it undergoes infinite extension and surface tension forces are unable to balance the viscous stresses. Consider breakup in flows with $\mathbf{D}:\mathbf{mm}$ constant in time (for example, an axisymmetric extensional flow with the drop axis initially coincident with the maximum direction of stretching). Rearranging Eq. (26) and defining a characteristic length $R/p^{1/3}$, we obtain the condition, for a drop in equilibrium,

$$\frac{\mathbf{D}:\mathbf{mm}}{(\mathbf{D}:\mathbf{D})^{1/2}} = e_\lambda = \left(\frac{1}{2(5)^{1/2}E} \right) \left(\frac{L_s^{1/2}}{1 + 0.8L_s^3} \right), \quad (27)$$

where L_s denotes the steady-state length and $E = p^{1/6}\text{Ca}$. A graphical interpretation of the roots L_s is given in Fig. 18. The horizontal line represents the asymptotic value of the efficiency (i.e., corresponding to $d\mathbf{m}/dt = 0$), which in three dimensions is $(2/3)^{1/2}$, and the value of the resistance is a function of the drop length for various values of the dimensionless strain rate E . For $E < E_c$ there are two steady states: one stable and the other unstable. For $E > E_c$ there are no steady states and the drop extends indefinitely.

4. Breakup Modes

Once a drop is subjected to a flow for which $\text{Ca} > \text{Ca}_{\text{crit}}$, it stretches and breaks depending on the degree of deformation, the viscosity ratio

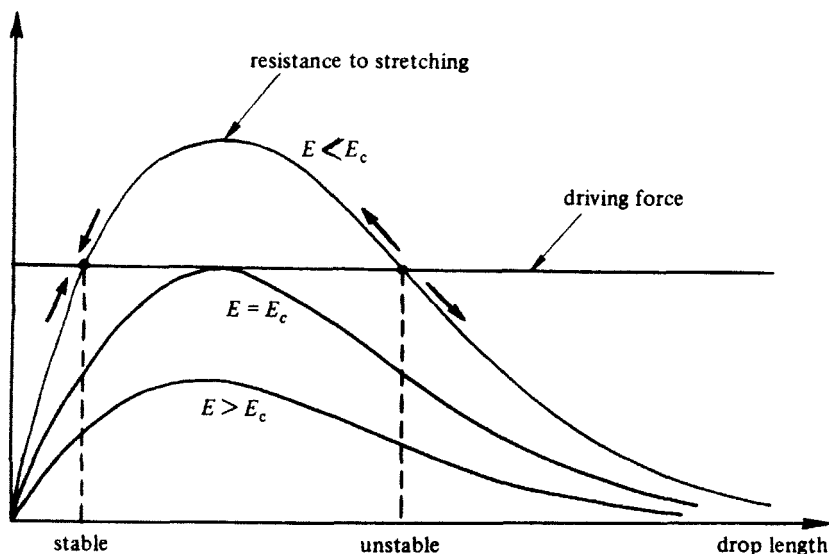


FIG. 18. Graphical interpretation of the criterion for breakup of pointed drops in an extensional flow (Khakhar and Ottino, 1986c).

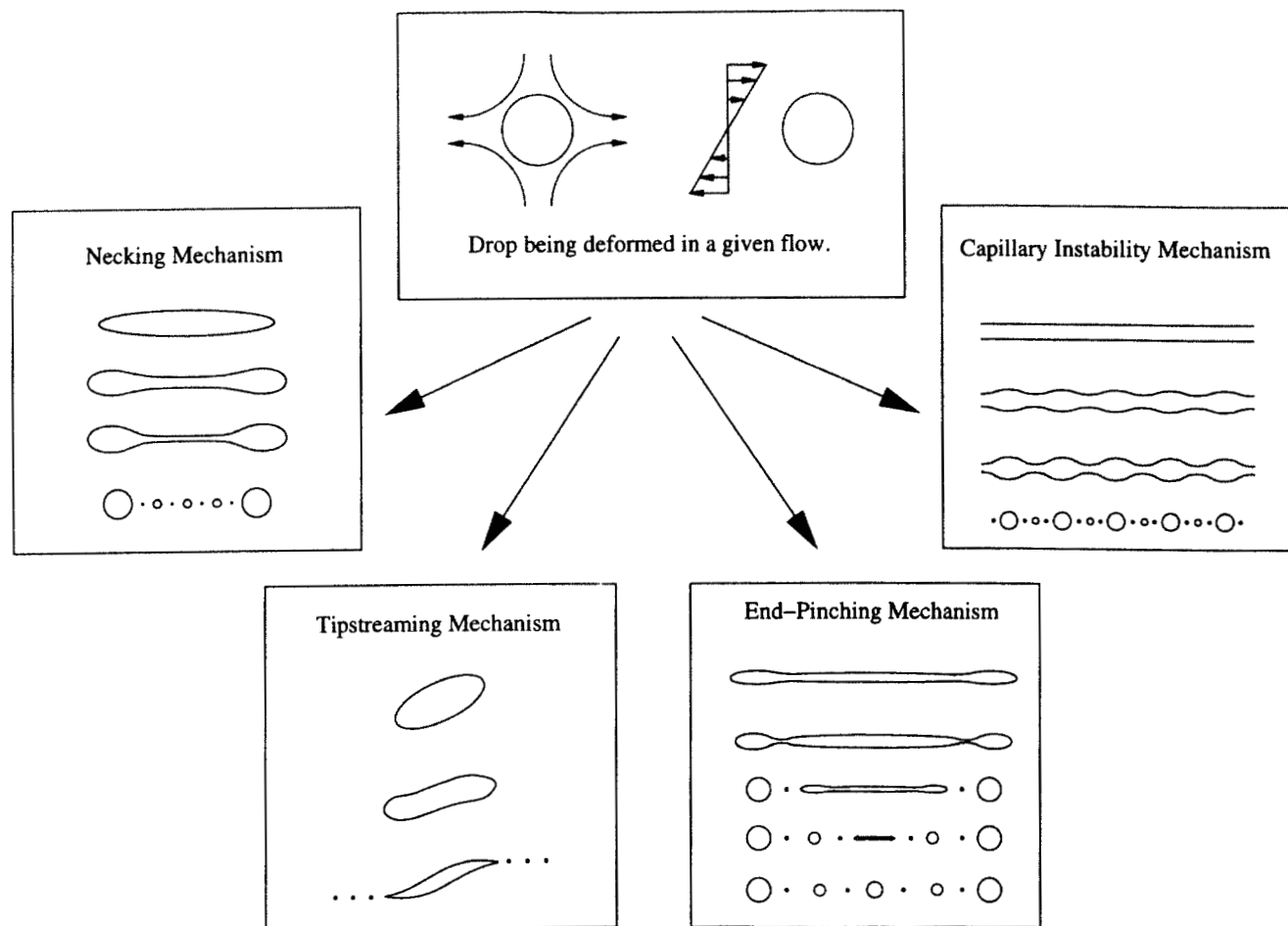
and the flow type (see, for example, Fig. 16). When a drop breaks, it does so by one of the four mechanisms illustrated in Fig. 19 (Stone, 1994). These four mechanisms will be briefly discussed here. For more details, see reviews by Eggers (1997), Stone (1994), Rallison (1984), and Acrivos (1983).

Moderately extended drops ($L/R_0 \lesssim 15$, where R_0 is the radius of a spherical drop of the same volume) break by a *necking* mechanism (Rumscheidt and Mason, 1961). In this type of breakup, the two ends of the drop form bulbous ends and a neck develops between them. The neck continuously thins until it breaks, leaving behind a few smaller drops between two large drops formed from the bulbous ends. This necking mechanism generally occurs during a sustained flow where Ca is relatively close to Ca_{crit} . Little has appeared in the literature on the number and size of drops formed upon breakage by necking. One general observation is that the number of drops produced is less than 10 (Grace, 1982).

The necking mechanism has also been investigated using theoretical and numerical techniques. The theoretical approach, based on small deformation analysis (Barthès-Biesel and Acrivos, 1973) for the case of low Ca or high p shows the formation of lobes on the drop for $Ca > Ca_{crit}$. Numerical techniques (Rallison, 1981) for $p = 1$ give similar results. The general conclusion is confirmation of the experimentally determined curve for Ca_{crit} ; the drops in this case may break up rather than extend indefinitely.

Tipstreaming, in which small drops break off from the tips of moderately extended, pointed drops, is another mechanism for drop breakup, though not of much significance to the dispersion process. Tipstreaming is generally attributed to gradients in interfacial tension along the surface of the drop (de Bruijn, 1993), but the exact conditions at which tipstreaming occurs are not well known.

Relaxation of a moderately extended drop under the influence of surface tension forces when the shear rate is low may lead to breakup by the *end-pinching* mechanism (Stone *et al.*, 1986; Stone and Leal, 1989). For example, this type of breakup occurs if a drop is deformed past a critical elongation ratio, $(L/R_0)_{crit}$, at Ca close to Ca_{crit} and then the flow is stopped abruptly. The critical elongation ratio necessary for breakup once the flow is stopped is dependent on p with a minimum deformation around $p \approx 0.2-2$, but is nearly independent of flow type (Stone *et al.*, 1986). Smaller-than-critical elongations result in relaxation of the drop to a spherical shape. The relaxation of the drop in this case is driven by the surface tension stress generated by the ends of the extended drop. The high viscosities and low surface tensions encountered in polymer processing lead to high relaxation times for the drop; hence, breakup by end pinching may not occur to any significant effect in such systems. However, this mechanism would be the dominant mode of breakup in the emulsification of low-viscosity liquids.



The three breakup mechanisms previously discussed occur for moderately extended drops; however, when $Ca \geq \kappa Ca_{\text{crit}}$, the drop is stretched affinely and becomes a highly extended thread. The extended thread is unstable to minor disturbances and will eventually disintegrate into a number of large drops with satellite drops between the larger mother drops (see Fig. 19). The driving force behind this process is provided by interfacial tension minimizing the surface area: All sinusoidal disturbances cause a decrease in surface area. However, only disturbances with a wavelength greater than the filament perimeter produce pressure variations along the filament (due to the normal stress boundary condition) that magnify the disturbance and lead to breakup. The analysis for how these disturbances grow depends on whether the thread is at rest or being stretched. Each of these two cases is considered next.

For the case of a thread at rest, the initial growth of a disturbance can be relatively well characterized by linear stability theory. In the initial stages, the deformation of the thread follows the growth of the fastest growing disturbance (Tomotika, 1935). Eventually the interfacial tension driven flow becomes nonlinear, leading to the formation of the smaller satellite drops (Tjahjadi *et al.*, 1992).

Although linear stability theory does not predict the correct number and size of drops, the time for breakup is reasonably estimated by the time for the amplitude of the fastest growing disturbance to become equal to the average radius (Tomotika, 1935):

$$t_{\text{break}} \approx \frac{2\mu_c R_o}{\sigma \Omega_m} \ln \left(\frac{(2/3)^{1/2} R_o}{\alpha_o} \right). \quad (28)$$

The nondimensional growth rate, Ω_m , is a unique function of the wave-number and p . Kuhn (1953) estimated the magnitude of the initial amplitude of the disturbances (α_o) to be 10^{-9} m based on thermal fluctuations. Mikami *et al.* (1975) gave a higher estimate of 10^{-8} to 10^{-7} m.

For the case of a thread breaking during flow, the analysis is complicated because the wavelength of each disturbance is stretched along with the thread. This causes the dominant disturbance to change over time, which results in a delay of actual breakup. Tomotika (1936) and Mikami *et al.* (1975) analyzed breakup of threads during flow for 3D extensional flow, and Khakhar and Ottino (1987) extended the analysis to general linear flows. Each of these works uses a perturbation analysis to describe an equation for the evolution of a disturbance.

In general, disturbances will damp, then grow, and then damp again as the wavelength of a particular disturbance increases due to stretching of the thread. However, disturbances cannot damp below the initial amplitude,

α_o , caused by thermal fluctuations. Hence, the initial damping stage is omitted and once the thread reaches a critical radius, R_{crit} , the disturbance starts to grow from α_o . If the amplitude of a disturbance reaches the average size of the thread, disintegration into drops occurs. Disturbances grow and damp at different rates depending on their initial wavenumber χ_o . The disturbance that reaches the amplitude of the average thread radius first is the dominant disturbance and causes breakup.

Mikami *et al.* (1975) and Khakhar and Ottino (1987) presented a numerical scheme for determining t_{grow} , which is the time for the dominant disturbance to grow from α_o to an amplitude equal to the average thread radius. The total breakup time, t_{break} , is the sum of t_{grow} and t_{crit} , where t_{crit} is the time to reach R_{crit} from R_o . The value of R_{crit} is also obtained from the numerical scheme for calculating t_{grow} . Tjahjadi and Ottino (1991) used this numerical scheme and fitted the results to the expression

$$R_{\text{crit}} \approx (37.8 \pm 3.8)10^{-4}e^{-0.89}p^{-0.44}\left(\frac{\sigma}{\mu_c G}\right)^\chi, \quad (29)$$

where $0.84 < \chi < 0.92$ for $10^{-3} \leq p \leq 10^2$ and R_{crit} is in cm. Janssen and Meijer (1993) took the approach of Tjahjadi and Ottino (1991) one step further and reduced all the results to a graphical representation of R_{drops} , R_{crit} , and t_{grow} that only depends on the dimensionless parameters p and $\mu_c \epsilon \alpha_o / \sigma$. The Illustration following this section indicates how to calculate t_{break} using these graphs.

Although the area of breakup can be divided into four distinct categories—necking, tipstreaming, end-pinching, and capillary instabilities—more than one mechanism may be present in a given flow. Stone *et al.* (1986) and Stone and Leal (1989) demonstrated that if a drop is stretched enough, both end-pinching and capillary instabilities will be present. The end-pinching mechanism dominates the breakup close to the ends and the capillary instabilities dominate the breakup of the drop toward the middle. An examination of the pictures of Tjahjadi and Ottino (1991) shows the presence of three breakup mechanisms, necking, end-pinching, and capillary instabilities, on different portions of the same extended thread; however, capillary instabilities dominate the breakup.

Illustration: Breakup time for threads during flow. Consider a thread being deformed in a 2D extensional flow, with the following material and process parameters:

$$\begin{aligned} \dot{\epsilon} &= 30 \text{ s}^{-1}, & \sigma &= 5 \times 10^{-3} \text{ N/m} \\ \mu_c &= 100 \text{ Pa} \cdot \text{s}, & L_o &= 1 \times 10^{-2} \text{ m} \\ \mu_d &= 100 \text{ Pa} \cdot \text{s}, & R_o &= 1 \times 10^{-5} \text{ m}. \end{aligned}$$

Janssen and Meijer (1993) have shown the calculation of the time for breakup of a thread during flow can be reduced to the graphs in Fig. 20, which only depend on the viscosity ratio, $p = 1$, and the parameter $\mu_c \dot{\epsilon} \alpha_o / \sigma = 6 \times 10^{-4}$ using $\alpha_o = 1 \times 10^{-9} \text{m}$ (Kuhn, 1953). Using these two parameters and Fig. 20, the following values are obtained:

$$R_{\text{crit}}/\alpha_o = 50, \quad R_{\text{drops}}/\alpha_o = 50, \quad e_{\text{f}}^* t_{\text{grow}} = 1.5.$$

Here, $e_{\text{f}} = \sqrt{2\dot{\epsilon}}/\dot{\gamma}$ and $t_{\text{grow}}^* = t_{\text{grow}} \dot{\gamma}$. R_{crit} is the radius of the thread at which the critical disturbance begins to grow, R_{drops} is the size of the drops produced once the thread breaks, and t_{grow} is the time for the disturbance to grow from its initial amplitude to half the average radius at which breakup occurs. For $\alpha_o = 1 \times 10^{-9} \text{m}$, we obtain $R_{\text{crit}} = 5 \times 10^{-8} \text{m}$, $R_{\text{drops}} = 5 \times 10^{-8} \text{m}$, and $t_{\text{grow}} = 0.04 \text{s}$. The time to reach R_{crit} , t_{crit} , is found from the equation for stretching in a 2D exponential flow:

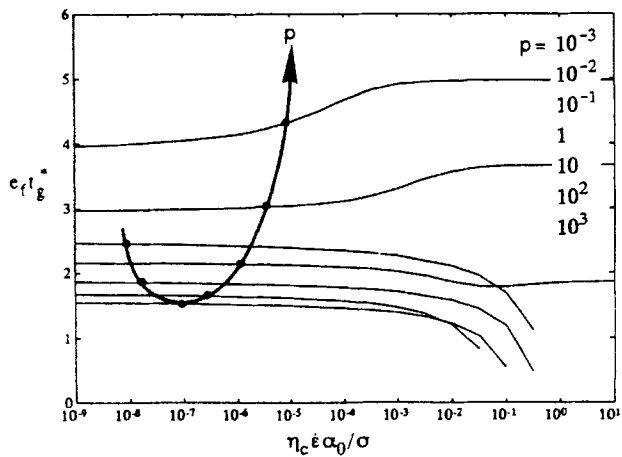
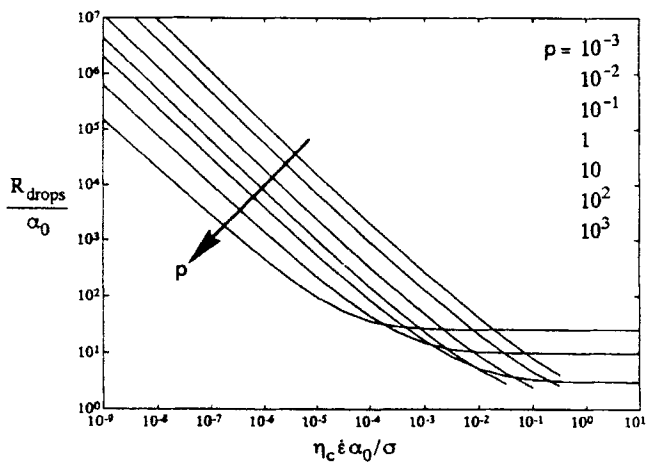
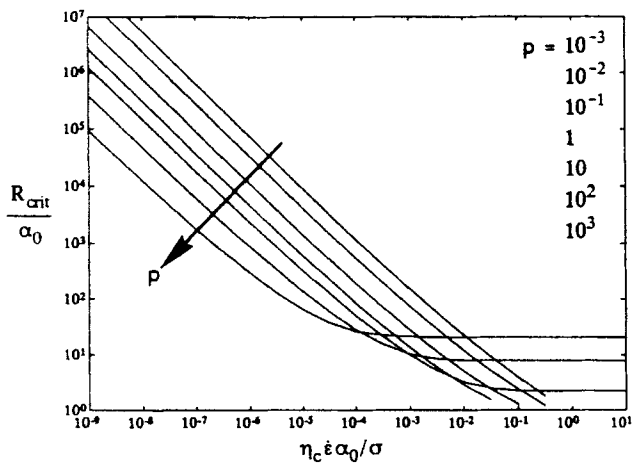
$$\frac{R_{\text{crit}}}{R_o} = \exp(-\dot{\epsilon} t) \rightarrow t_{\text{crit}} = 0.18 \text{ s}$$

$$t_{\text{break}} = t_{\text{crit}} + t_{\text{grow}} = 0.22 \text{ s}.$$

Illustration: Satellite formation in capillary breakup. The distribution of drops produced upon disintegration of a thread at rest is a unique function of the viscosity ratio. Tjahjadi *et al.* (1992) showed through inspection of experiments and numerical simulations that up to 19 satellite drops between the two larger mother drops could be formed. The number of satellite drops decreased as the viscosity ratio was increased. In low-viscosity systems [$p < O(0.1)$] the breakup mechanism is self-repeating: Every pinch-off results in the formation of a rounded surface and a conical one; the conical surface then becomes bulbous and a neck forms near the end, which again pinches off and the process repeats (Fig. 21). There is excellent agreement between numerical simulations and the experimental results (Fig. 21).

Illustration: Comparison between necking and capillary breakup. Consider drops of different sizes in a mixture exposed to a 2D extensional flow. The mode of breakup depends on the drop sizes. Large drops ($R \gg Ca_{\text{crit}} \sigma / \mu_c \dot{\gamma}$) are stretched into long threads by the flow and undergo capillary breakup, while smaller drops ($R \approx Ca_{\text{crit}} \sigma / \mu_c \dot{\gamma}$) experience breakup by necking. As a limit case, we consider necking to result in binary breakup, i.e., two daughter droplets and no satellite droplets are produced on breakup. The drop size of the daughter droplets is then

$$R \approx \frac{Ca_{\text{crit}} \sigma}{\mu_c \dot{\gamma}} 2^{-1/3}. \quad (30)$$



The radius of drops produced by capillary breakup is independent of the initial drop size, and is determined essentially by the viscosity ratio. Figure 22 shows a comparison of the drop size produced on breakup by the two different mechanisms (Janssen and Meijer, 1993). The size of the daughter drops produced by capillary breakup is significantly smaller than that for binary breakup for the case of high viscosity ratios. However, in practical situations in which coalescence and breakup occur during mixing, a range of drop sizes would exist, and thus the binary breakup radius gives an upper limit for the drop size.

Illustration: Drop size distributions produced by chaotic flows. Affinely deformed drops generate long filaments with a stretching distribution based on the log-normal distribution. The amount of stretching (λ) determines the radius of the filament locally as

$$R \sim \frac{1}{\lambda^{1/2}}. \quad (31)$$

Upon breakup, the filament breaks into a set of *primary* or mother drops whose sizes are, to a first approximation, proportional to R . The size of drops produced when the filament breaks can then be obtained from the distribution of R . Each mother drop produced upon breakup carries a distribution of satellites of diminishing size; for example, each mother drop of radius r has associated with it one large satellite of radius $r^{(1)}$, two smaller satellites of radius $r^{(2)}$, four satellites of radius $r^{(3)}$, and so on. For breakup at rest, the distribution of smaller drops is a unique function of the viscosity ratio.

If we assume that drops break only once, the drop-size distribution can be predicted based on the log-normal stretching distributions typical of mixing flows. Assuming a mean stretch of 10^4 gives a range of stretching from 1 to 10^{10} (Muzzio *et al.*, 1991a). Therefore, the corresponding distribution of mother drops is log-normal with a range from R_0 to $10^{-5}R_0$, where R_0 is the radius of the initial drop. The distribution for each satellite drop will be the same as that of the mother drop, except the position of the distribution will be shifted by a factor of r/r' and the amplitude multiplied by the number of satellite drops per mother drop. When all of the individual

FIG. 20. Radius of drops produced on capillary breakup in hyperbolic extensional flow (R_{drops}), radius of the thread at which the disturbance that causes breakup begins to grow (R_{crit}), and the time for growth of the disturbance (t_{grow}) for different values of the dimensionless parameters p and $\mu_c \dot{\epsilon} \alpha_0 / \sigma$. The time for capillary breakup of the extending thread (t_{break}) can be obtained from these graphs (see Illustration for sample calculations) (Janssen and Meijer, 1993).

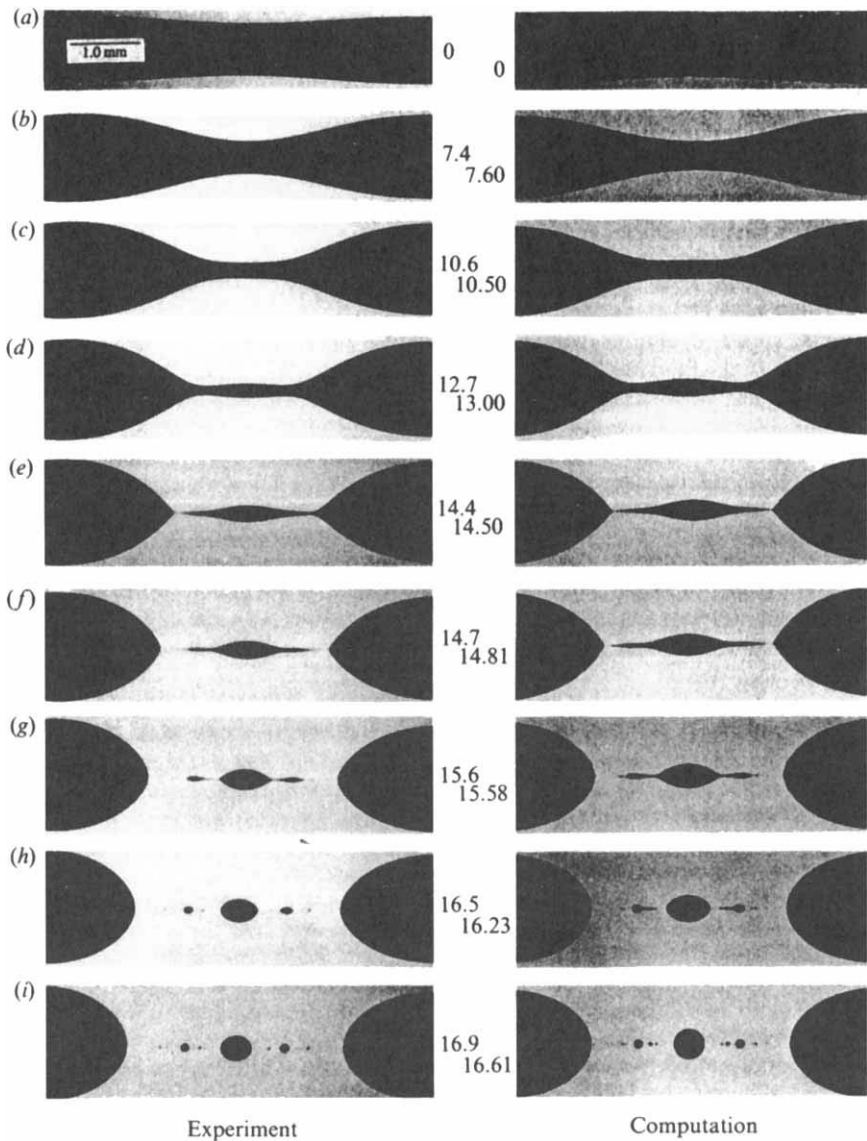


FIG. 21. Formation of satellite drops during the breakup of a filament at rest. A comparison between computations and experimental results is shown (Tjahjadi, Stone, and Ottino, 1992). Numbers refer to dimensionless times with $t = 0$ corresponding to Fig (a).

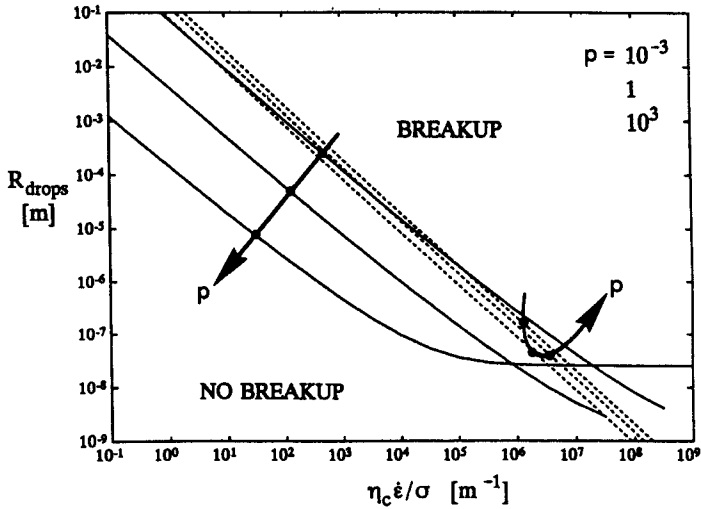


FIG. 22. Radius of drops produced by capillary breakup (solid lines) and binary breakup (dotted lines) in a hyperbolic extensional flow for different viscosity ratios (p) and scaled shear rate ($\mu_c \dot{\gamma} / \sigma$) (Janssen and Meijer, 1993). The initial amplitude of the surface disturbances is $\alpha_0 = 10^{-9}$ m. Note that significantly smaller drops are produced by capillary breakup for high viscosity ratios.

distributions are added, to give the overall drop distribution, a log-normal distribution is approached, as illustrated in Fig. 23.

The preceding example, as well as the repetitive nature of stretching and breakup, suggests that the experimentally determined equilibrium drop size distribution $f(V, p)$ might be self-similar [$f(V, p)dV$ is the number of drops with sizes between V and $V + dV$]. Figure 24 shows the distribution of drops obtained experimentally in the journal bearing flow resulting from repeated stretching and breakup. Figure 25 shows that rescaled experimental drop-size distributions $V^2 f(V, p)$ vs $V/\langle V \rangle$, where $\langle V \rangle$ is the arithmetic mean of volume sizes, collapses all data into a single curve. (Muzzio et al. 1991b).

Illustration: Effect of viscosity ratio on drop size distributions.

Experiments show that the equilibrium size distributions corresponding to high viscosity ratio drops are more nonuniform than those corresponding to low viscosity ratios, and that, in general, the mean drop size decreases as the viscosity ratio p increases (Tjahjadi and Ottino, 1991). The experiments pertain to the case of low number densities of drops when coalescence is negligible. There seem to be two distinct mechanisms: one-time breakup and repeated breakup. Low viscosity drops stretch passively but extend relatively little before they break, resulting in the formation of large droplets; these droplets undergo subsequent stretching, folding, and breakup.

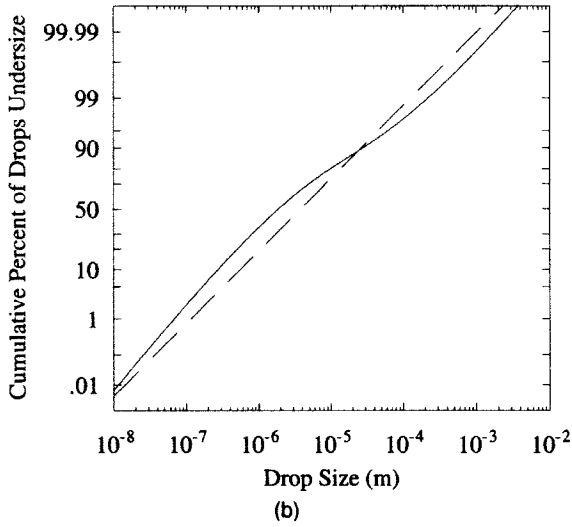
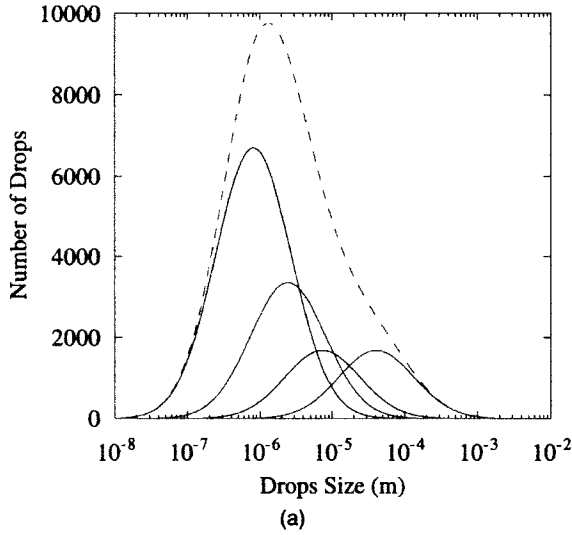


FIG. 23. (a) Distribution of drop sizes for mother droplets and satellite droplets (solid lines) produced during the breakup of a filament (average size = 2×10^{-5} m) in a chaotic flow. The total distribution is also shown (dashed line). A log-normal distribution of stretching with a mean stretch of 10^{-4} was used. (b) The cumulative distribution of mother droplets and satellite droplets (solid line) approaches a log-normal distribution (dashed line).

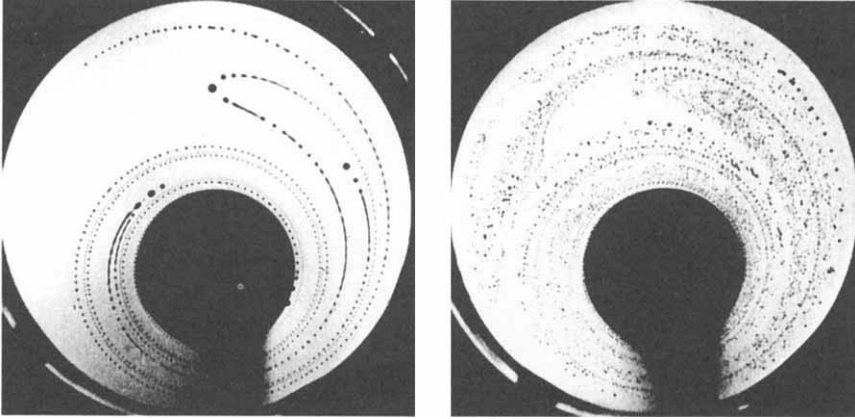


FIG. 24. Experimental results for drop breakup in a journal bearing flow. The Figure on the right shows repeated stretching and breakup, which is observed for low-viscosity drops (Tjahjadi and Ottino, 1991).

Under identical conditions, high-viscosity-ratio drops stretch substantially, $O(10^3-10^4)$, before they break producing very small fragments; these small fragments rarely break again. It is apparent, contrary to a long-held belief, that the finest dispersion does not correspond to $p = 1$.

HEURISTICS

- *Necking:*

Breakup by necking occurs in sustained flows when Ca is close to Ca_{crit} . The number of drops produced upon breakup by necking is generally less than 10.

The time for breakup by necking increases with p .

- *End-Pinching:*

Breakup by end-pinching occurs when a drop is deformed at Ca close to Ca_{crit} , and the flow is stopped abruptly.

Breakup by end-pinching is most difficult for very viscous or inviscid drops.

- *Capillary Instabilities:*

Breakup due to capillary instabilities dominates when the length of the filament is more than 15 times the initial radius of the drop.

The size of daughter droplets produced is independent of the initial drop size.

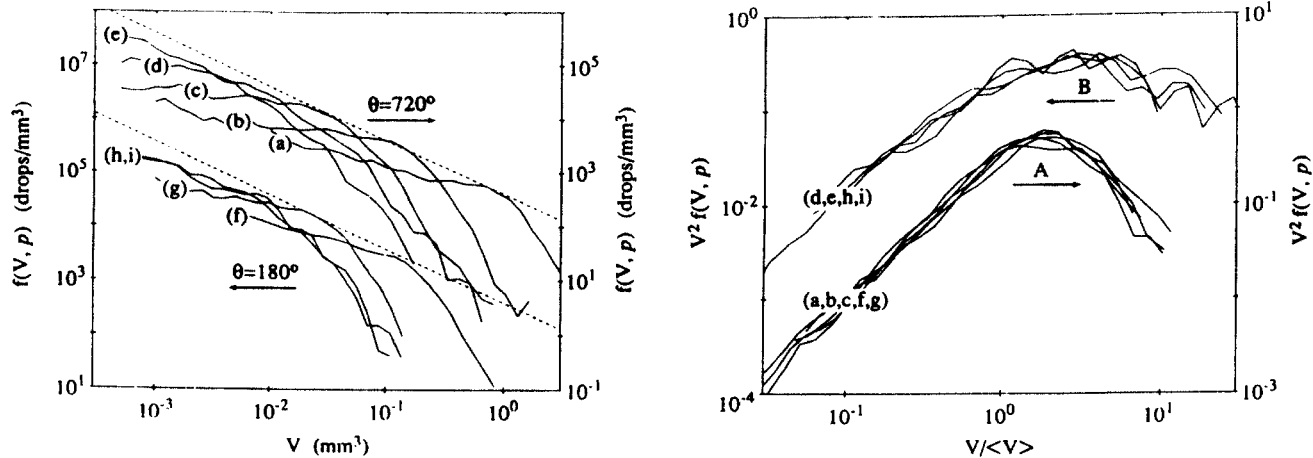


FIG. 25. Drop size distributions $[f(V, p)]$ based on drop volume (V) obtained by repeated stretching and breakup in a journal bearing flow for different viscosity ratios (p) (left). The curves for the different distributions overlap when the distribution is rescaled (right) (Muzzio, Tjahjadi, and Ottino, 1991).

The number of satellite drops produced upon breakup by capillary instabilities decreases as p increases (minimum of 3 to maximum of 16).

Breakup during flow is delayed relative to breakup at rest, so in general the easiest way to break an extended thread is to stop the flow.

Viscosity ratio $p = 1$ does not produce the finest dispersion; average drop sizes decrease with viscosity ratio.

B. COALESCENCE

1. Collisions

As dispersion proceeds drops come into close contact with each other and may coalesce. Coalescence is commonly divided into three sequential steps (Chesters, 1991): "collision" or close approach of two droplets, drainage of the liquid between the two drops, and rupture of the film (see Fig. 26).

The collision frequency between drops may be estimated by means of Smoluchowski's theory (see, for example, Levich, 1962). The collision frequency ($\omega \equiv$ number of collisions per unit time per unit volume) for randomly distributed rigid equal-size spheres, occupying a volume fraction ϕ , is given by

$$\omega \approx \frac{4\dot{\gamma}\phi n}{\pi}, \quad (32)$$

where n is the number density of drops (number per unit volume). Because hydrodynamic interactions are neglected, this equation gives at best an order-of-magnitude estimate for the collision frequency. However, it is important to note that the result is independent of flow type if $\dot{\gamma}$ is interpreted as $\sqrt{2\mathbf{D}:\mathbf{D}}$ (see following Illustration). The collision rate for small drops considering hydrodynamic interactions is given in Wang, Zinchenko, and Davis (1994). A thorough analysis of coagulation in the presence of hydrodynamic interactions, interparticle forces, and Brownian diffusion in random velocity fields is given by Brunk *et al.* (1997).

Illustration: Effect of flow type on shear induced collisions in homogeneous linear flows. The collision frequency for a general linear flow [Eq. (15)] is obtained following Smoluchowski's (1917) approach as (Bidkar and Khakhar, 1990)

$$\omega = 2d^3n \int_0^{2\pi} d\phi \int_0^\pi \sin\theta d\theta |\mathbf{D}:\mathbf{mm}| \quad (33)$$

in spherical coordinates (r, θ, ϕ) , where $d = 2R$ is the collision radius and \mathbf{m} is the unit normal to the collision surface. If the coordinate axes are

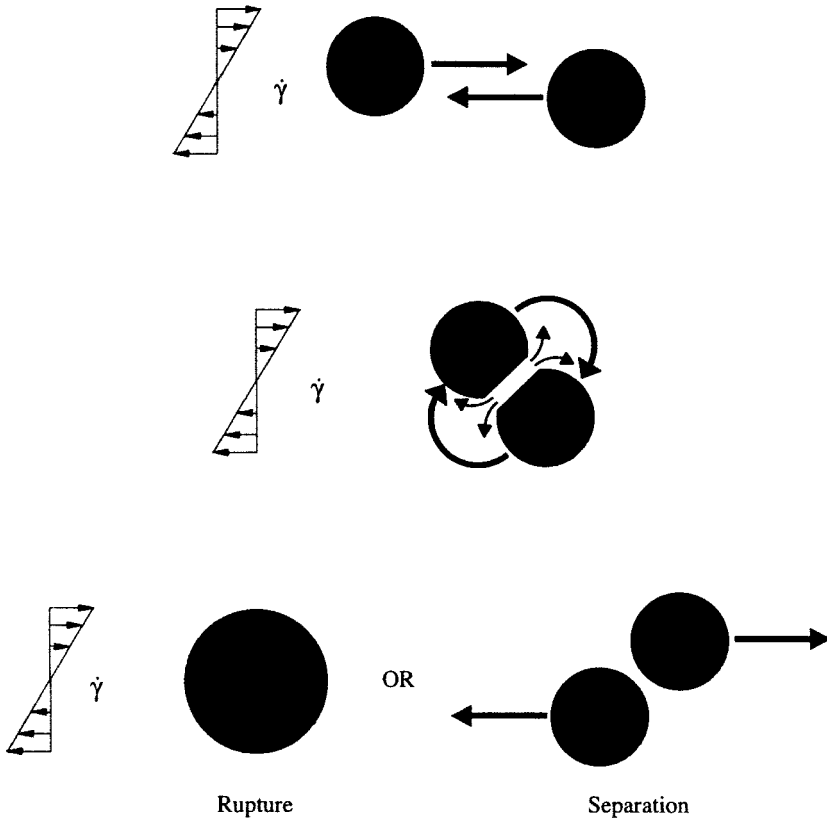


FIG. 26. Schematic representation of the three basic steps of coalescence.

chosen to be the principal axes, the tensor \mathbf{D} is diagonal, with the diagonal elements given by the roots of

$$\lambda^3 - \frac{1}{4}\lambda + \det(\tilde{\mathbf{D}}) = 0, \quad (34)$$

where $\tilde{\mathbf{D}} = \mathbf{D}/\dot{\gamma}$ and $\dot{\gamma} = \sqrt{2\mathbf{D}:\mathbf{D}}$. Thus, in the context of Smoluchowski's theory, the only parameter that specifies the flow type is $\det(\tilde{\mathbf{D}})$, which has a range of possible values $(-1/12\sqrt{3}, 1/12\sqrt{3})$. Clearly, vorticity plays no role in the process. For 2D flows, $\det(\tilde{\mathbf{D}}) = 0$, so that the collision frequency is independent of flow type and is given by

$$\omega_{2D} = \frac{4}{\pi} \dot{\gamma} n \phi. \quad (35)$$

For general linear flows, the limit case of axisymmetric flows [$|\det(\tilde{\mathbf{D}})| =$

$1/12\sqrt{3}]$ gives

$$\omega_{\text{axs}} = \frac{16}{9\pi} \dot{\gamma} n \phi = \frac{\pi}{3} \omega_{2D}. \quad (36)$$

These results show that the Smoluchowski collision frequency is independent of flow type for planar flows and that the maximum collision frequency (obtained for axisymmetric flows) is only 5% larger than that for planar flows.

2. Film Drainage

Once a “collision” occurs, the liquid between the drops is squeezed, forming a film. As the drops are continually squeezed by the external flow field, the drops rotate as a dumbbell and the film drains. At some distance h_o , the drops begin to influence each other and their rate of approach, dh/dt , decreases and is now governed by the rate of film drainage.

The rate of approach, dh/dt , is determined by the different boundary conditions of the interface, which characterize the *mobility* and *rigidity* of the interface. The mobility of the interface is essentially determined by the viscosity ratio and determines the type of flow occurring during film drainage. The rigidity of the interface is determined by the interfacial tension and determines the degree of flattening of the drop. These boundary conditions, along with the different expressions for dh/dt , are displayed in Fig. 27 (Chesters, 1991).

The required time for complete film drainage is given by integrating the equations for dh/dt from h_o to the critical film thickness at which film drainage ends and rupture begins. If the driving force for film drainage is taken, as a first approximation, to be the Stokes drag force acting on the drops,

$$F \approx 6\pi\mu_c\dot{\gamma}R_o, \quad (37)$$

integrating dh/dt is straightforward. This is clearly a simplified picture, but consistent with the assumptions used for calculation of the collision rate [Eq. (32)]. A more accurate estimate of the force may be obtained from Wang *et al.* (1994). The film drainage times for the different boundary conditions are given in Fig. 27. The expressions differ significantly, particularly with regard to the dependence on the applied force (F) and initial separation (h_o). In all cases, except for the perfectly mobile interface, the drainage time is directly proportional to the continuous phase viscosity (μ_c) and interfacial tension is important only in those cases where the drops are deformed. The equations in Fig. 27 are based on the formation of a flat circular film between the drops of radius a , and this dimension can be calculated from the applied force.

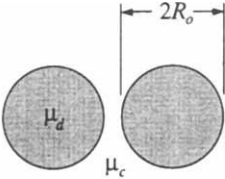
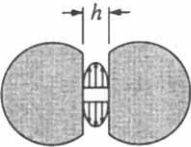
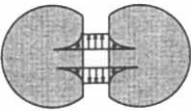
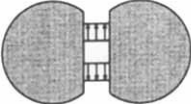
		Drainage Rate	Drainage Time	Criteria
Rigid Drops		$-\frac{dh}{dt} \approx \frac{2hF}{3\pi\mu_c R_o^2}$	$t_{drain} \approx \frac{3\pi\mu_c R_o^2}{2F} \ln\left(\frac{h_o}{h_{crit}}\right)$	$\frac{a}{R} < 2\left(\frac{h}{R}\right)^{1/2}$
Immobile Interfaces		$-\frac{dh}{dt} \approx \frac{8\pi\sigma^2 h^3}{3\mu_c R_o^2 F}$	$t_{drain} \approx \frac{3\mu_c R_o^2 F}{16\pi\sigma^2} \left(\frac{1}{h_{crit}^2} - \frac{1}{h_o^2} \right)$	$p > \frac{3a}{h}$
Partially Mobile Interfaces		$-\frac{dh}{dt} \approx \frac{2(2\pi\sigma/R_o)^{3/2} h^2}{\pi\mu_d F^{1/2}}$	$t_{drain} \approx \frac{\pi\mu_d F^{1/2}}{2(2\pi\sigma/R_o)^{3/2}} \left(\frac{1}{h_{crit}} - \frac{1}{h_o} \right)$	$\frac{6h}{a} < p < \frac{3a}{h}$
Fully Mobile Interfaces		$-\frac{dh}{dt} \approx \frac{2\sigma h}{3\mu_c R_o}$	$t_{drain} \approx \frac{3\mu_c R_o}{2\sigma} \ln\left(\frac{h_o}{h_{crit}}\right)$	$p < \frac{6h}{a}$

FIG. 27. Various modes of film drainage and the corresponding equations for the rate of film thinning and drainage time are shown. The criteria for specific modes are also indicated.

If a critical film thickness is not reached during film drainage, the drops separate from each other. Conversely, if the critical film thickness is reached, the film ruptures—as a result of van der Waals forces—and the drops coalesce. This generally occurs at thin spots, because van der Waals forces are inversely proportional to h^4 (Verwey and Overbeek, 1948). The value of h_{crit} can be determined by setting the van der Waals forces equal to the driving force for film drainage, giving (Verwey and Overbeek, 1948)

$$h_{\text{crit}} \approx \left(\frac{HR_0}{8\pi\sigma} \right)^{1/3}, \quad (38)$$

where H is the Hamaker constant.

A few general conclusions can be drawn from the equations presented in Fig. 27. In general, the drainage time is shortest when the drops are rigid (top equation). Smaller drops are more likely to coalesce than larger ones because the drainage time decreases with drop size. Since the drainage time decreases with force in all cases except the fully mobile interface, coalescence is more likely in lower shear rate zones where the force is lower [Eq. (37)]. Furthermore, surfactants and high-viscosity dispersed phases, both of which reduce the mobility of the interface, result in longer drainage times and thus lower probabilities of coalescence.

HEURISTICS

- Collision frequency is nearly independent of flow type.
 - Coalescence is important for dispersed phase volumes fraction (ϕ) greater than about 0.005; the rate of coalescence increases with ϕ .
 - Smaller drops are more likely to coalesce after collision than larger drops.
 - Coalescence is more likely to take place in regions of low shear rate.
 - Coalescence becomes more likely as the mobility of the interface increases.
-

C. BREAKUP AND COALESCENCE IN COMPLEX FLOWS

There have been several attempts at models incorporating breakup and coalescence. Two concepts underlie many of these models: binary breakup and a flow subdivision into weak and strong flows. These ideas were first used by Manas-Zloczower, Nir, and Tadmor (1982, 1984) in modeling the dispersion of carbon black in an elastomer in a Banbury internal mixer. A similar approach was taken by Janssen and Meijer (1995) to model blending of two polymers in an extruder. In this case the extruder was divided into two types of zones, strong and weak. The strong zones correspond to regions

of high shear with short residence times, where stretching of drops into threads and breakup of threads during flow takes place. The weak zones correspond to regions of low shear and long residence times, where breakup of threads at rest and coalescence of drops occurs. Janssen and Meijer (1995) modeled the strong zone as elongational flow and the weak zone as simple shear flow. After each zone, conditions were checked for stretching, capillary breakup, and coalescence according to local coalescence and breakup theory. An initial drop size distribution was passed through a series of alternating strong and weak zones a specific number of times, resulting in a final drop size distribution. Using this model the effects of material properties and process parameters on the final drop size distribution were evaluated. Another model was proposed by Huneault, Shi, and Utracki (1995), again, to model dispersion in extruders. In this case, however, a simplified flow analysis was used to model the flow in the extruder, which gave estimates for the average values of Ca . According to the average Ca in each zone, the average drop diameter was evolved according to a number of rules that included binary breakup. The droplet size distribution in simple shear flow was studied by Patlazhan and Lindt (1996) using a population balance approach based on simple models to predict droplet breakage and coalescence rates.

Let us consider the so-called viscous immiscible liquid mixing (VILM) model (DeRoussel, 1998). This model incorporates most of the important physical processes occurring during drop breakup described in the previous sections, though simplifications are inevitable. The basic approach is similar to that of Janssen and Meijer (1995)—a strong zone modeled by elongational flow in which stretching and breakup by capillary instabilities during flow occur and a weak zone modeled by shear flow in which coalescence and breakup by capillary instabilities at rest occur. The physical aspects of the VILM model that are not included in the model of Janssen and Meijer are summarized as follows:

- Stretching distributions are incorporated into the strong zone.
- Strong and weak zones are divided into subzones that allow for a distribution of shear and elongation rates and residence times.
- Threads breaking by capillary instabilities break into a distribution of drops rather than drop sizes of equal size.
- Coalescence between drops of different size is allowed.
- Variation of the driving force during film drainage is taken into account.

The basic procedure of the VILM model is to send an initial distribution of drops through a specified number of strong and weak zones. With each pass through the strong and weak zones, the evolution of the drop distribution is determined based on the fundamentals of breakup and coalescence.

The dispersed phase is considered to be in the form of either extended threads or spherical drops. In the strong zone, the evolution of drops and threads is essentially the same, except for drops that have $Ca < Ca_{crit}$ and hence remain underformed. The stretching of drops (if $Ca > 5Ca_{crit}$) and threads is affine and proceeds according to $L/R_o \sim \exp(\dot{\epsilon}t)$ and $R/R_o \sim \exp(-\dot{\epsilon}t/2)$. If the residence time in the strong zone is long enough, $\tau_s > t_{crit} + t_{grow}$, the thread breaks into a number of drops with a distribution of sizes. The size of the mother droplets is determined by the wavelength of the fastest-growing disturbance. Corresponding to each mother droplet is a distribution of satellite droplets that depends on the viscosity ratio (see Fig. 21). The distributions obtained by Tjahjadi, Stone, and Ottino (1992) for the breakup of a stationary thread are used in the computations.

The elongation rates for each of the subzones in the strong zone are chosen so that the amount of stretching incurred matches a given stretching distribution. So, if stretching distributions are known for a given mixer, a connection can be made between the relatively simple parameters of the VILM model and the complex flow of the mixer. Techniques for determining the stretching distributions in a mixer are addressed in Muzzio, Swanson, and Ottino (1991a) and Hobbs and Muzzio (1997).

Computations for the weak zone are carried out in discrete time steps with the time step taken to be the average time between collisions, as given by Smoluchowski's theory [Eq. (32)]. At each time step, the following procedure is performed. Two drops are chosen at random and placed in a collision array along with the time the collision occurred and the drainage time for these two particular drops. Each extended thread is checked to see if it has been at rest long enough for breakup due to capillary instabilities to occur. If enough time has elapsed for the thread to break, the corresponding number of drops replaces the thread. The collision array is checked to see if any of the drop pairs have been in contact long enough for the film to drain. When sufficient time has elapsed, the two colliding drops coalesce to form a single larger one. At the end of the time in the weak zone, all drop pairs remaining in the collision array are returned to the drop general population and the next cycle or subzone is started.

The foregoing procedure requires a calculation of the drainage time for each collision. When the number of collisions that occur during a single pass through the weak zone becomes large, $O(10^7)$, the procedure takes too long and is no longer practical. In order to deal with this complication, the number of drops is reduced by a factor that gives a feasible collision frequency. The shape of the distribution is preserved when the number of drops is reduced, so nothing is lost in the simulation.

By using the procedure just discussed, the VILM model allows general trends to be found as process and material parameters are varied. Figure 28

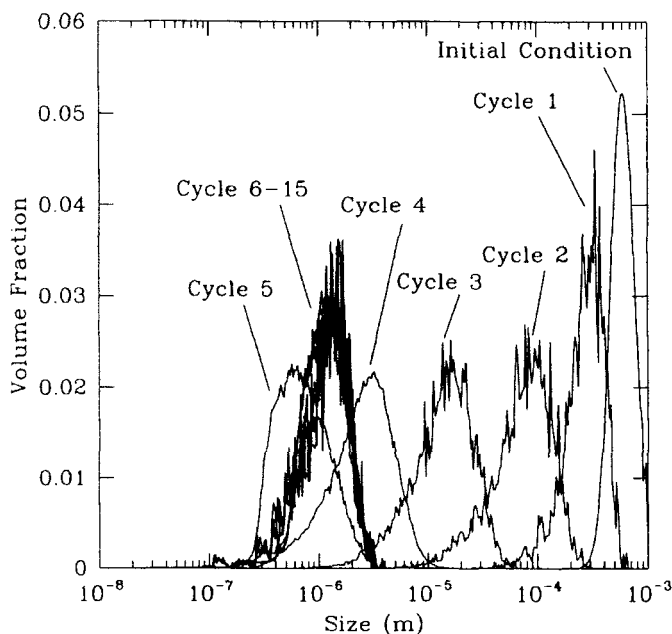


FIG. 28. Size distributions from a typical simulation produced by the VILM model. After six cycles a steady size is reached. Smaller sizes are obtained after five cycles as compared to the final distribution. The conditions for the simulation are $\mu_c = \mu_d = 100$ Pa s, $\phi = 0.2$, and $\sigma = 5 \times 10^{-3}$ N/m.

shows the results of a typical simulation in which an initial drop distribution passes through a number of cycles until a steady-state is reached after six cycles. An important point to note is that after five cycles the resulting distribution is at a smaller size than the final distribution. This phenomena is referred to as overemulsification in the emulsion technology literature (Becher and McCann, 1991), but apparently has not been documented in polymer processing. Overemulsification is a result of the many small satellite drops produced by capillary breakup. The mean drop size then increases with time because the small drops cannot break further and coalescence dominates. Thus, breakup dominates the early part of the process and coalescence dominates the later stages of mixing.

One variable that is commonly used to "classify" the morphology of a blend is the viscosity ratio. Quite often the average drop size is given as a function of the viscosity ratio. Figure 29 gives the results of a number of simulations in which the average size is plotted vs the viscosity ratio for different continuous and dispersed phase viscosities. As can be seen from this figure, for a given viscosity ratio the average size can vary a great deal.

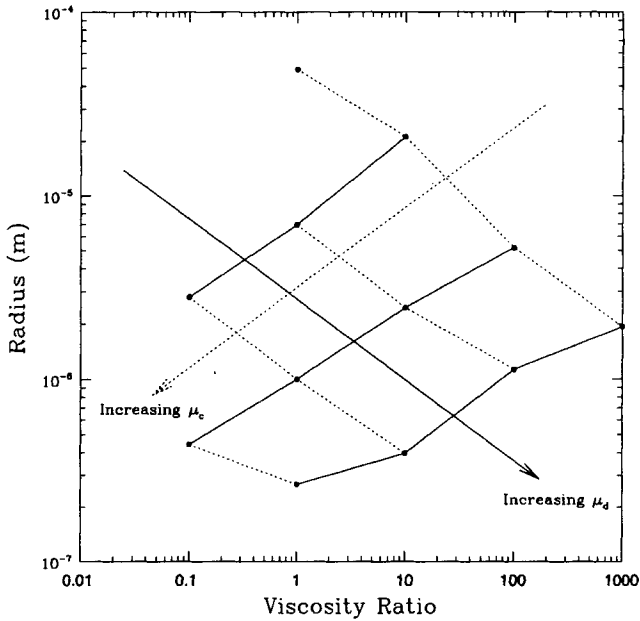


FIG. 29. Average steady-state size of the dispersed phase at different viscosity ratios. The solid and dashed lines represent simulations in which μ_d and μ_c are held constant. Other process parameters are the same as used for Fig. 28 (except $\phi \approx 0.05$). It is clear that the magnitudes of both viscosities must be considered rather than just the viscosity ratio. The lowest viscosity in each case is 1 Pa·s and the highest 1000 Pa·s. The curves are equally spaced on a logarithmic scale for viscosity.

Hence it is the values of each viscosity, dispersed and continuous, and not just the viscosity ratio that is important in determining the average size. The average size increases with a decrease in either continuous or dispersed phase viscosity for fixed operating conditions.

HEURISTICS

- The average drop size increases with decrease in continuous or dispersed phase viscosity.
 - Intermediate mixing times may produce the smallest drops; long mixing times result in an equilibrium size that is larger.
-

III. Fragmentation and Aggregation of Solids

1. Physical Picture

Powders dispersed in liquids consist of *agglomerates*—a collection of *aggregates*—which in turn are composed of *primary particles*. Agglomerates

break because of flow; aggregates do not. Often these particles are of colloidal size, with a size ratio agglomerates/aggregates of about 10^3 . In the case of carbon black, for example, aggregates are of the order of $0.1\ \mu\text{m}$ and agglomerates are of the order of $10\text{--}100\ \mu\text{m}$ and larger. Thus, the length reduction in solid dispersion is about of the same order of magnitude as in dispersion of liquids. Often we will refer to both aggregates and agglomerates as clusters, a cluster being composed of particles. The *size* of a cluster is given by the *number* of particles composing the cluster.

The objective of mixing—or dispersion—of solids is to break agglomerates to aggregate size, the process giving rise to broad, time-evolving cluster size distributions. The entire process of *dispersion* of a powder into a liquid involves several stages, which may all be occurring with some degree of overlap. Several scenarios have been proposed and, unavoidably, a proliferation of terms has ensued. For instance, Parfitt's (1992) scenario consists of four stages: *Incorporation* is the initial contact of the solid with the medium. *Wetting*, which follows incorporation, may in turn consist of (i) adhesion of the medium to the solid, (ii) immersion of the solid into the fluid, and (iii) spreading of the liquid into the porous solid. *Breakup* (or fragmentation) and *flocculation* (or aggregation) conclude the dispersion process. A much narrower definition of *dispersion* is commonly used in the polymer processing literature: fragmentation of agglomerates into aggregates, and the distribution of the aggregates into the medium.

In fact, the term fragmentation is commonly used in the physics literature to refer to a broader class of processes involving breakup of solids, such as rocks. Much of this literature can be adapted, *mutatis mutandi*, to the dispersion of agglomerates as is of interest here (see Fig. 1). Fragmentation may be in turn divided into two modes of breakup (Redner, 1990): *rupture* and *erosion*—rupture referring to the breakage of a *cluster* into several fragments of comparable size, erosion to the gradual shearing off of small fragments from larger clusters (Fig. 30). The main qualitative difference between these two mechanisms is energy input: low for erosion, high for rupture. Erosion dominates dispersion when stresses are low. Finally, materials may *shatter*, producing a large number of smaller fragments in a single event, as in the case of high-energy fragmentation. While the physical mechanisms may be different, there are similarities between fragmentation of solids and breakup of liquid drops, at least with respect to the size distribution of fragments produced on breakup: Tip streaming is analogous to erosion, necking to rupture, and capillary breakup to shattering.

Aggregation (*flocculation* is the term commonly used in the rubber industry) may be imagined as being the reverse of dispersion. Aggregates come together, interact via hydrodynamic forces and particle potentials, and eventually bind. Two bonding levels are possible: strong and weak. Strongly

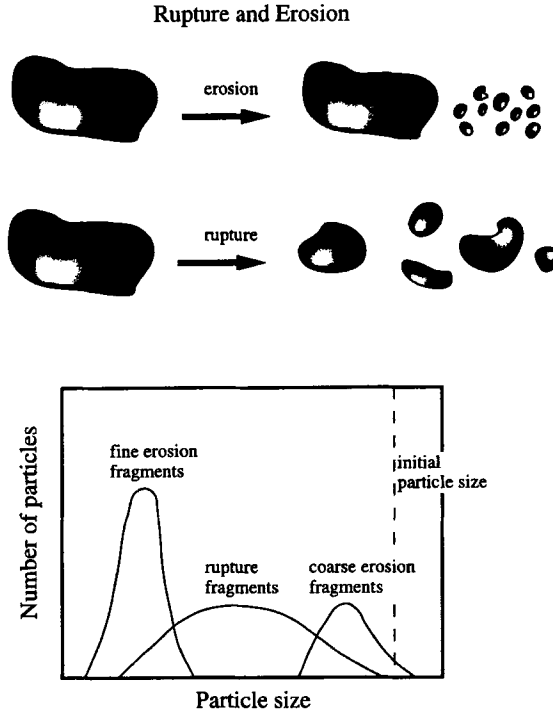


FIG. 30. Schematic view of rupture and erosion of particles and the typical size distribution of fragments obtained.

bound aggregates cannot be redispersed by future stirring; weakly bonded aggregates can be dispersed by stirring. As opposed to coalescence of droplets, structure in this case may be preserved and fractal-like structures (Fig. 31) are common. The mass of such clusters increases with radius according to R^D rather than R^3 for compact agglomerates, where $D < 3$ is the fractal dimension. As we shall see, flows can in fact be manipulated to tailor structures.

2. Small Scales: Particle Interactions

The current level of understanding of how aggregates form and break is not up to par with droplet breakup and coalescence. The reasons for this discrepancy are many: Aggregates involve multibody interactions; shapes may be irregular, potential forces that are imperfectly understood and quite susceptible to contamination effects.

Thus, analyses of how aggregates break have resorted to idealizations inspired by traditional fluid mechanical analysis, two limit cases being per-

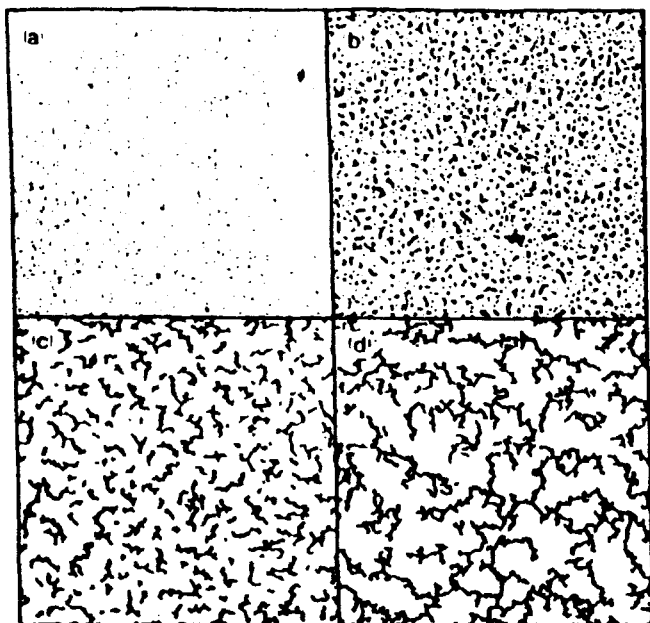


FIG. 31. Fractal structures obtained experimentally at different stages of aggregation of a colloidal monolayer of $1\ \mu\text{m}$ sulfonated polystyrene particles on the surface of an aqueous calcium chloride solution, initially uniformly distributed (Robinson and Earnshaw, 1992).

meable and impermeable spheres. Quite possibly the simplest model is to regard an agglomerate as a pair of bound spheres. As in the case of drop breakup, the analysis considers scales such that the surrounding flow is linear. The velocity of one particle relative to the other, taking into account hydrodynamic and potential interactions between the two particles, is

$$\mathbf{v} = \mathbf{D} \cdot \mathbf{r} + \boldsymbol{\omega} \times \mathbf{r} - \left\{ A(r) \frac{\boldsymbol{\pi}\boldsymbol{\pi}}{r^2} + B(r) \left[\mathbf{I} - \frac{\boldsymbol{\pi}\boldsymbol{\pi}}{r^2} \right] \right\} \cdot \mathbf{D} \cdot \mathbf{r} + \frac{C(r)}{6\pi\mu R} \mathbf{F}_c, \quad (39)$$

where \mathbf{r} is a vector joining the centers of the two spheres, \mathbf{D} is the rate of strain tensor, $\boldsymbol{\omega}$ is the vorticity of the driving flow, $A(r)$ and $B(r)$ are known functions (Batchelor and Green, 1972), and \mathbf{I} is the identity matrix. In the last term, \mathbf{F}_c is the physicochemical force between the particles, μ is the fluid viscosity, R is the radius of the particles, and $C(r)$ is a parameter that accounts for the particle proximity effect on drag (Spielman, 1970). The first three terms in this equation give the relative velocity between the spheres in a linear flow field under the influence of hydrodynamic interactions, and the last term gives the relative velocity due to the physicochemical

forces between the spheres. Rupture of this idealized aggregate occurs if hydrodynamic forces overcome the binding physicochemical forces as we show later. The equation also applies to the analysis of the aggregation of initially separated particles in a linear flow (Zeichner and Schowalter, 1977).

The physicochemical forces between colloidal particles are described by the DLVO theory (DLVO refers to Derjaguin and Landau, and Verwey and Overbeek). This theory predicts the potential between spherical particles due to attractive London forces and repulsive forces due to electrical double layers. This potential can be attractive, or both repulsive and attractive. Two minima may be observed: The primary minimum characterizes particles that are in close contact and are difficult to disperse, whereas the secondary minimum relates to looser dispersible particles. For more details, see Schowalter (1984). Undoubtedly, real cases may be far more complex: Many particles may be present, particles are not always the same size, and particles are rarely spherical. However, the fundamental physics of the problem is similar. The incorporation of all these aspects into a simulation involving tens of thousands of aggregates is daunting and models have resorted to idealized descriptions.

A. FRAGMENTATION

There is a large body of theoretical work dealing with fragmentation. General aspects, primarily in the context of mathematical aspects of particle size distributions produced on fragmentation, are covered by Redner (1990) and Cheng and Redner (1990), whereas a review of various modeling approaches and experimental results, addressing grinding of solids, is presented by Austin (1971). Of special interest is the distribution of fragments upon rupture. Power law forms for cumulative distributions based on particle radius are commonly obtained and, in many cases, the distribution of fragments produced in a single rupture event is *homogeneous* (i.e., the distribution depends only on the ratio of the mass of the fragment to the mass of the original particle). Erosion produces fragments much smaller than the original particle, and consequently the particle size distribution is bimodal. This body of literature provides a starting point for the understanding of the dispersion of agglomerates in viscous flows (Fig. 30).

Fragmentation of agglomerates is similar to rupture of solids in that both agglomerates and granular solids deform only slightly before breaking. Differences arise mainly from the complex internal structure of agglomerates. In addition, the weaker bonding in agglomerates results in fragmentation at relatively low stresses. Fragmentation may be caused by several mechanisms, for example, application of direct compressive loads and parti-

cle-particle and wall-particle impacts. However, here we focus only on fragmentation by hydrodynamic forces, which is of most relevance to polymer processing. By analogy with liquid droplets and the capillary number [Eq. (18)] the dimensionless parameter that characterizes the fragmentation process is the ratio of the viscous shear stress to the strength of the agglomerate. We term this ratio the *Fragmentation number*, Fa :

$$Fa = \frac{\mu\dot{\gamma}}{T}. \quad (40)$$

The term T denotes the characteristic cohesive strength of the agglomerate and plays a role analogous to the surface tension stress (σ/R) in the definition of the Capillary number for liquid drops. Unlike surface tension, however, the agglomerate strength is not a material property but depends on internal structure, density (degree of compaction), moisture, and many other variables. A similar definition of a dimensionless Fragmentation number appears in previous studies (e.g., Rwei, Manas-Zloczower, and Feke, 1990), though it was not termed as such.

1. Agglomerate Strength

The cohesive strength of an agglomerate owes its origins to interparticle bonds due to electrostatic charges, van der Waals forces, or moisture. Experimental methods for the measurement of the characteristic agglomerate strength include the tensile testing of compacted pellets (Rumpf, 1962; Hartley and Parfitt, 1984), notched bending tests of compacted beams (Kendall, 1988), and compression testing of compacted beds by penetration of a conical tester (Lee, Feke, and Manas-Zloczower, 1993). The three tests measure different properties: the tensile strength, the tensile strength in the presence of flaws, and the cohesivity, respectively. Values obtained from different test methods for the same agglomerate would clearly be different; trends with changes in parameters are, however, similar.

Two idealized models have been reasonably successful in predicting the strength of agglomerates and we review them here. Rumpf (1962) assumed the agglomerates to be spatially uniform and composed of identical spheres of radius a bound to touching neighbors by van der Waals forces. Considering a planar rupture surface, the tensile strength T is

$$T \approx \frac{H}{48az_0^2} \frac{\phi}{1 - \phi}, \quad (41)$$

where H is the Hamaker constant, ϕ is the solids volume fraction, and z_0 is the equilibrium separation distance between the sphere surfaces. Kendall

(1988), on the other hand, used the Griffith criterion for crack growth to obtain

$$T \approx 15.6 \frac{\phi^4 \Gamma_c^{5/6} \Gamma^{1/6}}{(2ac)^{1/2}}, \quad (42)$$

where Γ is the interfacial energy, Γ_c is the fracture energy, and c is the initial length of the crack (edge notch). The two mechanisms, fracture at a plane and crack growth, give very different expressions, particularly with respect to dependence on the solids volume fraction (ϕ) and the aggregate (primary particle) radius (a). Surprisingly, agglomerates may rupture by either of these mechanisms. For example, experiments using titanium dioxide *agglomerates* carried out by Lee, Feke, and Manas-Zloczower (1993) found the strength of agglomerates ($a \approx 0.16 \mu\text{m}$) to follow Rumpf's model, whereas Kendall (1988) found the agglomerates ($a \approx 0.23 \mu\text{m}$) to follow the crack growth model. A notable difference was the order of magnitude lower strength measured by Lee *et al.* (1993) as compared to the agglomerates of Kendall (1988); however, this may be due to the different test methods used.

Illustration: Effect of flow type on agglomerate separation after rupture. The nature of the local flow significantly affects the separation of fragments produced on rupture of an agglomerate, as shown by Manas-Zloczower and Feke (1988), for equal-sized spherical fragments. Significantly higher shear rates are required for separation in a simple shear flow as compared to extensional flows. As the following analysis demonstrates, the process of separation is very similar to the breakup of slender drops (Khakhar and Ottino, 1986b,c; Ottino, 1989); thus, previous results are useful for generalizing the analysis of fragment separation for all linear flows.

The spherical fragments, initially in close contact, move relative to each other according to Eq. (B.1). The underlying physics is revealed more clearly by recasting equation (B.1) in the following dimensionless form:

$$\frac{1}{r} \frac{dr}{dt} = (1 - A(r)) \mathbf{D} : \mathbf{mm} - C(r) \frac{F_c}{Fa}, \quad (43)$$

$$\frac{d\mathbf{m}}{dt} = [(1 - B(r)) \mathbf{D} - \Omega] \cdot \mathbf{m} - (1 - B(r)) (\mathbf{D} : \mathbf{mm}) \mathbf{m}. \quad (44)$$

Here r is the center-to-center distance, and \mathbf{m} is a unit vector along the line joining the centers of the two fragments, so that $\mathbf{r} = r\mathbf{m}$. Distances are made dimensionless with respect to the radius of a fragment (a), shear rates and time with respect to the characteristic shear rate $\dot{\gamma} = \sqrt{2\mathbf{D} : \mathbf{D}}$, and $F_c = |\mathbf{F}_c|$ with respect to H/a . These equations are identical in form to

those for the breakup for a slender drop (Khakhar and Ottino, 1986b) discussed earlier.

Several conclusions result from the preceding equations: They reveal that the dimensionless parameter of the system is the fragmentation number (Fa) with the characteristic strength given by

$$T = \frac{H}{6\pi a^3}. \quad (45)$$

The rate of separation of the fragments depends on the functions $A(r)$, $C(r)$, F_c , and the fragmentation number, while the rate of rotation depends only on the function $B(r)$. Further, it is apparent that the separation between the fragments increases only when the hydrodynamic force exceeds the binding physicochemical force. The pair of fragments rotates as a material element in an apparent flow with an effective velocity gradient tensor

$$\mathbf{M} = \mathbf{D} + \Omega/(1 - B). \quad (46)$$

Since B is positive, the apparent flow appears to have a higher vorticity relative to the strain rate than the imposed flow.

Based on the foregoing discussion, a criterion for the separation of the fragments is easily obtained. If at least one eigenvalue of the tensor \mathbf{M} is positive, the pair orients along the corresponding principal axis and the critical Fragmentation number for separation is given by

$$Fa_{\text{sep}} = \frac{\sqrt{2}}{e_\lambda} \frac{1}{12z_0^2}, \quad (47)$$

where $e_\lambda/\sqrt{2}$ is the asymptotic value of $\mathbf{D}:\mathbf{mm}$ (i.e., the largest positive eigenvalue of \mathbf{M}) and $z_0 = (r - 2)$ is the equilibrium separation. For $Fa > Fa_{\text{sep}}$ the fragments separate indefinitely. In arriving at the preceding equation, the physicochemical force was estimated for a pair of equal-sized spheres as $F_c = 1/12z_0^2$ (Rumpf, 1962), and the result $(1 - A)/C = 1$ for small separations was used. Special cases of this result were presented by Manas-Zloczower and Feke (1988). For purely extensional flows ($\Omega = \mathbf{0}$), we have $e_\lambda = 1/\sqrt{2}$ for planar flows and $e_\lambda = \sqrt{2/3}$ for axisymmetric flows. In the case of simple shear flow, eigenvalues are imaginary; hence, no asymptotic orientation exists and the separation distance oscillates with time as the fragments rotate in the flow. Separation of fragments in this flow occurs, according to Manas-Zloczower and Feke (1988), when the potential energy due to the van der Waals forces at the maximum separation distance is less than the thermal energy. This criterion gives the critical separation as

$$z_c \approx \frac{Ha}{12k_B T}, \quad (48)$$

where k_B is the Boltzmann constant. The critical fragmentation number for separation should be at least as large as that for planar extension; numerical simulation is required to obtain Fa_{sep} at which the criterion $z > z_c$ is satisfied.

2. Rupture—Critical Fragmentation Number

Agglomerates in a sheared fluid rupture when the hydrodynamic stress exceeds a critical value; in dimensionless form the criterion for rupture is $Fa > Fa_{crit}$. Rupture occurs within a short time of application of the critical stress, and thus can be distinguished from erosion, which occurs over much longer time scales.

Experimental data for the critical fragmentation number is sparse and certainly much less than what is available for droplets. Rwei, Manas-Zloczower, and Feke (1990) carried out experiments to determine the critical stress for the rupture of compact agglomerates in simple shear flow. Carbon black pellets of different densities (ρ) and silicone oils of different viscosities were used. The tensile strength of the agglomerates was measured and is well correlated by Kendall's (1988) model: $T \approx K\rho^4$ with $K \approx 1.7 \times 10^6$ Pa (g/cm³)⁻⁴. The critical shear stress applied at the point of rupture was found to be $\mu\dot{\gamma}_c \approx A\rho^4$ with $A \approx 8.7 \times 10^4$ Pa (g/cm³)⁻⁴ for the different density pellets and the fluids of varying viscosity. The reported data thus gives $Fa_{crit} \approx 0.05$ independent of pellet density. The dependence of Fa_{crit} on the agglomerate size was not studied. (Note: The magnitude of Fa_{crit} depends on the method used for measuring the strength of the agglomerate, T .) The size distribution of the fragments formed upon rupture is log-normal. This seems to be in agreement with the theory for random breakage discussed later in this section.

Rupture of fractal (focculated) aggregates of polystyrene latices in simple shear flow and converging flow was studied by Sonntag and Russel (1986, 1987b). For simple shear flow and low electrolyte concentrations, the critical fragmentation number decreases sharply with agglomerate radius (R) as

$$Fa_{crit} \approx 1.6 \times 10^4 \left(\frac{R}{a} \right)^{-3}, \quad (49)$$

where the agglomerate strength, $T = 595$ dyn/cm², is obtained by fitting a theory (discussed later) to the experimental data. The fractal dimension of the agglomerates is $D \approx 2.5$. Ionic effects at high electrolyte concentrations are well accounted for by assuming T to be proportional to the force between two primary particles calculated using the DLVO theory (the

bond strength between the primary particles increases with increasing ionic strength). In the converging flow, the mass of the critical agglomerates decreases linearly with increasing shear rate, like the shear flow, but the radius of gyration is nearly constant. Such behavior could be due to the formation of elongated fragments upon rupture.

Theoretical prediction of the critical fragmentation number requires an estimate of the hydrodynamic stress acting on the agglomerate. For the case of spherical impermeable agglomerates Bagster and Tomi (1974) showed that rupture in simple shear flow occurs on a plane through the center of the agglomerate, and Fa_{crit} is independent of the agglomerate size. In the analysis, the hydrodynamic stress on the surface is given by

$$\mathbf{F} = 5\mu\mathbf{D} \cdot \mathbf{r} \quad (50)$$

(Brenner, 1958). Feke and Manas-Zloczower (1991) extended this analysis to the case of spherical agglomerates with a single flaw considering rupture to occur by crack growth. Again Fa_{crit} is independent of size. A significant result is that rupture is more likely in simple shear flow, as compared to extensional flows, since the agglomerate rotates in a simple shear flow and the rupture surface (flaw) experiences the entire range of stresses possible.

The case of permeable porous agglomerates gives qualitatively different results. Adler and Mills (1979) showed that Fa_{crit} decreases with agglomerate size initially, but approaches the impermeable limit for large agglomerates ($R/k^{1/2} \gg 1$, where μ/k is the permeability). Sonntag and Russel (1987a) analyzed fractal structures using a similar approach. The fractal structure is incorporated into the mean field approach by considering a radially varying solids volume fraction

$$\phi(r) \approx \phi_0 \left(\frac{r}{a} \right)^{D-3}, \quad (51)$$

with the strength given by $T = K\phi^n$ (similar to Kendall's model). This model predicts the experimentally determined dependence of Fa_{crit} on agglomerate size when $n = 4.45$ (Fig. 32). In both the models for porous agglomerates, hydrodynamic stresses within the sphere are calculated using the Brinkman equation with creeping flow in the surrounding fluid. The Mises rupture criterion

$$(\mathbf{T}_D : \mathbf{T}_D)^{1/2} > T \quad (52)$$

is used in both analyses, where \mathbf{T}_D is the deviatoric part of the stress tensor (i.e., $\mathbf{T} = -P\mathbf{I} + \mathbf{T}_D$). Thus, rupture can occur at any point in the sphere.

Most recently, Horwath, Manas-Zloczower, and Feke (1992a, b) carried out a numerical study of the rupture of fractal clusters generated by different aggregation protocols (more details of these protocols are given in Section

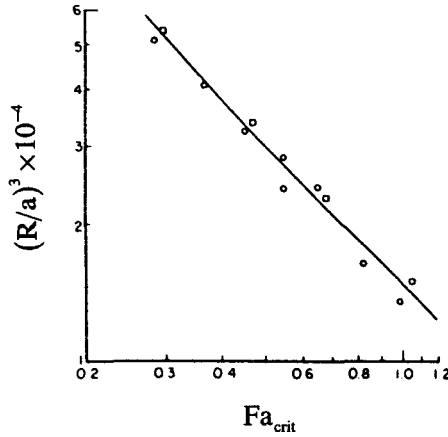


FIG. 32. Relationship between Fa_{crit} and the dimensionless cluster size (R/a) for fractal clusters ($D \approx 2.5$) of polystyrene latex in a simple shear flow. Data points are experimental results and the solid line is the theoretical prediction (Sonntag and Russel, 1986, 1987a).

III, B on aggregation). The clusters are modeled as impervious spheres and the hydrodynamic force is calculated following the approach of Bagster and Tomi (1974). The cluster ruptures if the resultant stress on the bonds between clusters exceeds a specified bond strength. The critical fragmentation number decreases with agglomerate radius for clusters with low fractal dimension (D) and is nearly independent of cluster size for compact clusters. This is in agreement with previous theories. The magnitude of Fa_{crit} , however, does not seem to have a strong correlation with the fractal dimension of the cluster.

3. Erosion

Erosion of agglomerates due to hydrodynamic stresses occurs over long time scales and at low values of the fragmentation number ($Fa \ll Fa_{crit}$). The fragments eroded are much smaller than the parent particle (volume of fragment $< 10\%$ of volume of parent). Of primary interest from the viewpoint of dispersion of agglomerates is the rate of erosion and the size distribution of eroded fragments. Only a few studies focusing on these aspects have been carried out, and we summarize the main results here.

Erosion kinetics for compact spherical structures are well described by

$$\frac{R_0 - R(t)}{R_0} \approx k_e \dot{\gamma} t \quad (53)$$

at short times of erosion, where R is the radius of the parent agglomerate, R_0 is the initial radius, and k_e is a dimensionless erosion rate constant. This

equation implies that the rate of erosion (volume eroded per unit time) is directly proportional to the surface area of the parent. Thus, k_e is a first-order rate constant, and for long times $R \approx R_0 \exp(-k_e \dot{\gamma} t)$.

In the case of compact *cohesionless clusters* (no attractive forces between aggregates forming agglomerate), Powell and Mason (1982) found k_e to be independent of shear rate but dependent on flow type and the ratio (a/R_0) , where a is the radius of the primary particle (aggregate). In contrast, Rwei, Manas-Zloczower, and Feke (1991), in a study of compact carbon black agglomerates in simple shear flow, found k_e to depend only on the fragmentation number (Fa) based on experiments carried out at different shear rates and pellet densities (Fig. 33). The critical shear rate below which erosion stops was found to be $\mu\dot{\gamma}_{c,e} \approx 100$ Pa by extrapolating data obtained at different stresses to a zero erosion rate. Using the strength of agglomerates determined in their earlier work (Rwei *et al.*, 1990), the critical fragmentation number for erosion is obtained as $Fa_{c,e} \approx 2 \times 10^{-3}$, which is an order of magnitude lower than Fa_{crit} . The size (radius) distribution of the fragments was found to be Gaussian with a mean and standard deviation proportional to the initial radius of the parent. In a separate study, carried out at significantly higher values of Fa , Rwei, Manas-Zloczower, and Feke (1992) found the radius to decrease exponentially with time.

Physicochemical interaction between the agglomerate and fluid is an additional factor that affects the rate of erosion. For example, in a study of erosion under simple shear flow using four different types of titanium dioxide agglomerates in silicone oil, Lee, Feke, and Manas-Zloczower (1993) found k_e to be proportional to the product FaW_a , where W_a is the work of adhesion of the fluid to the particles (nearly equal to the dispersive component of the fluid interfacial tension). Further, increasing the particle porosity sharply increased the erosion rate. This is a consequence of the faster penetration of the fluid into the more porous agglomerates (initially dry), resulting in the reduction of the cohesive strength of the bonds between the primary particles. There is much that remains to be done in this area. For example, erosion of fractal structures does not seem to have been sufficiently studied.

Illustration: Kinetics of dispersion: the two-zone model. The models for agglomerate rupture when integrated with a flow model are useful for the modeling of dispersion in practical mixers, as was discussed for the case of drop dispersion. Manas-Zloczower, Nir, and Tadmor (1982), in an early study, presented a model for the dispersion of carbon black in rubber in a Banbury mixer (Fig. 34). The model is based on several simplifying assumptions: Fragmentation is assumed to occur by rupture alone, and each rupture produces two equal-sized fragments. Rupture is assumed to occur

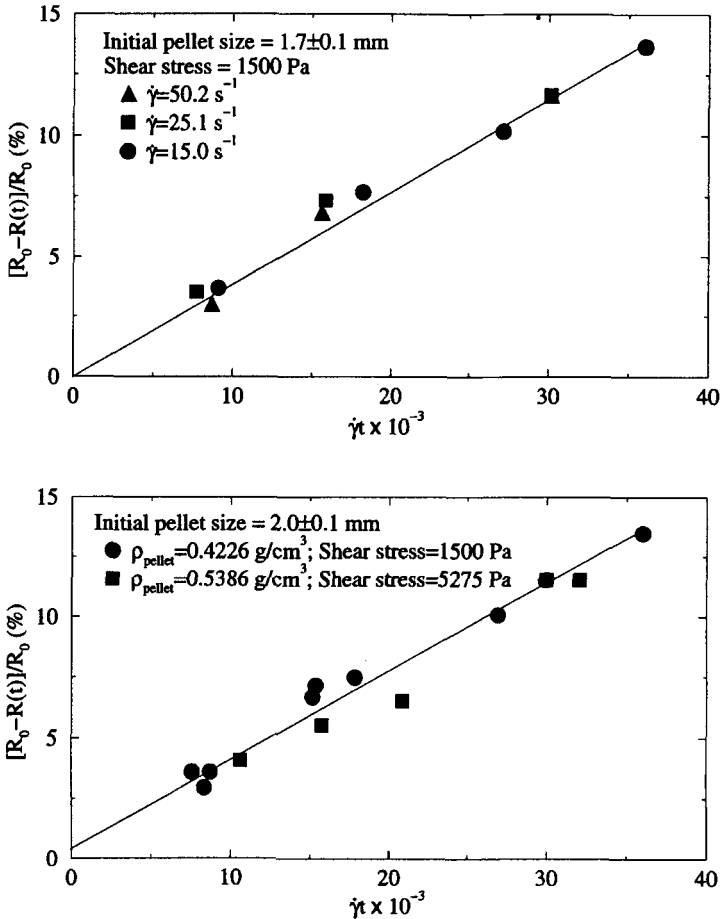


FIG. 33. Variation of dimensionless radius with dimensionless time for compact carbon black particles suspended in silicone oil undergoing a simple shear flow. *Top*: Data for initial radius $R_0 \approx 1.7$ mm for different viscosities and different shear rates, but with $Fa \approx 0.28$. *Bottom*: Data for initial radius $R_0 \approx 2.0$ mm for different densities and different shear rates, but with $Fa \approx 0.28$. For all cases the erosion rate constant $k_e \approx 0.37$. (See Eq. 53).

along a specific plane in the agglomerate (similar to the model of Kendall, 1988), but the strength of the agglomerate is calculated using Rumpf's (1962) model. Hydrodynamic forces are calculated assuming the agglomerate to be a pair of touching spheres [Eq. (39)]. The flow in the Banbury mixer is taken to be a well-mixed low-shear zone from which a stream is continuously passed through a small high-shear zone and recycled. Only a fraction of the agglomerates passing through the high-shear zone rupture,

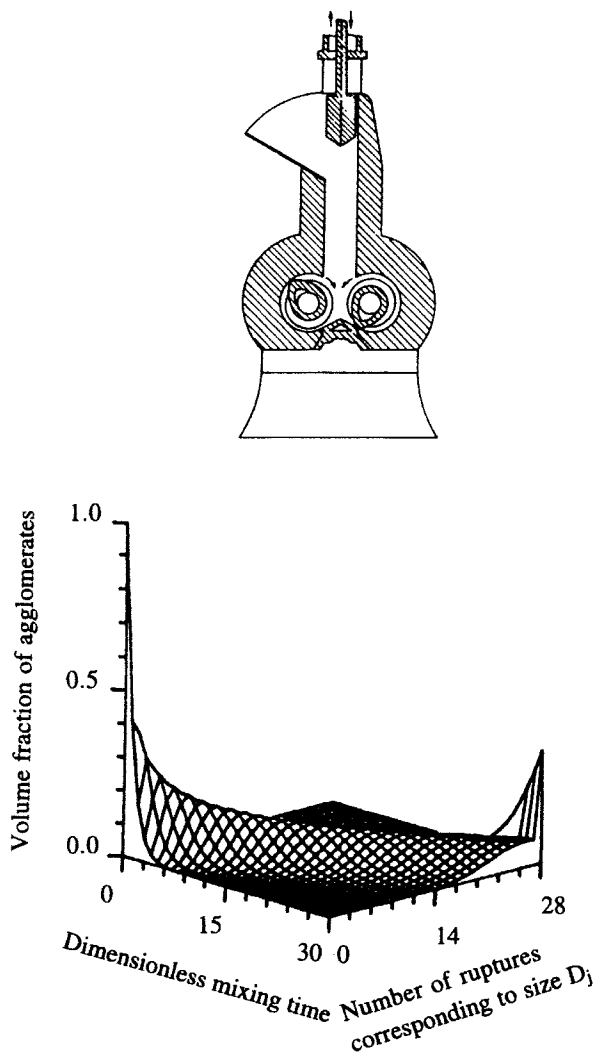


FIG. 34. *Top*: Schematic view of a Banbury mixer. *Bottom*: Evolution of the agglomerate size distribution with time predicted by the two-zone model with parameter values corresponding to the dispersion of carbon black in rubber in a Banbury mixer. The size of an agglomerate after j ruptures is given by $D_j = D_0/2^{j/3}$, where D_0 is the initial size of the agglomerates. The size of the aggregate (primary particle) corresponds to $j = 28$ (Manas-Zloczower, Nir, and Tadmor, 1982).

and this is determined by whether or not the rupture plane is exposed to a sufficiently high force. An agglomerate may break once at most during a single pass through the high-shear zone, and no fragmentation takes place in the low-shear zone. Statistical arguments are used to obtain the distribution for the number of passes made by an agglomerate through the high-shear zone, and to obtain the agglomerate size distribution.

In spite of the simplifying assumptions made in the model, the results give a qualitative insight into the operation of the process. Figure 34 shows the evolution of the agglomerate size distribution with time for a representative case. At the start of the process only large agglomerates (diameter D_0) are present; with increasing mixing time the distribution broadens and the peak shifts to smaller sizes. At the same time a new peak is formed corresponding to the aggregate size; aggregates cannot be further ruptured by the flow.

Illustration: Simultaneous erosion and rupture. Agglomerates when sheared at $Fa > Fa_{crit}$ fragment by both rupture and erosion mechanisms. Experiments of Rwei, Manas-Zloczower, and Feke (1992) for carbon black agglomerates in molten polystyrene show that rupture of the particles occurs within a short time of application of the shear flow, and a log-normal distribution of fragment sizes is produced. Subsequent shearing results only in a slow reduction of the average agglomerate size, and the average radius decreases exponentially with time ($R = R_0 \exp(-k_e \dot{\gamma} t)$) which is characteristic of erosion. Thus rupture and erosion can be considered to occur sequentially in homogeneous flows because of their different time scales. However, in flows with spatially varying shear rates, erosion would occur in all regions of the flow with varying rates depending on the local value of Fa , while rupture would result during the first visit of an agglomerate to a high shear zone where $Fa > Fa_{crit}$.

4. Global Scales: Particle Size Distributions

Analysis of the particle size distributions produced in fragmentation processes go back to the early work of Kolmogorov (1941). Considering that the size of fragments produced on breakage are random, Kolmogorov (1941) used statistical arguments, similar to those outlined earlier for the stretching distributions, to show that the size distribution is log-normal. A more general starting point for the study of dispersion of powdered solids is provided by the so-called fragmentation theory (Redner, 1990). Irreversible, continuous breakup of solids in a well-mixed batch system can be described by the linear fragmentation equation,

$$\frac{\partial c}{\partial t} = -a(x)c(x, t) + \int_x^\infty a(y)f(x|y)c(y, t) dy, \quad (54)$$

where $c(x, t)$ is the concentration of clusters of mass x at time t , $a(x)$ is the overall rate of breakup of clusters of size x , and $f(x|y)$, the relative rate of breakup, is the expected number of clusters of size x produced from the breakage of a cluster of size y .

The breakup kernels, $a(x)$ and $f(x|y)$, determine the kinetics of the fragmentation process. However, general conclusions can be drawn without exact specification of these kernels by scaling analysis of the fragmentation equations. For example, if small clusters break up like larger clusters, behavior experimentally observed in many systems, the breakage kernels are homogeneous. The overall rate of breakup in this case is given by $a(x) \sim x^\lambda$, where λ is known as the homogeneity index. Homogeneity also implies that the distribution of fragments produced on breakup is

$$f(x|y) = \frac{1}{y} b\left(\frac{x}{y}\right). \quad (55)$$

The average number of particles produced on a single breakup event is then $\int_0^1 b(r)dr$, and $\int_0^1 rb(r)dr = 1$, because of conservation of mass.

The fragmentation equation can be scaled into the following time-invariant form for the case of homogeneous kernels:

$$w \left[2\phi + \eta \frac{d\phi}{d\eta} \right] = -\eta^\lambda \phi + \int_\eta^\infty \xi^{\lambda-1} \phi(\xi) b\left(\frac{\eta}{\xi}\right) d\xi. \quad (56)$$

Here, both concentration and size are rescaled with respect to the average agglomerate size $s(t)$ as

$$\eta = x/s(t), \quad \phi(\eta) = c(x, t)/s^{-\theta}. \quad (57)$$

For conservation of mass it is required that $\theta = 2$. For the scaled equation (56) to be time-invariant, the separation constant (w) given by

$$w = -\frac{ds}{dt} s^{-(1+\lambda)} \quad (58)$$

must be independent of time. In general, this condition is satisfied at long times as the particle size distribution asymptotically approaches the self-similar distribution, independent of the initial condition.

Filippov (1961) rigorously showed the above scaling to be valid when λ is positive; if $\lambda < 0$ the scaling breaks down as mass is lost to the formation of infinitesimal size fragments (Filippov, 1961). For positive values of λ , Eq. (58) gives $s \sim t^{-1/\lambda}$ at long times.

The moments of order α of the bare and scaled size distribution are defined as

$$M_\alpha(t) \equiv \int_0^\infty x^\alpha c(x, t) dx, \quad \text{and} \quad m_\alpha \equiv \int_0^\infty x^\alpha \phi(x) dx, \quad (59)$$

respectively, and have the form of Mellin transforms (Morse and Feshbach, 1953). The moments have a physical significance for the process: for example, M_0 is the total number of clusters per unit volume, and M_1 is the total mass per unit volume. The *number* average size is then $s_n(t) = M_1/M_0$, and the *weight* average size is $s_w(t) = M_2/M_1$. Finally, the *polydispersity*, which characterizes the width of the distribution, is

$$P = \frac{s_w}{s_n} = \frac{M_2 M_0}{M_1^2}. \quad (60)$$

The scaled moments for the case of homogeneous kernels are obtained as

$$m_{\alpha+\lambda} = w \frac{1-\alpha}{L_\alpha-1} m_\alpha, \quad \text{with} \quad L_\alpha \equiv \int_0^1 r^\alpha b(r) dr \quad (61)$$

in the limit of long times when the scaling solution is valid. This recursive relationship between the scaled moments, and use of inverse Mellin transforms, allows the determination of the form of the scaling distribution for the tails of the size distribution (Cheng and Redner, 1990). In the limit of large mass [$x \gg s(t)$], the size distribution is

$$c(x, t) \sim \exp(-\text{const. } tx^\lambda). \quad (62)$$

The cluster size distribution in the limit of small mass [$x \ll s(t)$] depends on the properties of the agglomerates undergoing fragmentation. If infinitesimal particles are formed on a single breakage, that is, $b(r) \sim r^\nu$, then

$$c(x, t) \sim x^\nu \quad \text{as} \quad x \rightarrow 0, \quad (63)$$

and if clusters are broken into small fragments by several steps, then the distribution is log-normal in the limit of small x . This is in agreement with the theory of Kolmogorov (1941). Thus, limiting forms of the cluster size distribution are obtained by invoking only the assumption of homogeneous breakup kernels.

Several works over the past decade or so (Ziff, 1991; Ziff and McGrady, 1986; McGrady and Ziff, 1987, 1988; and Williams, 1990) have addressed the behavior of systems with specified breakup kernels. Certain specific forms for the breakup kernels lead to analytical solutions for the cluster size distribution. For example, Ziff (1991) obtained explicit forms of the size distribution for homogeneous breakup kernels of the form

$$b(r) = \alpha q r^{\alpha-2} + \beta(1-q)r^{\beta-2}, \quad (64)$$

where q , α , and β are adjustable parameters, which allow for fitting of a range of breakup processes. The limiting forms of these solutions are predicted by the preceding analysis.

5. Erosion-Controlled Fragmentation

The dynamics of the particle size distribution produced by fragmentation processes dominated by erosion are qualitatively different from those involving rupture. Although rate of breakage function is homogeneous [$a(x) = kx^1$] because the rate of erosion is proportional to surface area, the distribution of fragments produced on breakage, in general, is not homogeneous. As seen earlier, erosion produces small fragments with a relatively narrow Gaussian distribution. Thus, each erosion step may be considered as a binary breakup process forming one fragment of size ε and one of size $y - \varepsilon$, with $y \gg \varepsilon$. With these assumptions the relative rate of breakup becomes

$$f(x|y) = \delta(x - (y - \varepsilon)) + \delta(x - \varepsilon), \quad (65)$$

where y is the mass of the parent agglomerate and ε is the mass of the primary particle (aggregate).

A solution to this problem (Hansen and Ottino, 1996a) reveals that the cluster size distribution is bimodal, as expected, with $c(x,t)$ for large x dependent upon the initial conditions (Fig. 35a). The distribution thus does not approach a self-similar form and the scaling results just given are not valid for this problem. This is a result of the non-homogeneous relative rate of breakup.

Experimental data on erosion processes is limited—but there is some data from the comparable process of attrition. Neil and Bridgwater (1994) determine, by sieving, the cumulative mass fraction of clusters $M(l)$, with a characteristic length less than l . Hansen and Ottino (1996a) assume that $x \approx \pi \rho l^3/6$, where ρ is the density of the solids. Figure 35b shows the fitting to available experimental data. Deviation of the experimental data from the model could be due to inefficiencies in the sieving process, the assumed relationship between x and l , and/or the presence of rupture. Better data are clearly needed before hard conclusions can be drawn (concentrations would be more enlightening than cumulative mass, and the reported size distributions are relatively narrow). It is nevertheless apparent that the relative constancy of $M(l)$ with l indicates the presence of a bimodal distribution.

Advection is important in fragmentation processes, and an initially homogeneous system may evolve spatial variations due to spatially dependent fragmentation rates. For example, Fig. 36 shows the spatial distribution of eroded clusters in the journal bearing flow operating under good mixing

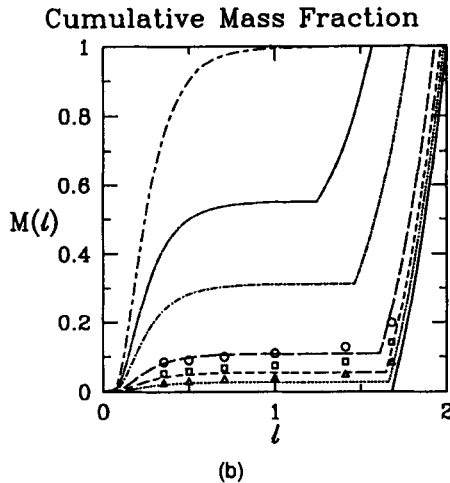
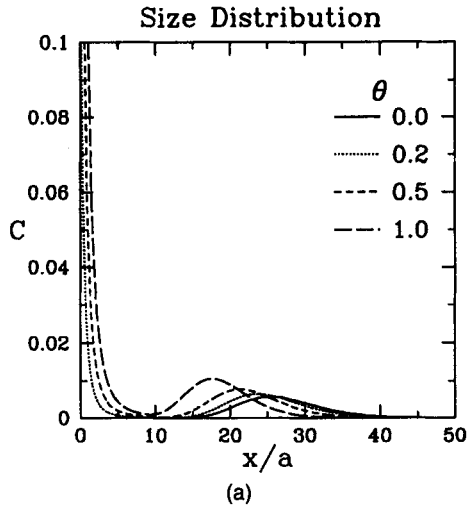


FIG. 35. (a) Size distributions $[c(x, q)]$ obtained for erosion-controlled fragmentation for increasing fragmentation time (q). (b) Comparison of theoretically predicted cumulative size distribution for erosion-controlled fragmentation to experimental data (Hansen and Ottino, 1996a).

and poor mixing conditions (Hansen, 1997). Clusters are eroded by hydrodynamic stresses and parent clusters are coded in the figure according to size. The aggregates eroded from the cluster are not shown. The poorly mixed system (Fig. 36a) shows large clusters (clusters eroded to a lesser extent) trapped in a regular island in which the shear rates are low, and

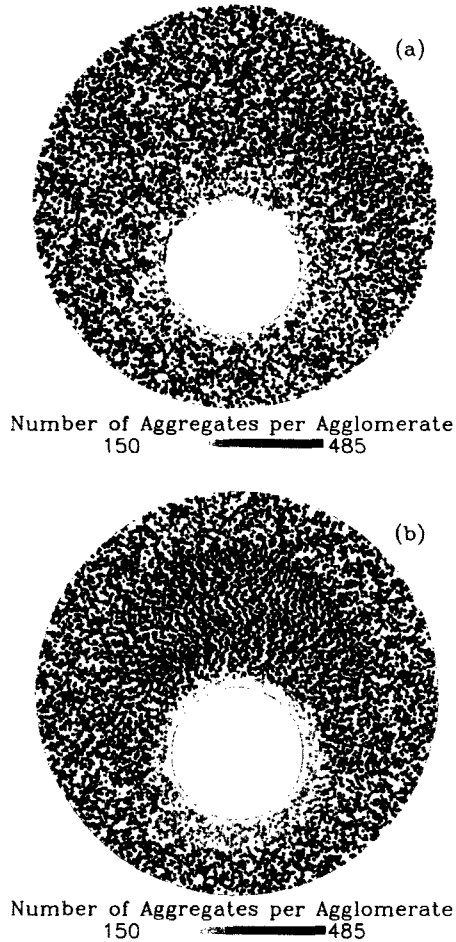


FIG. 36. The spatial variation of agglomerate sizes in simulations of erosion in the journal bearing flow. Initially there are 10000 agglomerates consisting of 400–500 aggregates. The grey scale represents the number of aggregates in the agglomerates. (a) Poorly mixed flow after four periods. (b) Well-mixed flow after one period (Hansen, *et al.* 1998).

small clusters near the inner cylinder where the shear rates are high. However, even the well-mixed system shows spatial variations of cluster sizes, indicating that the rate of mixing is not fast enough to eliminate the fluctuations produced by the spatially dependent fragmentation rate. Such spatial variations would undoubtedly cause deviations from predictions of mean field theories for the cluster size distribution.

Illustration: Size reduction by simultaneous erosion and rupture. Consider now continuous irreversible breakup by both rupture and erosion

mechanisms in a well-mixed system. As in the model of erosion discussed earlier, we assume that clusters consist of particles of mass ε , and that $\varepsilon \ll s(t)$, so that the discrete size distribution may be approximated as a continuum. The fragmentation equation for simultaneous rupture and erosion for the case of homogeneous rupture kernels is (Hansen and Ottino, 1996a)

$$\begin{aligned} \frac{\partial c(x, t)}{\partial t} = K \left\{ \frac{\partial}{\partial x} [x^\lambda c(x, t)] + \frac{\delta(x - \varepsilon)}{\varepsilon} \int_\varepsilon^\infty y^\lambda c(y, t) dy \right\} \\ - x^\sigma c(x, t) + \int_x^\infty y^{\sigma-1} b_r(x/y) c(y, t) dy, \end{aligned} \quad (66)$$

where λ and σ are the homogeneity indices for erosion and rupture, respectively. The first term on the right-hand side accounts for erosion, and the next two terms account for rupture.

A characteristic parameter of the process is the ratio of the overall rate of erosion relative to the overall rate of rupture given by

$$H \sim Ks(t)^{\lambda-\sigma-1}. \quad (67)$$

This ratio determines the applicability of the scaling solution: If $\lambda < \sigma + 1$, the scaling solution breaks down as $s(t)$ approaches zero.

Consider next the case of binary rupture when $\lambda = 0$, $s = 1$, and $b_r(x/y) = 2$. Assuming that fragments once eroded do not fragment further, an approximate form of the evolution equation for clusters larger than size ε is

$$\frac{\partial^2 c}{\partial x \partial t} = K \frac{\partial^2 c}{\partial x^2} - x \frac{\partial c}{\partial x} - 3c(x, t). \quad (68)$$

The mass of the eroded fragments can then be obtained from the mass balance. The solution breaks down as the average size (s) approaches the aggregate size (ε). Following Ziff and McGrady (1985), particle size distribution is obtained as

$$c(x, t) = (1 + t/s)^2 \exp[-(t + s)x - K(t^2/2 + ts)] \quad (69)$$

for the initial condition $c(x, 0) = e^{-sx}$. Since the kinetic equation (68) is linear, the solutions for other initial conditions are easily obtained by superposition.

HEURISTICS

- Erosion:

Occurs even at low fragmentation numbers, and over long time scales
Rate of erosion is directly proportional to the fragmentation number

and the surface area of the parent agglomerate

Bimodal cluster size distribution

Model computations indicate that for short times, polydispersity is inversely proportional to average size

Size distribution is not self-similar

- Rupture:

Occurs rapidly once the fragmentation number exceeds the critical value

Size distributions of fragments produced in a single rupture event are self-similar

For fractal agglomerates, the critical fragmentation number is inversely proportional to its volume $(R/a)^3$

Homogeneous breakage kernels with positive homogeneity index ($\lambda > 0$) produce self-similar size distributions at long times

B. AGGREGATION

Aggregation of particles may occur, in general, due to Brownian motion, buoyancy-induced motion (creaming), and relative motion between particles due to an applied flow. Flow-induced aggregation dominates in polymer processing applications because of the high viscosities of polymer melts. Controlled studies—the counterpart of the fragmentation studies described in the previous section—may be carried out in simple flows, such as in the shear field produced in a cone and plate device (Chimmili, 1996). The number of such studies appears to be small.

At the simplest level, the rate of flow-induced aggregation of compact spherical particles is described by Smoluchowski's theory [Eq. (32)]. Such expressions may then be incorporated into population balance equations to determine the evolution of the agglomerate size distribution with time. However with increase in agglomerate size, complex (fractal) structures may be generated that preclude analysis by simple methods as above.

Let us illustrate first how different (idealized) aggregation processes may result in different structures. There is extensive literature on *diffusion-limited aggregation* (DLA) (for a comprehensive review, see Meakin, 1988). Three methods of simulation are common: (standard) diffusion-limited aggregation (DLA), reaction-limited aggregation (RLA), and linear trajectory aggregation (LTA). DLA structures are generated by placing a seed particle in the middle of a lattice. Other particles are placed in the lattice

and follow a random walk trajectory. These moving particles bind onto the growing seed upon contact to form a cluster. In general, clusters produced by DLA simulations are fractal, and the fractal dimension of the clusters is approximately 2.5 (Fig. 37). The difference between RLA and DLA is that a sticking probability governs the binding in RLA. Thus, particles penetrate further into the growing agglomerate, and denser agglomerates are formed. The dimension of RLA clusters is greater than 2.5 and increases with a decreasing sticking probability. LTA is similar to DLA, with particles following a random linear trajectory instead of a random walk. LTA, which models agglomerates formed by mechanical motion such as a mixing processes, yields compact structures with a fractal dimension close to 3.

Unlike the simulations which only consider particle-cluster interactions discussed earlier, hierarchical cluster-cluster aggregation (HCCA) allows for the formation of clusters from two clusters of the same size. Clusters formed by this method are not as dense as clusters formed by particle-cluster simulations, because a cluster cannot penetrate into another cluster as far as a single particle can (Fig. 37). The fractal dimension of HCCA clusters varies from 2.0 to 2.3 depending on the model used to generate the structure: DLA, RLA, or LTA. For additional details, the reader may consult Meakin (1988).

The direct relevance of these diffusion-driven aggregation models to flow-driven aggregation is somewhat questionable, though they serve to highlight the influence of the aggregation process on the structures produced. These models have been used to synthesize structures to investigate how they break (Horwatt *et al.* 1992a,b).

Flow-induced aggregation may also result in the formation of agglomerates with complex (fractal) structure (Jiang and Logan, 1996). An understanding of the structures formed in the aggregation process is important—the kinetics of the aggregation is significantly affected by the type of structures formed, as we will see in the following sections. The kinetics in turn affect the evolution of the agglomerate size distribution, which is the quantity of primary interest from a practical viewpoint.

1. Global Scales: Agglomerate Size Distributions

Analytical approaches to obtain the agglomerate size distribution are possible for well-mixed systems and when the rate of aggregation of clusters is defined by simple functions. In general, irreversible aggregation in well-mixed systems is described by Smoluchowski's coagulation equation, which

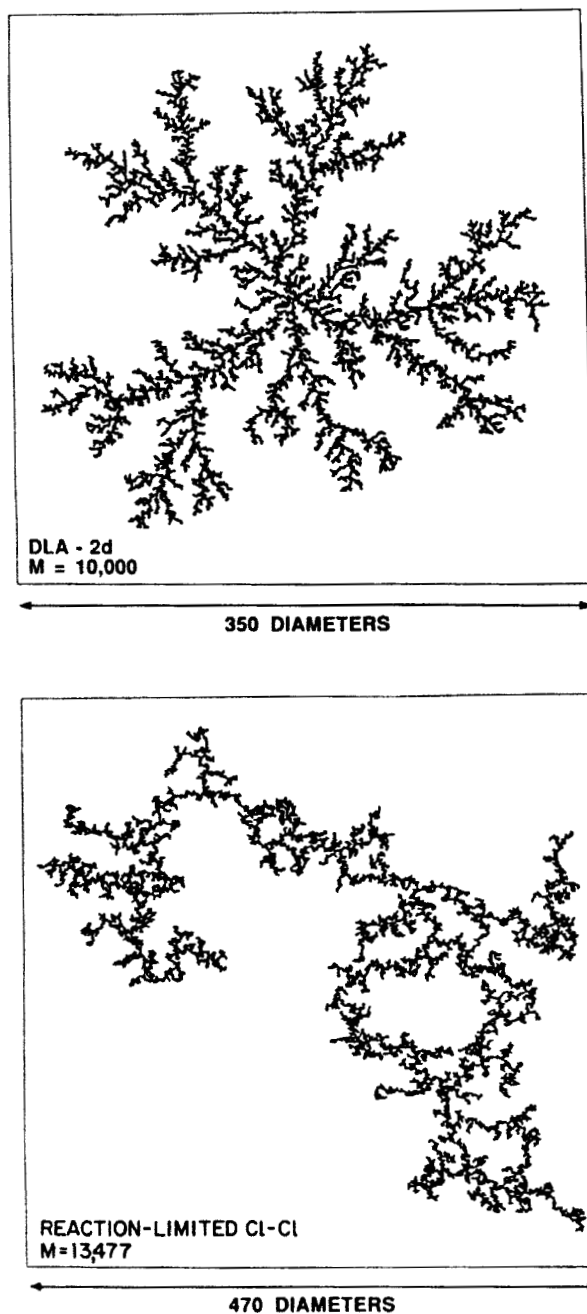


FIG. 37. Typical clusters obtained by diffusion-limited aggregation (DLA). *Top*: Two-dimensional diffusion-limited aggregation. *Bottom*: Reaction-limited hierarchical cluster-cluster aggregation (HCCA) (Meakin, 1988 with permission, from the *Annual Review of Physical Chemistry*, Vol. 39, © by Annual Reviews www.Annual/Reviews.org).

for a continuous distribution of cluster sizes can be written as

$$\begin{aligned} \frac{\partial c(x, t)}{\partial t} = & \frac{1}{2} \int_0^x K(x-y, y) c(x-y, t) c(y, t) dy \\ & - c(x, t) \int_0^\infty K(x, y) c(y, t) dy, \end{aligned} \quad (70)$$

where $c(x, t)$ is the concentration of clusters of mass x at time t and $K(x, y)$ is the rate of aggregation of clusters of masses x and y (van Dongen and Ernst, 1988). The first term on the right-hand side accounts for the formation of a cluster of size x due to aggregation of two clusters of size $x-y$ and y , whereas the second term represents the loss of clusters of mass x . There are significant parallels between this equation and the fragmentation equation.

Scaling solutions, as in the case of fragmentation, are possible if the kernel $K(x, y)$ is homogeneous, which requires that

$$K(\xi x, \xi y) = \xi^\kappa K(x, y), \quad (71)$$

where κ is the homogeneity index. This condition is not very restrictive; for example, the aggregation rate given by Smoluchowski's theory [Eq. (32)] is homogeneous with $\kappa = 1$. Time-invariant scaled solutions are obtained in this case if the concentration is scaled as

$$c(x, t) = x^{-2} \psi(\eta), \quad (72)$$

where $\eta = x/s(t)$ and $s(t)$ is the average size, as defined earlier. The relationship between the scaled concentration for fragmentation (ϕ) and ψ is then

$$\psi(\eta) = \eta^2 \phi(\eta). \quad (73)$$

This scaling (or self-similarity) is verified by numerous computational and theoretical studies (for a review, see Meakin, 1992).

For many well-studied rate of aggregation kernels, the average cluster size grows algebraically, $s(t) \sim t^z$. In fact, when $K(x, y)$ is homogeneous and κ , as defined in Eq. (73), is less than unity, we get $z = 1/(1-\kappa)$. When $\lambda > 1$, loss of mass to the formation of infinite size clusters—the opposite of shattering in fragmentation, termed gelling—occurs in finite time.

Smoluchowski's equation, like the fragmentation equation, can be written in terms of the scaling distribution. Furthermore, general forms may be determined for the tails of the scaling distribution—limits of small mass, $x/s(t) \ll 1$, and large mass, $x/s(t) \gg 1$. The details can be found in van Dongen and Ernst (1988).

If the scaling form given earlier holds, then the bare and scaled moments are related by

$$M_\alpha = s(t)^{\alpha-1} m_\alpha. \quad (74)$$

Hence, the polydispersity [Eq. (60)] is independent of time, provided $\int_0^\infty \phi(\eta) d\eta$ is bounded. Moreover, if $\phi(\eta) = e^{-\eta}$, as is expected for a rate of aggregation independent of mass (Schumann, 1940), the polydispersity is equal to 2. Also note that

$$\frac{M_\alpha}{M_{\alpha-1}} \sim \frac{M_2}{M_1}, \quad (75)$$

and therefore number average and weight average sizes are proportional to each other when scaling used for the fragmentation equation is applicable and the integral of $\phi(\eta)$ is bounded.

Illustration: Short-time behavior in well mixed systems. Consider the initial evolution of the size distribution of an aggregation process for small deviations from monodisperse initial conditions. Assume, as well, that the system is well-mixed so that spatial inhomogeneities may be ignored. Of particular interest is the growth rate of the average cluster size and how the polydispersity scales with the average cluster size.

This can be done by developing equations for the moments—for example, multiplying Smoluchowski's equation by $x^\alpha dx$, integrating from 0 to infinity, and manipulating the limits of integration yields (Hansen and Ottino, 1996b):

$$\frac{dM_\alpha}{dt} = \frac{1}{2} \int_0^\infty \int_0^\infty [(x+y)^\alpha - (x^\alpha + y^\alpha)] K(x, y) c(x, t) c(y, t) dx dy. \quad (76)$$

Expanding the new kernel,

$$Q_\alpha(x, y) = [(x+y)^\alpha - (x^\alpha + y^\alpha)] K(x, y), \quad (77)$$

in a series about the average cluster size yields

$$Q_\alpha(x, y) \approx s^{\alpha+1} \left\{ Q_\alpha(1, 1) + \frac{\partial Q_\alpha(1, 1)}{\partial x} \left(\frac{x}{s} - 1 \right) + \frac{\partial Q_\alpha(1, 1)}{\partial y} \left(\frac{y}{s} - 1 \right) + \dots \right\}, \quad (78)$$

where $\partial Q_\alpha(1, 1)/\partial x$ denotes $\partial Q_\alpha/\partial x$ evaluated at $x = 1$ and $y = 1$ (this assumes that most of the clusters are relatively close to the average cluster size, i.e., the polydispersity is close to unity). Considering the number average cluster size $s(t) = M_1/M_0$, we determine that

$$\frac{ds}{dt} = \frac{M_1}{2M_0^2} \int_0^\infty \int_0^\infty K(x, y) c(x, t) c(y, t) dx dy, \quad (79)$$

which can be rewritten in terms of the moments as

$$\frac{ds}{dt} \approx \frac{M_1}{2} \left\{ K(1,1) + \frac{\partial^2 K(1,1)}{\partial x^2} \left[\frac{M_2 M_0}{M_1^2} - 1 \right] + \dots \right\} s^\kappa, \quad (80)$$

where the higher-order terms include combinations of larger moments that are small when the polydispersity is near unity. Hence, when the polydispersity is close to unity the average cluster size is described by

$$s(t) = \begin{cases} s_0 \left(1 + (1 - \kappa) \frac{t}{\tau} \right)^{1/(1-\kappa)} & \text{for } \kappa \neq 1 \\ s_0 \exp\left(\frac{t}{\tau}\right) & \text{for } \kappa = 1 \end{cases} \quad \text{with } \tau = \frac{2s_0^{1-\kappa}}{M_1 K(1,1)}. \quad (81)$$

Here s_0 denotes the initial average cluster size.

Similar arguments can be used to determine the behavior of the zeroth and second moments. For example, the polydispersity evolves according to

$$P \approx \frac{1}{\beta} \left[\left(\frac{s(t)}{s_0} \right)^\beta - 1 \right] + 1, \text{ where } \beta = \left[\frac{4}{K(1,1)} \frac{\partial K(1,1)}{\partial x} - 1 \right], \quad (82)$$

for polydispersities near unity.

It should be noted that the predictions for the number average cluster size and polydispersity agree with analytical results for $K(x, y) = 1, x + y$, and xy . Furthermore, the short-time form of number average size in Eq. (81) matches the form of $s(t)$ predicted by the scaling ansatz. Computational simulations (Hansen and Ottino, 1996b) also verify these predictions (Fig. 38).

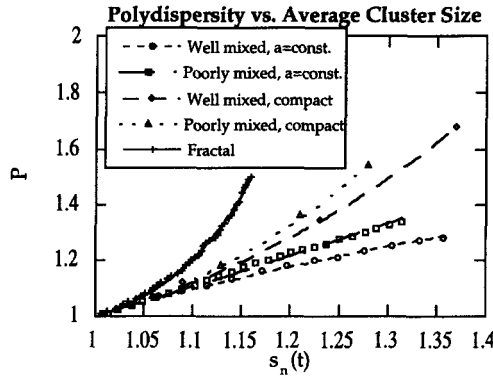


FIG. 38. Variation of polydispersity with average cluster size at short times in a journal bearing flow. The symbols are from simulations and the lines are fits from Eq. (82). The regular flow is the journal bearing flow with only the inner cylinder rotating (Hansen and Ottino, 1996b).

2. Size Distributions for Flow-Induced Aggregation

In this section, we consider flow-induced aggregation without diffusion, i.e., when the Péclet number, $Pe \equiv VL/D$, where V and L are the characteristic velocity and length and D is the Brownian diffusion coefficient, is much greater than unity. For simplicity, we neglect the hydrodynamic interactions of the clusters and highlight the effects of advection on the evolution of the cluster size distribution and the formation of fractal structures.

Torres, Russel, and Schowalter (1991a,b) have examined structure formation due to aggregation driven by shear and elongational flows. Two cases were computationally examined: *particle-cluster* aggregation, and *cluster-cluster* aggregation. In the case of particle-cluster aggregation, a particle is placed at a random position relative to the cluster and is advected by the flow. Rapid coagulation is assumed so that the particle aggregates with the cluster upon collision. The cluster-cluster aggregation procedure is similar but with the particle replaced by a cluster of the same size as the site cluster. Clusters formed in particle-cluster simulations are denser than suggested by experiments (Torres *et al.*, 1991a). On the other hand, the cluster-cluster simulations agree with experiments in shear flows carried out by the same investigators, suggesting that the formation of clusters is dominated by cluster-cluster aggregation. The fractal dimension of the aggregates formed in both shear and elongational flows by the cluster-cluster simulations is about 1.8 (Torres *et al.*, 1991b).

Only a few studies have considered aggregation in complex flows, in particular chaotic flows. Unlike studies of aggregation by kinetic equations, these simulations allow for spatial variations. A computational study (Muzzio and Ottino, 1988), focusing on compact clusters in a 2D chaotic flow (blinking vortex flow), shows that islands of regularity may cause spatial variations in the rate of aggregation, and that aggregation in “well-mixed” chaotic systems is similar mathematically to Brownian aggregation and can be described by Smoluchowski’s equation. The effect of mixing on the fractal nature of clusters is considered explicitly by Danielson *et al.* (1991). They determined that the fractal dimension can be controlled by varying the degree of mixing in chaotic flows. The variation of fractal dimension with mixing is due to the nature of interactions of monomers and larger clusters in different mixing schemes. If the system is not well mixed (large islands), the large clusters, which are trapped in islands, do not interact with each other and the process resembles the particle-cluster aggregation of Torres *et al.* (1991b). However, if the system is well mixed (no islands), then larger clusters interact with each other and aggregation resembles cluster-cluster aggregation. Thus, the fractal dimension of a cluster is expected to decrease with better mixing.

We focus on aggregation in model, regular and chaotic, flows. Two aggregation scenarios are considered: In (i) the clusters retain a compact geometry—forming disks and spheres—whereas in (ii) fractal structures are formed. The primary focus of (i) is *kinetics and self-similarity* of size distributions, while the main focus of (ii) is the *fractal structure* of the clusters and its dependence with the flow.

Illustration: Aggregation in chaotic flows with constant capture radius.

Here we consider aggregation in a physically realizable chaotic flow, the journal bearing flow or the vortex mixing flow described earlier. The computations mimic fast coagulation; particles seeded in the flow are convected passively and aggregate upon contact. In this example the clusters retain a spherical structure and the capture radius is independent of the cluster size.

The evolution of the average cluster size is shown in Fig. 39a. In a well-mixed system the growth of the average cluster size is linear with time (Hansen and Ottino, 1996b). In a poorly mixed system, a system with small chaotic regions, the average cluster size grows less fast $(1 + t/\tau)^{0.6}$, with a small variation in the exponent with the capture radius of the clusters. The growth of the average cluster in a regular flow, i.e., no chaos present, is included for completeness. Intuitively, one may expect the aggregation in the poorly mixed system to be a hybrid of aggregation in the well-mixed flow and in the regular flow, but this is not the case. Surprisingly, the growth rate of the average cluster in the regular flow, approaching linear growth, is faster than in the poorly mixed flow.

As previously discussed, we expect the scaling to hold if the polydispersity, P , remains constant with respect to time. For the well-mixed system the polydispersity reaches about 2 when the average cluster size is approximately 10 particles, and statistically fluctuates about 2 until the mean field approximation and the scaling break down, when the number of clusters remaining in the system is about 100 or so. The polydispersity of the size distribution in the poorly mixed system never reaches a steady value. The ratio M_3M_1/M_2^2 , which is constant if the scaling holds and mass is conserved, is also unsteady in the poorly mixed flow, indicating that the cluster size distribution is not self-similar in poorly mixed flows. The polydispersities of the clusters in the poorly-mixed and well-mixed flows are compared in Fig. 39b. The polydispersity of clusters in a regular flow, also included in Fig. 39b, initially increases, then slowly approaches unity as the number of clusters approaches 1. The higher polydispersity for clusters formed in the poorly mixed flow is indicative of the wider range of cluster sizes present in the system.

The self-similar nature of the cluster size distributions for the well-mixed flow is shown in Fig. 39c. Because of the discrete nature of cluster size in

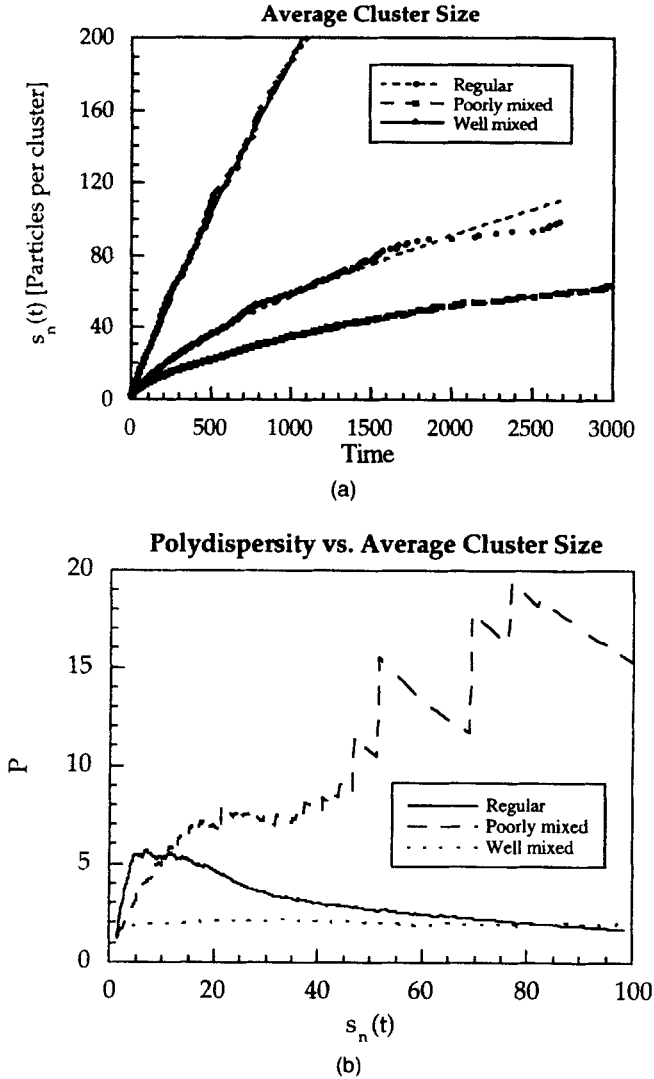


FIG. 39. (a) The growth of average cluster size for clusters with a constant capture radius in various 2D flows. (b) Variation of polydispersity with average cluster size. (c) Scaled distribution of the cluster sizes at different times. The regular flow is the journal bearing flow with only the inner cylinder rotating. One time unit is equivalent to the total displacement of the boundaries equal to the circumference of the outer cylinder (Hansen and Ottino, 1996b).

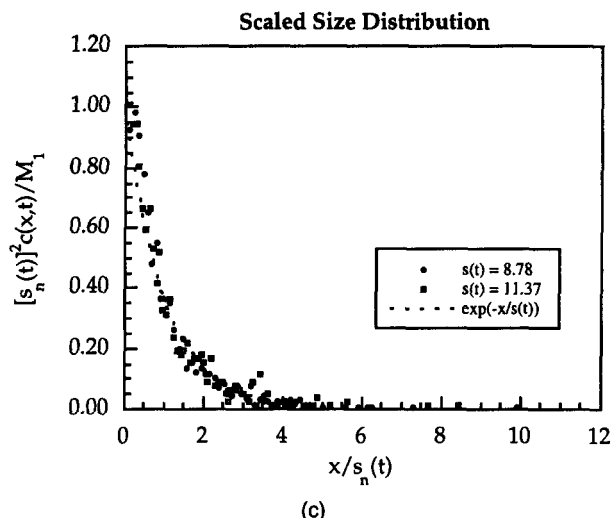


FIG. 39 (continued)

the simulations, this figure shows the cumulative mass fraction, as it is less prone to statistical fluctuations (a scaled cluster size distribution is also included for clarity). It should be noted that the cumulative size distribution scales as

$$M(x, t) = \int_0^x y c(y, t) dy = \int_0^{x/s(t)} \eta \phi(\eta) d\eta. \quad (83)$$

Thus, we plot $M(x, t)/M_1$ vs $x/s(t)$. As noted earlier, the cluster size distribution and the first moment of the size distribution are averaged over the entire journal bearing. As indicated by the behavior of P in Fig. 39b, the cluster size distribution becomes self-similar when the average size is about 10 particles per cluster.

Illustration: Aggregation of area-conserving clusters in two dimensional chaotic flows. Particles, convected passively in a two-dimensional chaotic flow, aggregate on contact to form clusters. The capture radius of the clusters increases with the size of the cluster. Since these simulations are in two dimensions, the area of the aggregating clusters is conserved.

The rate of aggregation of clusters with the same capture radius in two dimensions is proportional to the area of the cluster (Muzzio and Ottino, 1988). If this dependence of the rate of aggregation on cluster size holds for clusters with different capture radii, then the aggregation in these simulations is on the verge of gelation (van Dongen and Ernst, 1988). Simulations show that for aggregation of area-conserving clusters the formation of one large cluster predominates, but an infinite cluster is not formed since the

system is finite. This large cluster is formed before the scaling distribution is reached.

In a system with a small chaotic region, the rate of aggregation in the regular region is significantly slower than in the chaotic region. Thus, the polydispersity of the clusters remains large until the regular region is “broken” by the increasing capture radius of the cluster. However, the regular region retains its identity if the capture radius of the clusters does not become large enough that clusters in the regular region aggregate with clusters in the chaotic region.

As shown in Fig. 40, the average cluster size in a well-mixed or chaotic system evolves as $(1 + t/\tau)^6$. There are small variations in the exponent with the area fraction of the clusters. The growth rate of the average cluster size in a poorly mixed system follow the same form; however, the exponent is quite different. In a poorly mixed system, the exponent is dependent on the area fraction of clusters. For one flow studied, when the area fraction of clusters is 0.02 the exponent is 0.81. When the area fraction of clusters is increased to 0.1, the rate of aggregation increases dramatically—the exponent is 25. In fact, it is difficult to determine if this high rate of aggregation is algebraic or exponential. This implies that above some critical area fraction of clusters the large clusters are more likely to aggregate, whereas small clusters are more likely to aggregate below some critical area fraction of clusters. In the poorly mixed system, it appears that the growth rate changes as aggregation proceeds because clusters in the chaotic region become large enough to aggregate with clusters in the regular region.

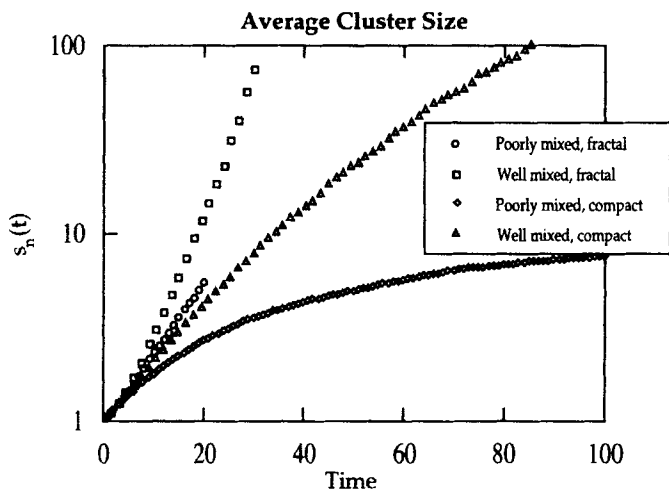


FIG. 40. Growth of average cluster size for area conserving clusters and fractal clusters in the journal bearing flow (Hansen and Ottino, 1996b).

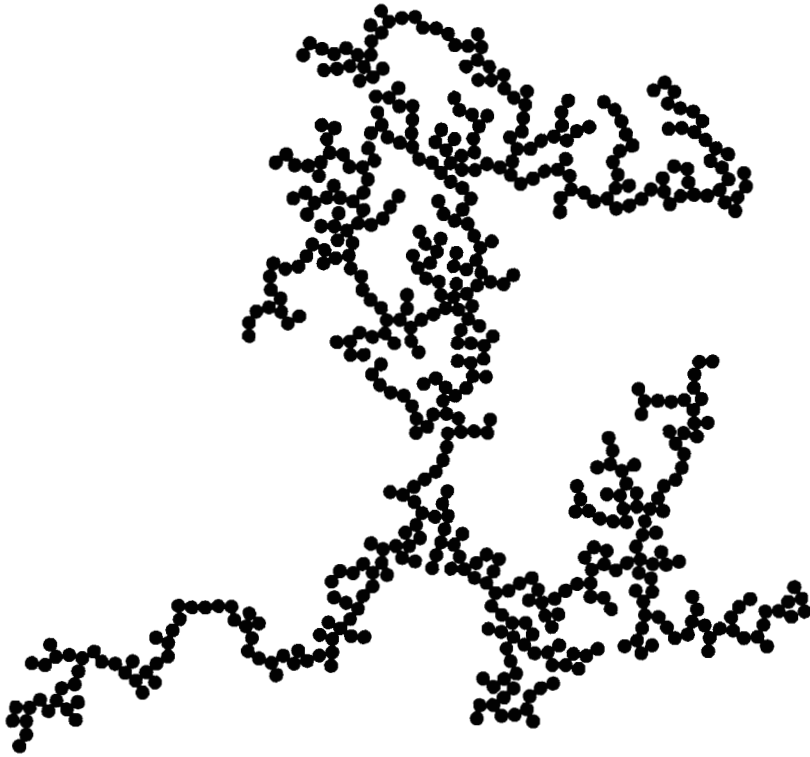


FIG. 41. Typical 2D fractal structure obtained by aggregation of particles in the journal bearing flow. Fractal dimension of the cluster is 1.54 (Hansen and Ottino, 1996b).

Illustration: Aggregation of fractal structures in chaotic flows. In a further study of aggregation in two-dimensional chaotic flows, the passively convected clusters retain their geometry after aggregation, i.e., fractal structures are formed. A typical fractal cluster resulting from these simulations is shown in Fig. 41.

The kinetics of fractal structures differ significantly from the kinetics of compact structures. As with the area-conserving compact structures, no self-similar distribution is observed. However, fractal clusters grow faster than compact structures. This is highlighted in Fig. 40, which illustrates that the average cluster size of fractal structures grows nearly exponentially, while the average cluster size of compact structures grows algebraically. The growth of fractal structures in the poorly mixed system is accurately described by $s(t) = s_0 \exp(t/\tau)$; however, aggregation in the well-mixed system may only be approximated by the exponential form. Interestingly, the overall rate of aggregation of fractal structures is first order, while the

overall rate of aggregation of clusters with a constant capture radius is second order in the well-mixed system. The rate of aggregation of area-conserving clusters fits between first order and second order.

Note that only one system, the one corresponding to constant capture radius clusters in chaotic flows, behaves as expected via mean field predictions. In general, the average cluster size grows fastest in the well-mixed system. However, in some cases the average cluster size in the regular flow grows faster than in the poorly mixed system.

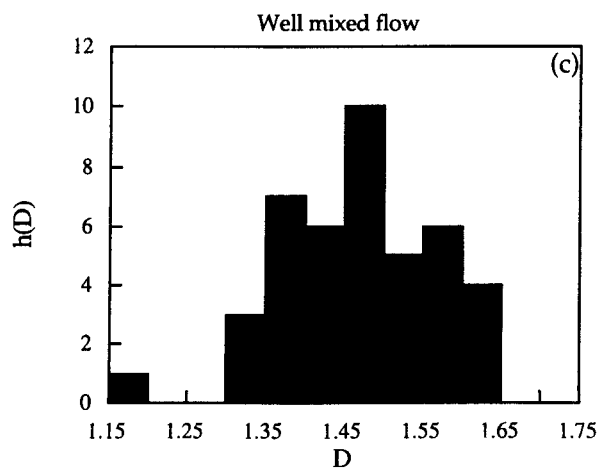
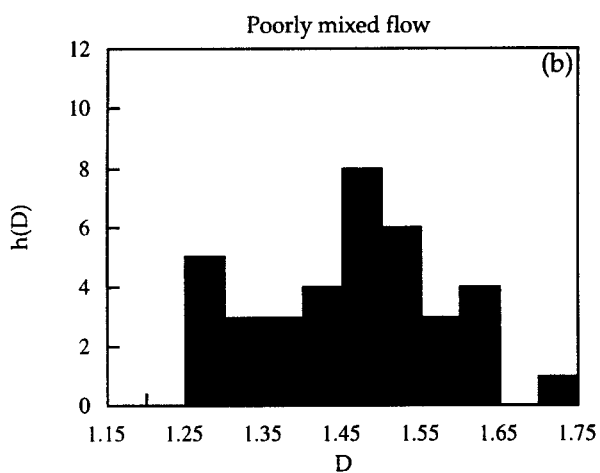
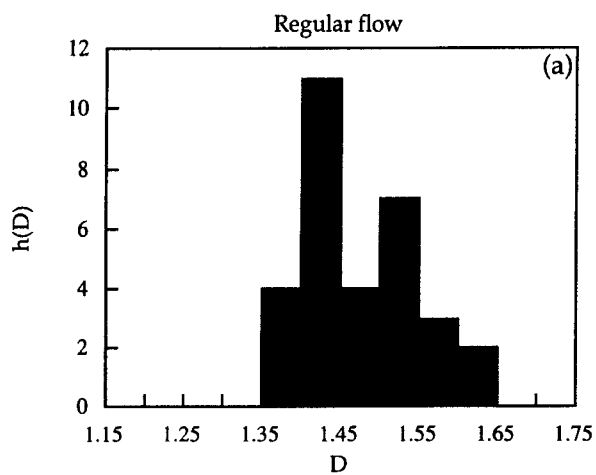
Furthermore, since the average cluster size of fractal clusters grows exponentially, we do not expect the scaling to hold. The argument is that κ would be unity if the scaling ansatz were applicable here, but that the scaling is not valid for $\kappa \geq 1$ and therefore not applicable to this case. Indeed, the polydispersity does not approach a constant value, indicating that the scaling does not apply. Again, significant differences between the polydispersities of fractal structures and compact structures are shown in Fig. 38. Initially, P increases rapidly; as is shown in Fig. 38, the polydispersity of fractal clusters grows faster than the polydispersity of their compact counterparts. Furthermore, in these simulations, P of fractal structures approaches unity sooner.

The long-time behavior of the polydispersity suggests that only one system, the well-mixed system with constant capture radius, may be described by the scaling ansatz. The scaling breaks down in poorly mixed systems because of spatial fluctuations. In other systems, aggregation of area-conserving or fractal clusters, the scaling breaks down because aggregation is dominated by formation of one or several large clusters.

The fractal nature of the structures is also of interest. Because of the wide range of flow in the journal bearing, a distribution of fractal clusters is produced. When the area fraction of clusters is 0.02, the median fractal dimension of the clusters is dependent on the flow, similar to the study by Danielson *et al.* (1991). The median fractal dimension of clusters formed in the well-mixed system is 1.47, whereas the median fractal dimension of clusters formed in the poorly mixed case is 1.55. Furthermore, the range of fractal dimensions is higher in the well-mixed case.

The results are different when the area fraction of clusters increases. The distribution of the fractal dimension of the clusters for a system with an area fraction of clusters of 0.10 is shown in Fig. 42. The median fractal dimension of the clusters is independent of the flow and is approximately

FIG. 42. Distribution of the fractal dimensions of the clusters generated by aggregation in the journal bearing flow for different flow types (Hansen and Ottino, 1996b).



1.47. Since the fractal dimension of the clusters is closer to the dimension of the clusters in the well-mixed system with a lower area fraction of clusters, this suggests that as the area fraction of clusters increases, the island of regularity gets broken up by the increasing capture radius of the clusters. Thus, aggregation in the poorly mixed system behaves similarly to that in the well-mixed system when aggregation occurs between the two disjoint regions of the flow.

HEURISTICS

- Rate of aggregation of compact clusters in well-mixed systems follows Smoluchowski's theory.
- Fractal dimension of clusters formed by flow-induced aggregation is independent of local flow type.
- Fractal dimension depends on mixing in chaotic flows: good mixing (no islands) gives lower fractal dimensions.
- Model computations indicate that the *average cluster size*:

Grows algebraically for compact structures; linearly for constant capture radius clusters in a well-mixed system.

Grows exponentially for fractal structures.

Has the fastest rate of growth in well-mixed systems.

- Model computations indicate that the *polydispersity*:

For short times is predicted by Eq. (82)

For long times is

- (i) Constant ~ 2 for constant capture radius clusters in a well-mixed system.
 - (ii) Nonconstant for poorly mixed systems, and for area-conserving compact and fractal clusters.
-

IV. Concluding Remarks

The modeling of mixing processes has undergone exciting progress in the past few years. Computations have reached maturity and exploitation of concepts and results in the context of realistic devices is now a reality (Avalosse and Crochet, 1997a,b). But much, if not all, of the advances have been restricted to single-phase fluids. One would expect that similar advances will take place in dispersion of solids and liquids in viscous flows. One may also speculate as to whether modeling or theory will drive experi-

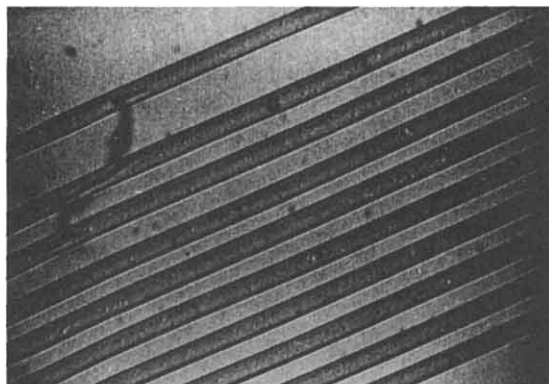
ments or the other way around. One might argue that as things are now, theory is ahead and that more experiments are badly needed. But the theory picture, described at length in the previous sections, is clearly incomplete and one may argue that more realism is needed.

As pointed out earlier most of the examples involve "one-sided" interactions: the microstructures are acted on by the chaotic flow, but they do not modify the flow structure itself. Not much has been done regarding these interactions in the context of chaos and mixing, and it is probably useful to point out here whatever little is known. An example of coupling involves dilute viscoelastic fluids (polymer solutions) in chaotic flows. A general finding is that the *rate* of mixing seems always to be slowed down by elasticity. A second general example along the lines of microstructures and flow is the presence of a dispersed phase that alters the flow patterns, and computational studies have shown how regular islands can be broken as a consequence. Little is known, in general, in this case as well.

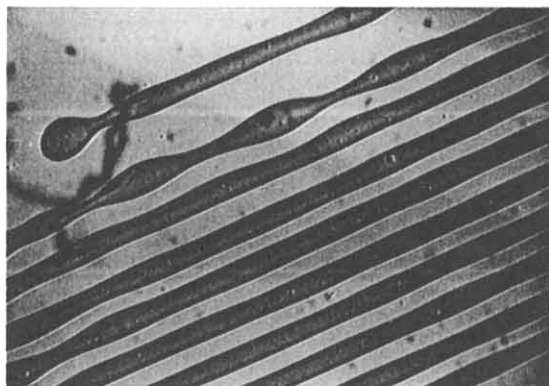
The caveats notwithstanding practical applications based on already existing theory seem possible. Zumbrunnen *et al.* have studied experimentally the possibility of developing fine-scale structures of dispersed phases by exploiting chaotic three-dimensional flows (Liu and Zumbrunnen, 1996; Zumbrunnen, Miles, and Liu, 1996), and Liu and Zumbrunnen (1997) note that significant improvements in impact properties of a polystyrene matrix can be achieved by adding small volume fraction ($\sim 9\%$) of low-density polyethylene. As opposed to conventional dispersion methods, where the minor phase may consist of randomly distributed small droplets, controlled chaotic mixing produces highly connected stretched and folded structures that can be preserved upon solidification.

The interaction between the dispersed-phase elements at high volume fractions has an impact on breakup and aggregation, which is not well understood. For example, Elemans *et al.* (1997) found that when closely spaced stationary threads break by the growth of capillary instabilities, the disturbances on adjacent threads are half a wavelength out of phase (Fig. 43), and the rate of growth of the instability is smaller. Such interaction effects may have practical applications, for example, in the formation of monodisperse emulsions (Mason and Bibette, 1996).

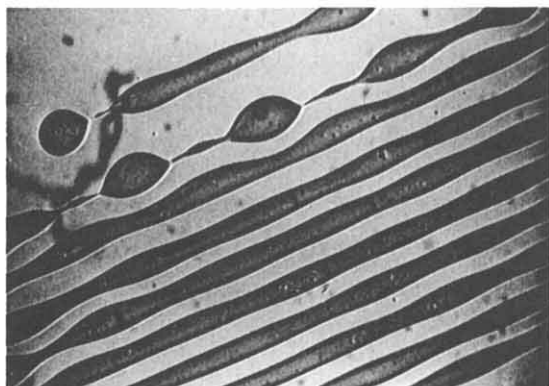
Although the fundamentals of breakup of drops are reasonably well-understood, the physics of the fragmentation of clusters is not as well grounded. Characterization of the structure and the measurement of the strength of agglomerates need to be addressed in greater detail. However, as in the case of liquid-liquid dispersions, existing concepts provide inspiration for possible new technologies, as suggested, for example, by Danescu and Zumbrunnen (1997) for the case of conductive composites involving small volume fraction of a conductive component. Both extremes, no-



(a)

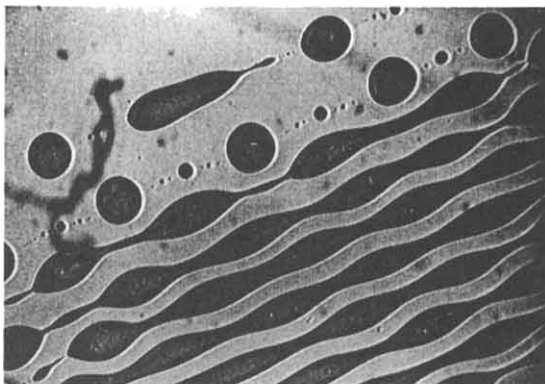


(b)

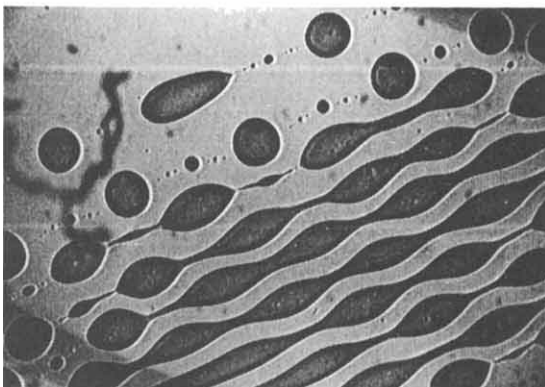


(c)

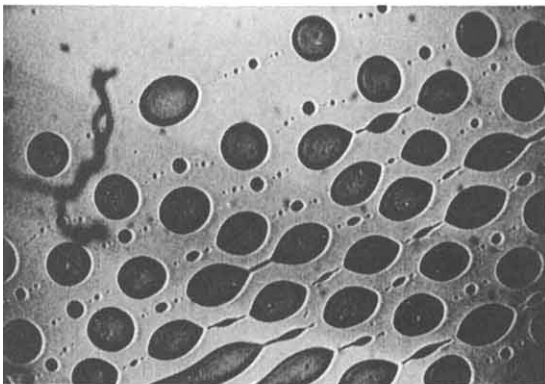
FIG. 43. Capillary breakup of closely spaced molten nylon-6 threads in molten polystyrene. Photographs at different times are shown (frames "a" through "f" correspond to 0, 210, 270, 360, 390, and 510 s). The initial thread diameter is $70\text{ }\mu\text{m}$ (Elemans *et al.*, 1997).



(d)



(e)



(f)

FIG. 43 (*continued*)

mixing and “perfect” mixing, lead to poor overall conductivities. No-mixing corresponds to the case of large isolated agglomerates in a polymer matrix; “perfect” mixing, to randomly placed aggregates having little contact with each other. At low volume fractions there are no sample-spanning clusters percolating through the sample, and the conductivity is poor. The best conductivities result when the particles are still recognizable as being aligned in long, thin interconnected structures, before further mixing randomizes the particles and connectivity is lost. There has been, for some time, industrial empirical evidence that “too much mixing” may not be good, and in this case, existing theory provides a rationalization of the observed events.

Integrating the fundamental processes at drop/cluster length scales to realistic flow fields is another area that is still developing, and the gap between the work presented here and more practical extrusion applications (Rauwendaal, 1994; White, 1990) needs to be bridged. Advances in this field would undoubtedly have an impact on the analysis and design of mixing equipment, as well as on optimization of processing conditions for mixers. All these issues require in-depth study before applications emerge.

It should be stressed again that the application of the concepts presented here is relevant to polymer and rubber processing and composite applications—which now form a fertile ground for the application of these ideas—as well to a variety of consumer products industries where product value is intimately tied to the creation of unique structures. Examples in this area may range from food products such as ice cream and margarine to laundry and personal care products such as dishwasher liquids, creams, and lotions. The creation of an organized body of knowledge geared toward the consumer product area presents considerable opportunities (Villadsen, 1997).

ACKNOWLEDGMENT

The research presented here has been supported over the past decade or so by grants to JMO awarded by the National Science Foundation, the Department of Energy—Basic Energy Sciences, and 3M.

REFERENCES

- Acrivos, A., The breakup of small drops and bubbles in shear flows. *4th International Conference on Physicochemical Hydrodynamics, Ann. N. Y. Acad. Sci.*, **404**, 1–11 (1983).

- Adler, P. M., and Mills, P. M., Motion and rupture of a porous sphere in a linear flow field. *J. Rheol.* **23**, 25–37 (1979).
- Aref, H., Stirring by chaotic advection. *J. Fluid Mech.* **143**, 1–21 (1984).
- Austin, L. G., A review introduction to the mathematical description of grinding as a rate process. *Powder Technol.* **5**, 1–17 (1971).
- Avalosse, Th., Simulation numerique du melange laminaire par elements finis. Ph.D. Thesis, Université Catholique de Louvain, Belgium (1993).
- Avalosse, Th., and Crochet, M. J., Finite element simulation of mixing: 1. Two-dimensional flow in periodic geometry. *AIChE J.* **43**, 577–587 (1997a).
- Avalosse, Th., and Crochet, M. J., Finite element simulation of mixing: 2. Three-dimensional flow through a Kenics mixer. *AIChE J.* **43**, 588–597 (1997b).
- Bagster, D. F., and Tomi, D., The stresses within a sphere in simple flow fields. *Chem. Eng. Sci.* **29**, 1773–1783 (1974).
- Barthès-Biesel, D., and Acrivos, A., Deformation and burst of a liquid droplet freely suspended in a linear shear field. *J. Fluid Mech.* **61**, 1–21 (1973).
- Batchelor, G. K., and Green J. T., The hydrodynamic interaction of two small freely-moving spheres in a linear flow field. *J. Fluid Mech.* **56**, 375–400 (1972).
- Becher, P., and McCann, M., The process of emulsification: A computer model. *Langmuir* **7**, 1325–1331 (1991).
- Bentley, B. J., and Leal, L. G., A computer-controlled four-roll mill for investigations of particle and drop dynamics in two-dimensional linear shear flows. *J. Fluid Mech.* **167**, 219–240 (1986).
- Bidkar, U. R., and Khakhar, D. V., Collision rates in chaotic flows: Dilute suspensions. *Phys. Rev. A* **42**, 5964–5969 (1990).
- Bigg, D., and Middleman, S., Laminar mixing of a pair of fluids in a rectangular cavity. *Ind. Eng. Chem. Fundam.* **13**, 184–190 (1974).
- Brenner, H., Dissipation of energy due to solid particles suspended in a viscous liquid. *Phys. Fluids* **1**, 338–346 (1958).
- Brunk, B. K., Koch, D. L., and Lion, L. W., Hydrodynamic pair diffusion in isotropic random velocity fields with application to turbulent coagulation. *Phys. Fluids* **9**, 2670–2691 (1997).
- Chaiken, J., Chevray, R., Tabor, M., and Tan, Q. M., Experimental study of Lagrangian turbulence in Stokes flow, *Proc. Roy. Soc. Lond.* **A408**, 165–174 (1986).
- Chakravarthy, V. S., and Ottino, J. M., Mixing of two viscous fluids in a rectangular cavity. *Chem. Eng. Sci.* **51**, 3613–3622 (1996).
- Chella, R., and Ottino, J. M., Fluid mechanics of mixing in a single-screw extruder. *I&EC Fundamentals* **24**, 2, 170–180 (1985).
- Chella, R., and Viñals, J., Mixing of a two phase fluid by cavity flow. *Phys. Rev. E* **53**, 3832–3840 (1996).
- Cheng, Z., and Redner, S., Kinetics of fragmentation. *J. Phys. A: Math. Gen.* **23**, 1233–1258 (1990).
- Chesters, A. K., The modeling of coalescence processes in fluid–liquid dispersions: A review of current understanding. *Trans. Inst. Engrs.* **69**, 259–270 (1991).
- Chimmili, S., Shear induced agglomeration in particulate suspensions. M. Sci. thesis, West Virginia University (1996).
- Danescu, R. I., and Zumbrennen, D. A., Creation of conducting networks among particles in polymer melts by chaotic mixing. *J. Thermoplast Composites*, **11**, 299–320 (1998).
- Danielson, T. J., Muzzio, F. J., and Ottino, J. M., Aggregation and structure formation in chaotic and regular flows. *Phys. Rev. Lett.* **66**, 3128–3131 (1991).
- de Bruijn, R. A., Tipstreaming of drops in simple shear flows. *Chem. Eng. Sci.* **48**, 2, 277–284 (1993).

- DeRoussel, P., Mixing and dispersion of viscous liquids. Ph.D. Thesis in progress, Northwestern University (1998).
- Eggers, J., Nonlinear dynamics and breakup of free surface flows. *Rev. Modern Phys.* **69**, 865–930 (1997).
- Elemans, P. H. M., van Wunnik, J. M., and van Dam, R. A., Development of morphology in blends of immiscible polymers. *AIChE J.* **43**, 1649–1651 (1997).
- Erwin, L., Theory of mixing sections in single screw extruders. *Polym. Eng. Sci.* **18**, 7, 572–576 (1978).
- Feke, D. L., and Manas-Zloczower, I., Rupture of inhomogeneous spherical clusters by simple flows. *Chem. Eng. Sci.* **46**, 2153–2156 (1991).
- Filippov, A. F., On the distribution of the sizes of particles which undergo splitting. *Theory of Probab. and Its Appl.* (Engl. Transl.) **4**, 275–294 (1961).
- Franjone, J. G., and Ottino, J. M., Feasibility of numerical tracking of material lines and surfaces in chaotic flows. *Phys. Fluids* **30**, 3641–3643 (1987).
- Giesekus, H., Strömungen mit konstantem Geschwindigkeitsgradienten und die Bewegung von darin suspendierten Teilchen. *Rheol. Acta* **2**, 112–122 (1962).
- Grace, H. P., Dispersion phenomena in high viscosity immiscible fluid systems and application of static mixers as dispersion devices in such systems. *3rd Eng. Found. Conf. Mixing, Andover, N. H.*; Republished in *Chem. Eng. Commun.* **14**, 225–227 (1982).
- Hansen, S., Aggregation and fragmentation in chaotic flows of viscous fluids. Ph.D. Thesis, Northwestern University (1997).
- Hansen, S., and Ottino, J. M., Agglomerate erosion: A nonscaling solution to the fragmentation equation. *Phys. Rev. E* **53**, 4209–4212 (1996a).
- Hansen, S., and Ottino, J. M., Aggregation and cluster size evolution in nonhomogeneous flows. *J. Colloid Interface Sci.* **179**, 89–103 (1996b).
- Hanson, S., Khakhar, D. V., and Ottino, J. N., Dispersion of solids in nonhomogeneous viscous flows. *Chem. Eng. Sci.* **53**, 1803–1817 (1998).
- Hartley, P. A., and Parfitt, G. D., An improved split cell apparatus for the measurement of tensile strength of powders. *J. Phys. E, Sci. Instrum.* **17**, 347–349 (1984).
- Hobbs, D. M., and Muzzio, F. J., The Kenics static mixer: a three-dimensional chaotic flow. *Chem. Eng. J.* **67**(3), 133–166 (1997).
- Horwatt, S. W., Feke, D. L., and Manas-Zloczower, I., The influence of structural heterogeneities on the cohesivity and breakup of agglomerates in simple shear flow. *Powder Technol.* **72**, 113–119 (1992a).
- Horwatt, S. W., Manas-Zloczower, I., and Feke, D. L., Dispersion behavior of heterogeneous agglomerates at supercritical stresses. *Chem. Eng. Sci.* **47**, 1849–1855 (1992b).
- Huneault, M. A., Shi, Z. H., and Utracki, L. A., Development of polymer blend morphology during compounding in a twin-screw extruder. Part IV: A new computational model with coalescence. *Polym. Eng. Sci.* **35**(1), 115–127 (1995).
- Jana, S. C., Metcalfe, G., and Ottino, J. M., Experimental and computational studies of mixing in complex Stokes flow—the vortex mixing flow and the multicellular cavity flow. *J. Fluid Mech.* **269**, 199–246 (1994).
- Jana, S. C., Tjahjadi, M., and Ottino, J. M., Chaotic mixing of viscous fluids by periodic changes in geometry—baffled cavity flow. *AIChE J.* **40**, 1769–1781 (1994b).
- Janssen, J. M. H., Dynamics of liquid–liquid mixing. Ph.D. Thesis, Eindhoven University of Technology (1993).
- Janssen, J. M. H., and Meijer, H. E. H., Droplet breakup mechanisms: stepwise equilibrium versus transient dispersion. *J. Rheol.* **37**(4), 597–608 (1993).
- Janssen, J. M. H., and Meijer, H. E. H., Dynamics of liquid–liquid mixing: A 2-zone mixing model. *Polym. Eng. Sci.* **35**(22), 1766–1780 (1995).

- Jiang, Q., and Logan, B. E., Fractal dimensions of aggregates from shear devices. *J. AWWA*, February, pp. 100–113 (1996).
- Kao, S. V., and Mason, S. G., Dispersion of particles by shear. *Nature* **253**, 619–621 (1975).
- Kaper, T. J., and Wiggins, S., An analytical study of transport in Stokes flows exhibiting large scale chaos in the eccentric journal bearing. *J. Fluid Mech.* **253**, 211–243 (1993).
- Kendall, K., Agglomerate strength. *Powder Metallurgy* **31**, 28–31 (1988).
- Khakhar, D. V., and Ottino, J. M., Fluid mixing (stretching) by time periodic sequences for weak flows. *Phys. Fluids* **29**(11), 3503–3505 (1986a).
- Khakhar, D. V., and Ottino, J. M., A note on the linear vector model of Olbricht, Rallison, and Leal as applied to the breakup of slender axisymmetric drops. *J. Non-Newtonian Fluid Mech.* **21**, 127–131 (1986b).
- Khakhar, D. V., and Ottino, J. M., Deformation and breakup of slender drops in linear flows. *J. Fluid Mech.* **166**, 265–285 (1986c).
- Khakhar, D. V., and Ottino, J. M., Breakup of liquid threads in linear flows. *Int. J. Multiphase Flow* **13**(1), 71–86 (1987).
- Khakhar, D. V., Rising, H., and Ottino, J. M., An analysis of chaotic mixing in two chaotic flows. *J. Fluid Mech.* **172**, 419–451 (1986).
- Khakhar, D. V., Franjone, J. G. and Ottino, J. M., A case study of chaotic mixing in deterministic flows: the partitioned pipe mixer. *Chem. Eng. Sci.* **42**, 2909–2926 (1987).
- Kolmogorov, N. A., Über das logarithmisch normale Verteilungsgesetz der Dimensionen der Teilchen bei Zerstückelung. *Doklady Akad. Nauk. SSSR* **31**, 99–101 (1941); translated into English by Levin in NASA-TT F-12,287 (1969).
- Kuhn, W., Spontane Aufteilung von Flüssigkeitszylindern in klein Kugeln. *Kolloid Z.* **132**, 84–99 (1953).
- Kumar, S., and Homsy, G. M., Chaotic advection in creeping flow of viscoelastic fluids between slowly modulated eccentric cylinders. *Phys. Fluids* **8**, 1774–1787 (1996).
- Kusch, H. A., and Ottino, J. M., Experiments on mixing in continuous chaotic flows. *J. Fluid Mech.* **236**, 319–348 (1992).
- Lee, Y. J., Feke, D. L., and Manas-Zloczower, I., Dispersion of titanium dioxide agglomerates in viscous media. *Chem. Eng. Sci.* **48**, 3363–3372 (1993).
- Leong, C. W., and Ottino, J. M., Experiments on mixing due to chaotic advection in a cavity. *J. Fluid Mech.* **209**, 463–499 (1989).
- Leong, C. W., Chaotic mixing of viscous fluids in time-periodic cavity flows. Ph.D. Thesis, Univ. Massachusetts, Amherst (1990).
- Levich, V. G., “Physicochemical Hydrodynamics.” Prentice-Hall, Englewood Cliffs, NJ, 1962.
- Liu, Y. H., and Zumbrunnen, D. A., Emergence of fibrillar composites due to chaotic mixing of molten polymers. *Polymer Composites* **17**, 187–197 (1996).
- Liu, Y. H., and Zumbrunnen, D. A., Toughness enhancement in polymer blends due to the in-situ formation by chaotic mixing of fine-scale extended structures. *J. Mater. Sci.* **34**, 1921–1931 (1999).
- Manas-Zloczower, I., Dispersive mixing of solid additives, in “Mixing and Compounding of Polymers—Theory and Practice.” (I. Manas-Zloczower and Z. Tadmor, Ed.) Hanser Publishers, Munich, 1994, pp. 55–83.
- Manas-Zloczower, I., and Feke, D. L., Analysis of agglomerate separation in linear flow fields. *Intern. Polym. Process. II* **3/4**, 185–190 (1988).
- Manas-Zloczower, I., Nir, A., and Tadmor, Z., Dispersive mixing in internal mixers—a theoretical model based on agglomerate rupture. *Rubber Chem. Tech.* **55**, 1250–1285 (1982).
- Manas-Zloczower, I., Nir, A., and Tadmor, Z., Dispersive mixing in rubber and plastics. *Rubber Chem. Tech.* **57**, 583–620 (1984).

- Mason, T. G., and Bibette, J., Emulsification in viscoelastic media. *Phys. Rev. Lett.* **77**, 3481–3484 (1996).
- McGrady, E. D., and Ziff, R. M., Shattering transition in fragmentation. *Phys. Rev. Lett.* **58**, 892–895 (1987).
- McGrady, E. D., and Ziff, R. M., Analytical solutions to fragmentation equations with flow. *AIChE J.* **34**, 2073–2076 (1988).
- Meakin, P., Models for colloidal aggregation. *Ann. Rev. Phys. Chem.* **39**, 237–269 (1988).
- Meakin, P., Aggregation kinetics. *Physica Scripta* **46**, 295–331 (1992).
- Meijer, H. E. H., and Janssen, J. M. H., Mixing of immiscible liquids, in “Mixing and Compounding of Polymers—Theory and Practice.” (I. Manas-Zloczower and Z. Tadmor, Ed.), Hanser Publishers, Munich, 1994, pp. 85–147.
- Meijer, H. E. H., Lemstra, P. J., and Elemans, P. M. H., Structured polymer blends. *Makromol. Chem., Makromol. Symp.* **16**, 113–135 (1988).
- Mikami, T., Cox, R. G., and Mason, S. G., Breakup of extending liquid threads. *Int. J. Multiphase Flow* **2**, 113–138 (1975).
- Morse, P. M., and Feshbach, H., “Methods of Theoretical Physics.” McGraw-Hill, New York, 1953.
- Muzzio, F. J., and Ottino, J. M., Coagulation in chaotic flows. *Phys. Rev. A* **38**, 2516–2524 (1988).
- Muzzio, F. J., Swanson, P. D., and Ottino, J. M., The statistics of stretching and stirring in chaotic flows. *Phys. Fluids A* **5**, 822–834 (1991a).
- Muzzio, F. J., Tjahjadi, M., and Ottino, J. M., Self-similar drop size distributions produced by breakup in chaotic flows. *Phys. Rev. Lett.* **67**, 54–57 (1991b).
- Neil, A. U., and Bridgwater, J., Attrition of particulate solids under shear. *Powder Technol.* **80**, 207–209 (1994).
- Nieder Korn, T. C., and Ottino, J. M., Mixing of viscoelastic fluids in time-periodic flows. *J. Fluid Mech.* **256**, 243–268 (1993).
- Nieder Korn, T. C., and Ottino, J. M., Mixing of shear thinning fluids in time-periodic flows. *AIChE J.* **40**, 1782–1793 (1994).
- Olbricht, W. L., Rallison, J. M., and Leal, L. G., Strong flow criteria based on microstructure deformation. *J. Non-Newtonian Fluid Mech.* **10**, 291–318 (1982).
- Ottino, J. M., “The Kinematics of Mixing: Stretching, Chaos, and Transport.” Cambridge Univ. Press, Cambridge, U.K., 1989.
- Ottino, J. M., Mixing, chaotic advection and turbulence. *Ann. Rev. Fluid Mech.* **22**, 207–253 (1990).
- Parfitt, G. D., The mixing of cohesive powders, in “Mixing in the Process Industries” (N. Harnby, M. F. Edwards, and A. W. Nienow, Eds.). Elsevier, North-Holland, 1992, pp. 321–348.
- Patlathan, S. A., and Lindt, J. T., Kinetics of structure development in liquid–liquid dispersions under simple shear flow. Theory. *J. Rheol.* **40**, 1095–1113 (1996).
- Powell, R. L., and Mason, S. G., Dispersion by laminar flow. *AIChE J.* **28**, 286–293 (1982).
- Rallison, J. M., A numerical study of the deformation and burst of a viscous drop in general shear flows. *J. Fluid Mech.* **109**, 465–482 (1981).
- Rallison, J. M., The deformation of small viscous drops and bubbles in shear flows. *Ann. Revs. Fluid Mech.* **16**, 45–66 (1984).
- Rauwendaal, C., “Polymer Extrusion,” 3rd ed. Hanser Publishers, Munich, 1994.
- Redner, S., Fragmentation, in “Statistical Models for the Fracture of Disordered Media,” (H. J. Herrman and S. Roux, Eds.). Elsevier, North-Holland, 1990, pp. 321–348.
- Robinson, D. J., and Earnshaw, J. C., Experimental study of aggregation in two dimensions. I. Structural aspects. *Phys. Rev. A* **46**, 2045–2054 (1992).

- Rumpf, H., The strength of granules and agglomerates in "Agglomeration" (W. A. Knepper, Ed.). Wiley Interscience, New York, 1962.
- Rumscheidt, F. D., and Mason, S. G., Particle motions in sheared suspensions. XII. Deformation and burst of fluid drops in shear and hyperbolic flow. *J. Colloid Sci.* **16**, 238–261 (1961).
- Rwei, S. P., Manas-Zloczower, I., and Feke, D. L., Observation of carbon black agglomerate dispersion in simple shear flows. *Polym. Eng. Sci.* **30**, 701–706 (1990).
- Rwei, S. P., Manas-Zloczower, I., and Feke, D. L., Characterization of agglomerate dispersion by erosion in simple shear flows. *Polym. Eng. Sci.* **31**, 558–562 (1991).
- Rwei, S. P., Manas-Zloczower, I., and Feke, D. L., Analysis of the dispersion of carbon black in polymeric melts and its effect on compound properties. *Polym. Eng. Sci.* **32**, 130–135 (1992).
- Schepens, F. A. O., Chaotic mixing in the extended periodic cavity flow. Masters Thesis, Eindhoven University of Technology, 1996.
- Schowalter, W. R., Stability and coagulation of colloids in shear fields. *Ann. Rev. Fluid Mech.* **16**, 245–261 (1984).
- Schuman, T. E. W., Theoretical aspects of the size distribution of fog particles. *Quart. J. Meteorological. Soc.* **66**, 195–208 (1940).
- Smoluchowski, M., Versuch einer mathematischen Theorie der Koagulationskinetik kolloider Lösungen. *Z. Phys. Chem.* **92**, 129–168 (1917).
- Sonntag, R. C., and Russel, W. B., Structure and breakup of flocs subject to fluid stresses. I. Shear experiments. *J. Colloid Interface Sci.* **113**, 399–413 (1986).
- Sonntag, R. C., and Russel, W. B., Structure and breakup of flocs subject to fluid stresses. II. Theory, *J. Colloid Interface Sci.* **115**, 378–389 (1987a).
- Sonntag, R. C., and Russel, W. B., Structure and breakup of flocs subject to fluid stresses. III. Converging flow. *J. Colloid Interface Sci.* **115**, 390–395 (1987b).
- Spielman, L. A., Viscous interactions in Brownian coagulation. *J. Colloid Interface Sci.* **33**, 562–571 (1970).
- Srinivasan, M. P., and Stroeve, P., Subdrop ejection from double emulsion drops in shear flow. *J. Membrane Sci.* **26**, 231–236 (1986).
- Stone, H. A., Dynamics of drop deformation and breakup in viscous fluids. *Ann. Revs. Fluid Mech.* **26**, 65–102 (1994).
- Stone, H. A., and Leal, L. G., Relaxation and breakup of an initially extended drop in an otherwise quiescent fluid. *J. Fluid Mech.* **198**, 399–427 (1989).
- Stone, H. A., Bentley, B. J., and Leal, L. G., An experimental study of transient effects in the breakup of viscous drops. *J. Fluid Mech.* **173**, 131–158 (1986).
- Stroeve, P., and Varanasi, P. P., An experimental study of double emulsion drop breakup in uniform shear flow. *J. Coll. Int. Sci.* **99**, 360–373 (1984).
- Sundaraj, U., Dori, Y., and Macosko, C. W., Sheet formation in immiscible polymer blends: model experiments on an initial blend morphology. *Polymer* **36**, 1957–1968 (1995).
- Swanson, P. D., and Ottino, J. M., A comparative computational and experimental study of chaotic mixing of viscous fluids, *J. Fluid Mech.* **213**, 227–249 (1990).
- Tanner, R. I., A test particle approach to flow classification for viscoelastic fluids. *AIChE J.* **22**, 910–918 (1976).
- Taylor, G. I., The viscosity of a fluid containing a small drops of another fluid. *Proc. R. Soc.* **A138**, 41–48 (1932).
- Tjahjadi, M., and Ottino, J. M., Stretching and breakup of droplets in chaotic flows. *J. Fluid Mech.* **232**, 191–219 (1991).
- Tjahjadi, M., Stone, H. A., and Ottino, J. M., Satellite and subsatellite formation in capillary breakup. *J. Fluid Mech.* **243**, 297–317 (1992).

- Tomotika, S., On the instability of a cylindrical thread of a viscous liquid surrounded by another viscous fluid. *Proc. R. Soc. A* **150**, 322–337 (1935).
- Tomotika, S., Breaking up of a drop of viscous liquid immersed in another viscous fluid which is extending at a uniform rate. *Proc. R. Soc. A* **153**, 302–318 (1936).
- Torres, F. E., Russel, W. B., and Schowalter, W. R., Floc structure and growth kinetics for rapid shear coagulation of polystyrene colloids. *J. Colloid Interface Sci.* **142**, 554–574 (1991a).
- Torres, F. E., Russel, W. B., and Schowalter, W. R., Simulations of coagulation in viscous flows. *J. Colloid Interface Sci.* **145**, 51–73 (1991b).
- Ullbrecht, J. J., Stroeve, P., and Pradobh, P., Behavior of double emulsions in shear flows. *Rheol. Acta* **21**, 593–597 (1982).
- van Dongen, P. G. J., and Ernst, M. H., Scaling solutions of Smoluchowski's coagulation equation. *J. Stat. Phys.* **50**, 295–329 (1988).
- Varanasi, P. P., Ryan, M. E., and Stroeve, P., Experimental study on the breakup of model viscoelastic drops in uniform shear flow. *I&EC Research* **33**, 1858–1866 (1994).
- Verwey, E. J., and Overbeek, J. T. G., "Theory of the Stability of Lyophobic Colloids." Elsevier, 1948.
- Villadsen, J., Putting structure into chemical engineering. *Chem. Eng. Sci.* **52**, 2857–2864 (1997).
- Wang, H., Zinchenko, A., and Davis, R. H., The collision rate of small drops in linear flow fields. *J. Fluid Mech.* **265**, 161–188 (1994).
- White, J. L., "Twin Screw Extrusion." Hanser, Munich, 1990.
- Williams, M. M. R., An exact solution of the fragmentation equation. *Aerosol Sci. and Tech.* **12**, 538–546 (1990).
- Zeichner, G. R., and Schowalter, W. R., Use of trajectory analysis to study stability of colloidal dispersions in flow fields. *AIChE J.* **23**, 243–254 (1977).
- Zhang, D. F., and Zumbrunnen, D. A., Chaotic mixing of two similar fluids in the presence of a third dissimilar fluid. *AIChE J.* **42**, 3301–3309 (1996a).
- Zhang, D. F., and Zumbrunnen, D. A., Influences of fluidic interfaces on the formation of fine scale structures by chaotic mixing. *J. Fluids Eng.* **118**, 40–47 (1996b).
- Ziff, R. M., New solutions to the fragmentation equation. *J. Phys. A: Math. Gen.* **24**, 2821–2828 (1991).
- Ziff, R. M., and McGrady, E. D., The kinetics of cluster fragmentation and depolymerisation. *J. Phys. A: Math. Gen.* **18**, 3027–3037 (1985).
- Ziff, R. M., and McGrady, E. D., Kinetics of polymer degradation. *Macromolecules* **19**, 2513–2519 (1986).
- Zumbrunnen, D. A., Miles, K. C., and Liu, Y. H., Auto-processing of very fine-scale materials by chaotic mixing of melts. *Composites* **27A**, 37–47 (1996).